Dielectric Properties of Molecular Glass Formers; from the Liquid State to the Tunneling Regime

Der Universität Bayreuth

zur Erlangung des Grades eines

Doktors der Naturwissenschaften (Dr. rer. nat.)

vorgelegte Abhandlung

von

Catalin P. GAINARU

geboren am 27. Mai 1977 in Botosani, Rumänien

1. Gutachter: Prof. Dr. E.A. Rössler

2. Gutachter: Prof. Dr. R. Böhmer

"Make everything as simple as possible, but not simpler."

Albert Einstein

Contents

I. Introduction

I.1 The glass transition

The glass transition phenomenon has been recognized since a long time as one of the major topics in condensed matter physics. In spite of its considerable scientific impact there still exists a fairly widespread lack of understanding the nature of the glass transition.

A glass can be defined as a solid with irregular microscopic structure or, equivalently, as a liquid with infinite viscosity. The simplest way to produce a glass is by supercooling a liquid. Presumably, any liquid can be transformed into a glass if cooled fast enough to avoid crystallization. Supercooling a liquid results in a continuous slowing down of the structural relaxation process or, equivalently, a continuous increase of viscosity. This process, called *glass transition*, is purely kinetic in nature, as no thermodynamic phase transition is involved.

The temperature associated with the liquid surpassing a viscosity value of $\eta \approx 10^{12}$ *Pa·s* or with an increase of the time constant of the liquid structural relaxation beyond *100* seconds gives the conventional definition for the *glass transition temperature T_g*. Another criterion for T_g may be given by the temperature at which a step is recorded in the specific heat while heating the sample at *10 K/min*. This is called the *calorimetric* glass transition temperature. All the experiments probing structural relaxation, viscosity or specific heat yield similar values for T_g.

The glass is produced by the inability of the liquid structure to equilibrate on the *experimental time scale* at low temperatures. Since in the liquid, well above the melting point, the structural relaxation takes place on the time scale of picoseconds and on the time scale of hundreds of seconds around T_g, the structural relaxation time constant (or viscosity) changes by many decades upon supercooling. One of the most interesting features of supercooled liquids is that this change occurs in a rather small temperature range, as shown in Fig. I.1. Here the time constants of the glass former SiO_2 obeys a thermally activated behavior (straight line in Fig. I.1), *i.e.* their temperature dependence is given by an *Arrhenius law:* $\ln \eta \propto \ln \tau \propto \dfrac{E_a}{RT}$, with an activation energy E_a = constant. However, as the most glass formers, glycerol and o-terphenyl (*OTP*) show deviations from the Arrhenius behavior and a curvature in the "Arrhenius plot" is observed. Close to T_g, this non-Arrhenius temperature

dependence can be phenomenologically described by the Vogel-Fulcher-Tammann (*VFT*) equation [19,20]:

$$\eta(T) \propto \tau(T) = \tau_0 \exp(\frac{D}{T - T_0})$$

(I.1)
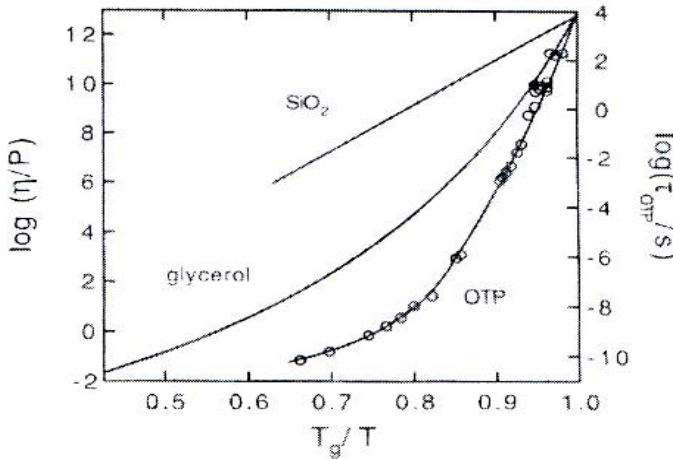
Fig. I.1 The Arrhenius plot for the viscosity for two supercooled liquids: SiO_2 and glycerol. In addition, time constants from dielectric measurements for o-terphenyl (*OTP*) are plotted as open circles. Figure from [18].

The good interpolation of the data with the *VFT* function can be interpreted as pointing to the existence of a non-zero temperature $T_0 < T_g$ at which the relaxation time of the supercooled liquid may diverge, *i.e.* a phase transition is expected here. However, since the relaxation time τ becomes inaccessibly large at such temperatures, it is impossible to actually verify this scenario.

Based on the temperature dependence of the viscosity, a classification of glass formers was introduced [21,22]: systems showing a weak change of viscosity at T_g in the above representation, $lg\eta$ vs. T_g/T, are called "strong" (*e.g. SiO_2*) while the others with a strong change are called "fragile" (*e.g. OTP*).

I.2 Relaxation processes in molecular glass forming systems

Dielectric spectroscopy (DS) is a powerful tool to investigate the extremely broad dynamic range involved in the glass transition (cf. Fig. I.1). Though dielectric measurements covering more than *18* decades in frequency were already performed, a conclusive picture of the evolution of molecular dynamics upon supercooling is still missing. This is due to the fact that there are not so many glass formers investigated in this full relevant relaxation time range. As most of commercially available dielectric spectrometers operate below some *GHz*, there are actually only two molecular liquids

investigated in the $10^{-6} - 10^{13}$ Hz range with dielectric spectroscopy, namely glycerol and propylene carbonate (*PC*) [25].

In order to reveal some characteristic relaxation features of the supercooled molecular liquids, the dielectric susceptibility of glycerol [25,26] is shown in Fig. I.2 (a). These data represent the *state-of-the-art* in the dielectric investigations of molecular glass formers. The main contribution to the dielectric spectra is given by the so-called α-*process.* For simple liquids this process is responsible for the ultimate correlation loss at long times; it characterizes the structural relaxation and controls macroscopic properties such as the flow, hence it governs the glass transition.
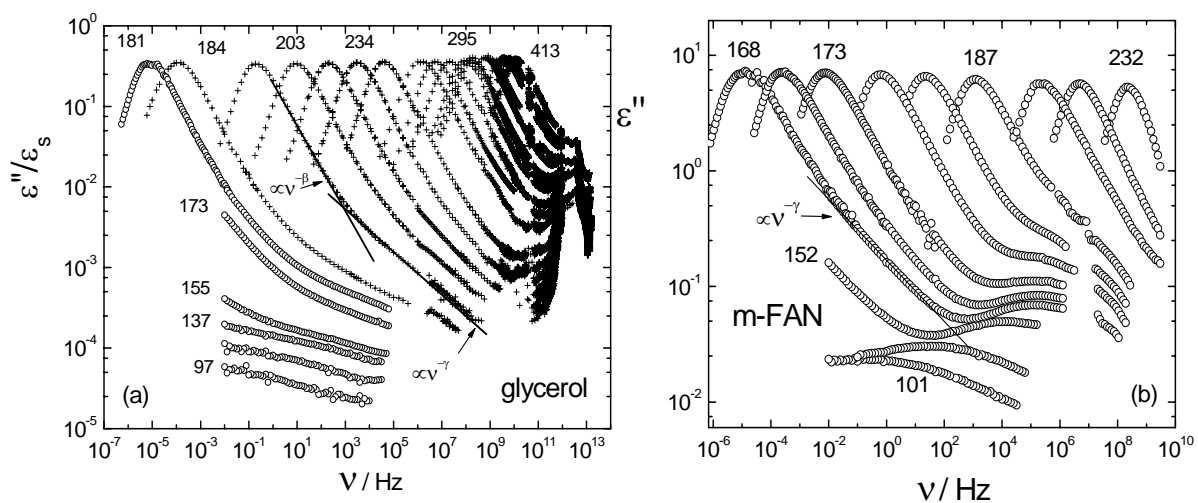
Fig. I.2 (a) Dielectric spectra of glycerol (T_g = 186 K) scaled by the static permittivity. The data plotted as crosses are from Lunkenheimer *et al.* [25] and the full circles are data measured by our group [26] scaled by the ε_s at T_g. (b) Dielectric spectra of m-fluoroaniline (*m-FAN, T_g = 172 K*), measured in our group [27]. Few temperatures (in K) are indicated.

Besides the non-Arrhenius temperature dependence of the α-relaxation times, another important feature of the α-relaxation peak is its asymmetric non-Debye spectral shape. There are several empirical expressions proposed to describe the the α-peak as, *e.g.*, the Cole-Davidson (*CD*) function. This function describe the high frequency side of the peak as a power-law ν^{β} with $0 < \beta < 1$. This function seems sufficient for interpolating the relaxation peak at the highest temperatures in Fig. I.2 (a).

The relaxation pattern gets more complicated while approaching T_g. A characteristic of the deeply supercooled state is the emergence of secondary relaxation features in addition to the α-relaxation close to T_g. One recognizes for glycerol in Fig. I.2 (a), at temperatures close and above T_g, an additional spectral contribution on the high-frequency flank of the α-peak, which can be described as a power-law ν^{γ} (with

3

exponent $\gamma < \beta$), the so-called *excess wing* (*EW*). This relaxation feature extends up to high frequencies (above GHz range) where a minimum in the susceptibility marks the crossover to the "fast dynamics". At the highest frequencies the so-called "microscopic peak", associated with vibrational dynamics ends the relaxation regime. The majority of the investigated glass formers exhibits in their dielectric spectra, in addition to EW, a second relaxation peak at frequencies higher than those associated with the α-process. An example is shown in Fig. I.2 (b) for m-fluoroaniline (*m-FAN)*. Secondary relaxation peaks were observed since long in polymers, where they are usually related to the dynamics of particular side groups. However, investigating simple molecular liquids formed by rigid molecules, Johari and Goldstein discovered that the secondary relaxation peaks may be present even for such simple compounds [28,29]. Ever since, it is commonly accepted that the so-called *Johari-Goldstein β-process* is an intrinsic property of the amorphous state.

A highly debated topic in the glass community is the validity of the frequency-temperature superposition, *i.e.* the invariance of the spectral shape of the α-relaxation while changing temperature. Besides its theoretical implications, it is a useful concept for handling experimental data acquired in a limited frequency range at different temperatures. Since different phenomenological approaches for disentangling the contribution of the α-peak from the overall relaxation including the secondary processes may lead to quite different results, the situation here appears not conclusive.

As observed in Fig. I.2, the secondary processes (*EW* and/or β-process) survive in the glass and give the major contribution to the dielectric response for temperatures down to say, $T_g/2$. However, systematic dielectric investigations of molecular glasses at even lower temperatures are not carried out up to date, as data here are sparse.

I.3 Scope and structure of the present study

The main purpose of the current work is to extend previous dielectric investigations of the molecular glass forming systems down to cryogenic temperatures say, close to 2 K. As the main experimental effort has been spent on the investigations at temperatures below T_g, only few molecular glass-formers are newly investigated in the supercooled regime, at $T > T_g$. However, having at hand a huge collection of data

compiled in the Bayreuth group in the last years, this work starts with describing the temperature evolution of the different spectral contributions (α-process, EW and β-process) for the molecular glass formers investigated above and also below T_g. A new phenomenological approach will be introduced to interpret the evolution of the dynamic susceptibility. This scenario stands for the applicability of the frequency temperature superposition for the α-peak in the whole temperature range down to T_g. The results of this approach call for strong reconsiderations for the evolution of the secondary processes in the supercooled regime, but also in the glass where they dominate the spectra. The dielectric results of glycerol will be discussed within this scenario together with those obtained by field cycling NMR and light scattering. From this comparison important conclusions will be drawn regarding the nature of the molecular dynamics associated with the EW.

The dielectric investigations will be extended down to cryogenic temperatures by applying a high precision bridge. Using this bridge, up to three decades in the frequency dependence of the dielectric loss of molecular glasses can be accessed at such low temperatures. This study will address the question down to what temperatures the dielectric spectra are still dominated by the contribution from the secondary processes emerging at $T > T_g$ and surviving in the glass. Moreover, it tries to identify some fingerprints of the "low temperatures anomalies" intensively discussed for inorganic glasses: whether the tunneling plateau can be reached in the accessible temperature range ($T > 2$ K) for molecular glasses, whether the spectra in the tunneling regime follow the predictions of the Standard Tunneling Model (STM) and whether one finds contributions from thermally activated Asymmetric Double Well Potential (ADWP) dynamics, a natural extension of the STM to higher temperatures.

The Thesis is structured as follows: the next Chapter (II) gives a brief description of the dielectric response of polar materials and the principles of the experimental techniques used within this work. Here, some functions taken from literature and used for the interpolation of the measured spectra are also discussed. Chapter III presents the state-of-the-art for the description of the evolution of dynamic susceptibility in molecular systems, cumulating the theoretical and phenomenological approaches preceding this work. The experimental results are discussed starting with Chapter IV, where new data, together with those previously obtained, are discussed within the new approach. Here, the evolution of the α-process, excess wing and β-

process is considered. Chapter V presents the low temperature investigations of the molecular glasses. The data are discussed within the predictions of theoretical models as STM and Gilroy-Phillips, aiming to describe the relaxation pattern observed as typical for inorganic glasses. In Chapter VI a comparison of three techniques (dielectric spectroscopy, field cycling NMR and light scattering) accessing the dynamic susceptibility of glycerol in a broad frequency and temperature range is presented. Ending the results, Chapter VII describes the dielectric response of 1,4 polybutadiene. This polymeric system shows a peculiar relaxational behaviour with respect to the one generally observed for the simple glass forming systems at low temperatures. All the findings within this work are summarized in Chapter VIII.

II. Dielectric Spectroscopy: Theory, Experiment and Phenomenological Description of the Dielectric Response

Dielectric spectroscopy relies on the property of materials to be polarized under the influence of an external electric field. The effect of a constant electric perturbation on a dielectric material as, *e.g.*, a supercooled molecular liquid, results in building-up of a non-zero macroscopic polarization. The value of the equilibrium polarization depends on temperature and material structure and the time needed for reaching this equilibrium value depends on the underlying microscopic dynamics. All in all, dielectric spectroscopy provides direct access to the microscopic molecular dynamics and, indirectly, certain structure information.

The main advantage of using this technique is the extremely large range in accessible time/frequency and the signal amplitude, *i.e.*, the complete dielectric response of molecular glass forming liquids can be monitored. Nowadays dielectric investigations can cover the spectral range of 10^{-6} *Hz – 1 THz*.

This Chapter will give a brief description of the dielectric response of polar materials and the principles of this experimental technique. The following parts are, more or less, a compilation from the books of Böttcher and Bordewijk [1,2] and Kremer and Schönhals [3].

II.1 Theoretical background

This Thesis will focus on the electric response of dielectric materials such as glass-forming molecular systems. Thus, most attention will be given to the polarization phenomena arising from the reorientational motion of molecular dipoles. Nevertheless, during experiments additional polarization mechanisms may interfere and they are briefly mentioned here [1,4,5]:

- shortly after an electric field is applied (at times smaller than say 10^{-13} *s*) dipole moments are induced by the change of the atoms position within the molecule or by the shift of the electronic cloud within the atoms. This gives a contribution to the total polarization, the so-called *induced polarization*. The corresponding fingerprint in the dielectric spectra is a number of resonance lines at frequencies beyond infrared band;

- any polar material contains electrically charged impurities whose diffusion will be manifested in the electric response as *conductivity*;

- at very low frequencies of the probing electric field, these free charges can accumulate at the electrod boundaries, a phenomenon called *electrode polarization*;

- if the material allows the presence of interfaces enclosing different structural domains, charges may accumulate at the embedding surfaces leading to the so-called *interfacial polarization* (or *Maxwell-Wagner polarization*).

Static response

Dielectric measurements can be performed in both time and frequency domain [2,3]. In a time domain experiment one applies a constant electric field with a moderate amplitude (below *10^3 Vcm^{-1}*) to a capacitor filled with the material under investigation. Let us assume the absence of the free charges (conductivity is neglected), and that the dielectric material consists only of rigid molecules with permanent dipole moments. In the absence of the field the molecular dipoles are randomly oriented. Shortly after the field is applied, the dipoles start to reorient due to the electric force. The minimum energy dictates a preferred alignment parallel with the field direction, thus a macroscopic dipole moment $\vec{P}$ is induced. This phenomenon is known as *orientational polarization.*

In the (quasi)static limit, *i.e.*, any change of the electric field $\vec{E}_0$ occurs slowly compared with the intrinsic motion of the constituent molecular dipoles, the total macroscopic polarization $\vec{P}$ builds-up to a value proportional with the applied field. Along the z-axis defined by $\vec{E}_0 = E_0 \vec{z}$

$$P = D - \varepsilon_0 E_0 = \varepsilon_0 (\varepsilon_s - 1) E_0 = \varepsilon_0 \chi_s E_0 \tag{II.1}$$

where ε_0 is the *vacuum permittivity*, ε_s is the *static permittivity* and $\chi_s = \varepsilon_s - 1$ is the *static susceptibility* of the material. *D* is the *electric displacement* and represents the density of electric charge induced on the sample surfaces. The material is considered isotropic, therefore ε_s and χ_s are scalars.

The overall polarization P arises from two contributions: the instantaneous polarization P_∞ due to the induced dipole moments, and the orientational polarization P_0 due to the reorientation of the permanent dipoles:

$$P = P_\infty + P_o = \varepsilon_0(\varepsilon_\infty - 1)E_0 + \varepsilon_0\Delta\varepsilon E_0 \qquad (II.2)$$

where $\varepsilon_s = \varepsilon_\infty + \Delta\varepsilon$ was substituted in Eq. (II.1), $\Delta\varepsilon$ being the *relaxation strength* and ε_∞ the permittivity related to the short-time response or, equivalently, to the response at very high frequencies, far above the ones associated with the molecular relaxation.

The *orientational polarization* $\vec{P}_0$ can be expressed as the macroscopic volume density of the vectorial sum over all permanent dipole moments contained in the material. Its projection on the z-axis defined by the electric field is given by:

$$P_0 = \frac{\sum_{i=1}^{N}\vec{\mu}_i}{V}\cdot\vec{z} = \frac{N}{V}\langle\mu\rangle_z \qquad (II.3)$$

Here N is the number of permanent dipoles in the volume V and $\langle\mu\rangle_z$ is the average over all projections of the dipole moments on the *z*-axis.

After the electric field is applied the dipoles in the new equilibrium state are only partially oriented parallel with the applied field due to the thermal fluctuations. One may consider their orientations as distributed within a solid angle $d\Omega = 2\pi\sin\theta d\theta$ around the *z*-axis and the distribution following the Boltzmann statistics. Accordingly:

$$\langle\mu\rangle_z = \frac{\int_o^\pi \mu_z \exp(\frac{\mu_z\cdot E_o}{\kappa T})2\pi\sin\theta d\theta}{\int_0^\pi \exp(\frac{\mu_z\cdot E_o}{\kappa T})2\pi\sin\theta d\theta} \qquad (II.4)$$

where $\mu_z = \mu\cos\theta$. After the integration, for small interaction energies ($\mu E_0 \ll kT$) the equation reduces to [1]:

$$\langle\mu\rangle_z = \frac{\mu^2}{3\kappa T}E_0 \qquad (II.5)$$

Identifying the orientation polarization P_0 in Eq. (II.2) and Eq. (II.3) we obtain, via Eq. (II.5), the *Curie law* [1,3]:

$$\Delta\varepsilon = \frac{N\mu^2}{3\varepsilon_0 V\kappa T} \qquad (II.6)$$

Most of the dielectric investigations of the molecular supercooled liquids indicate that the temperature dependence of the relaxation strength $\Delta\varepsilon$ may differ from the Curie-law [1,6]. This indicates that additional considerations are to be taken into account:

- the local field (*Lorentz field*) for a given dipole can differ from the external field E_0 (*Maxwell field*) due to the polarization of the dipole surroundings;

- a so called reaction field (*Onsager field*) may occur due to an additional polarization of the surroundings by the dipole itself [6];

- most important, the dipole – dipole interaction might play a significant role especially in the case of high values of the dipole moment [1,4].

Dynamic response

As already mentioned, if an external electric field is applied to a dielectric material the macroscopic polarization will not reach its equilibrium value instantaneously but after a certain time. By analogy, in a step-off experiment, the polarization decays with a delay with respect to the switched-off electric field (see Fig. II.1). In this way, one can introduce the *relaxation function* (*step-response function*) as:

$$\Phi(t) = \frac{P_o(t)}{P_o(0)} \tag{II.7}$$
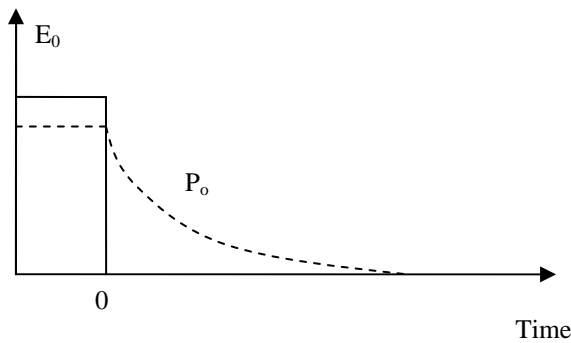
Fig.II.1. When the electric field E_0 (continuous line) is removed, the orientational polarization P_o (dashed line) starts to decrease in time towards the *0* value. The induced polarization P_∞ is neglected here.

Within the *linear response approximation* [2,7], the response of a system under the to an external perturbation is determined by the same mechanisms that also controls statistical equilibrium fluctuations within the system (*fluctuation-dissipation theorem*). Thus, one can identify the relaxation function $\Phi(t)$ with the autocorrelation function $\phi_P(t)$ of the macroscopic polarization noise in the absence of the field [2]:

$$\Phi(t) = \phi_P(t) \equiv \frac{\left\langle \vec{P}_o(0) \cdot \vec{P}_o(t) \right\rangle}{\left\langle \vec{P}_o(0) \cdot \vec{P}_o(0) \right\rangle} \tag{II.8}$$

The brackets denote ensemble average. Dielectric experiments access the response function $\Phi(t)$ or its Fourier transform and implicitly, via the fluctuation-dissipation theorem, the correlation function $\phi(t)$. We note here that the autocorrelation function $\phi_P(t)$ can also be directly accessed in the absence of any external electric field by monitoring directly the equilibrium polarization noise [8,9]. However, this requires a significant experimental effort.

The main interest is to access the microscopic dynamics of the material under study. Therefore it is necessary to establish a connection between the fluctuations of the macroscopic polarization and the dynamic fluctuations on the microscopic scale.

Introducing the molecular dipole moment $\vec{\mu}$, the correlation function $\phi_P(t)$ in Eq. (II.8) can be rewritten as:

$$\phi_P(t) = \frac{\sum_{i,j}^{N}\left\langle \vec{\mu}_i(0)\cdot\vec{\mu}_j(t)\right\rangle}{\sum_{i,j}^{N}\left\langle \vec{\mu}_i(0)\cdot\vec{\mu}_j(0)\right\rangle} = \frac{\sum_{i}^{N}\left\langle \vec{\mu}_i(0)\cdot\vec{\mu}_i(t)\right\rangle + \sum_{i\neq j}^{N}\left\langle \vec{\mu}_i(0)\cdot\vec{\mu}_j(t)\right\rangle}{N\mu^2 + \sum_{i\neq j}^{N}\left\langle \vec{\mu}_i(0)\cdot\vec{\mu}_j(0)\right\rangle} \tag{II.12}$$

Since $\phi_P(t)$ contains both auto- and cross-correlation terms, dielectric investigations of molecular systems probe both collective and single particle dynamics. *A priori*, it is difficult to separate the two contributions. However, provided that the cross-correlation terms can be neglected [2,10] one can identify the correlation function of the macroscopic polarization with the dipole-dipole autocorrelation function $\phi_\mu(t)$:

$$\phi_p(t) \approx \phi_\mu(t) = \frac{1}{N\mu^2}\sum_{i}^{N}\left\langle \vec{\mu}_i(0)\cdot\vec{\mu}_i(t)\right\rangle = \frac{1}{\mu^2}\left\langle \vec{\mu}(0)\cdot\vec{\mu}(t)\right\rangle = \left\langle \cos\vartheta(0)\cos\vartheta(t)\right\rangle \tag{II.13}$$

In glass forming systems the collective dynamics do not significantly differ from the single particle dynamics, hence dielectric spectroscopy probes in this case the dipole-dipole reorientation autocorrelation function in a good approximation.

Due to technical reasons, time domain experiments cannot be carried out for times shorter than milliseconds. In order to extend the investigations into a shorter time range, experiments are performed in the frequency domain, where the Fourier transform of $\Phi(t)$ is accessed.

For investigations in the frequency domain, the quantity of interest is the complex dielectric permittivity $\varepsilon^*(\omega)$. Relation (II.1) reads for alternating fields:

$$P^*(\omega) = \varepsilon_0(\varepsilon^*(\omega)-1)E(\omega) = \varepsilon_0\chi^*(\omega)E^*(\omega) \tag{II.9}$$

$\chi^*(\omega)$ is now the complex dielectric susceptibility. The permittivity relates to the response function as [2,3]:

$$\frac{\varepsilon^*(\omega) - \varepsilon_\infty}{\Delta\varepsilon} = 1 - i\omega \int_0^\infty \Phi(t) \exp(-i\omega t) d(t) \qquad (\text{II}.10)$$

The real and imaginary components of permittivity are interrelated by the *Kramers–Kronig relations*, thus they carry equivalent information. From the Kramers-Kronig analysis two important consequences can be drawn:

- the relaxation strength $\Delta\varepsilon$ is directly related to the integral over the relaxational part of the spectrum $\varepsilon''(\omega)$:

$$\Delta\varepsilon = \frac{2}{\pi} \int_{relax} \varepsilon''(\omega) d(\ln\omega) \qquad (\text{II}.11)$$

- the DC conductivity giving a contribution proportional with $1/\omega$ in $\varepsilon''(\omega)$ has no manifestation in the real part $\varepsilon'(\omega)$ [2,3].

II.2 Experimental details

In the following the physical principles of the dielectric techniques used for obtaining the data presented in this Thesis are briefly described.

As indicated in Fig. II.2, the experiments were performed using four spectrometers: three of them, operating in the frequency domain, are commercially available [11,13], and one measuring in the time domain is home-built [11]. Except high frequency experiments, all the others were performed using a dielectric cell suitable for the liquids investigation, constructed as suggested by Wagner and Richert [12] (see Fig. II.3). The cell was made from gold-plated Invar steel and in the absence of the sample, empty capacity ($\cong$ *40 pF*) varied within *0.5 %* in the temperature range from *4* to *300 K*. The experiments can be performed in a temperature range from *500 K* down to *2 K*.
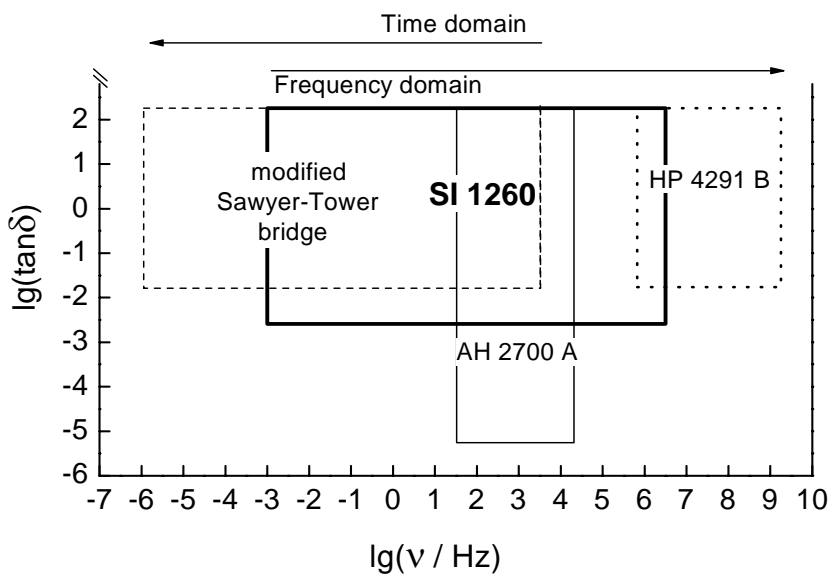
Fig. II.2 The dielectric spectrometers used to obtain the data presented in this Thesis; for every spectrometer the frequency and resolution (tanδ) ranges, *i.e.*, the accessible ranges are indicated.
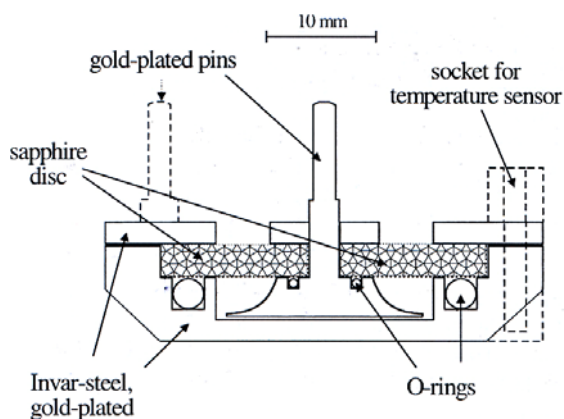
Fig. II.3 The sample cell user for the low frequency and time-domain spectroscopy in this work. Picture from [11].

13

II.2.1 Frequency domain measurements

The experiments in the frequency domain were performed using three different setups: one accesses a broadband intermediate frequency range, between 10^{-3} and 10^7 Hz, one the high frequency range, $10^6 - 2 \cdot 10^9$ Hz and the last setup is suited for high precision measurements in the frequency range *50 Hz–20 kHz*. For intermediate frequencies an Impedance Analyzer Schlumberger SI1260 together with a Broad Band Dielectric Converter (BDC) by Novocontrol were employed, and for the high frequency range a Hewlett Packard 4291 B network analyzer. Both spectrometers measure the frequency dependence of the complex impedance $Z^*(\omega)$ of the sample [11,13]:

1. The SI 1260 generates an alternating voltage $U^*(\omega,t) = U_0 e^{i\omega t}$ that is applied to a capacitor filled with the material under investigation. The amplitude and the phase shift of the resulting current are recorded $I^*(\omega,t) = I_0 e^{i(\omega t + \varphi)}$, yielding the complex impedance $Z^*(\omega) = \dfrac{U^*(\omega,t)}{I^*(\omega,t)}$. Since supercooled molecular liquids and glasses exhibit as high impedances, the BDC assures that the resulting low current amplitudes are monitored with high precision.

2. The HP 4291 B generates an electromagnetic wave along a coaxial line terminated by a small sample capacitor [91]. For a given frequency the amplitude and the phase shift of the reflected wave is recorded, yielding the complex reflection coefficient $\Gamma^*(\omega)$. The reflection coefficient is related to the impedance by $\Gamma^*(\omega) = \dfrac{Z^*(\omega) - Z_0^*}{Z^*(\omega) + Z_0^*}$, where Z_0^* is the characteristic impedance of the coaxial line, determined from the system calibration in the absence of a sample [91].

Modeling the sample as a pure capacitive reactance X_C^*, the permittivity $\varepsilon^*(\omega)$ can be related to the impedance by:

$$Z^*(\omega) = X_C^*(\omega) = \frac{1}{i\omega\varepsilon^*(\omega)C_g} \tag{II.14}$$

where the geometric factor $C_g = \varepsilon_0 \dfrac{S}{d}$ is given by the cell geometry (*S* is the area of the electrodes and *d* the distance between the electrodes) and is determined by the measurements of the unfilled capacitor.

The peculiarity of the high-precision bridge (AH 2700 A) is that it allows measurements of very low electric signals in a frequency range between *50 Hz* and *20 kHz*. This enables, for example, investigations of glasses at cryogenic temperatures. The resolution limit of the bridge incorporated in the setup is around *tanδ* ≈ *8x10⁻⁶*, as assured by the measurements of the empty cell from room temperature down to *4 K*.

Fig. II.4 displays the essentials of the AH bridge. A *50 Hz* to *20 kHz* sine wave generator excites the ratio transformer, which forms legs 1 and 2 of a basic bridge. Both legs have many transformer taps to ensure selection of precisely defined voltages. Leg 3 consists of a temperature-controlled fused-silica variable capacitor and a circuit simulating a very stable resistor. The sample represented in Fig. II.4 as a parallel circuit R_xC_x is connected to leg 4. A microprocessor performs the tasks of selecting Taps 1 and 2 in the transformer and of balancing C_0 and R_0 so that the current through the detector is minimized. The bridge allows to measure independently both resistive and capacitive components of the unknown impedance. If the zero current condition on the detector is fulfilled, the unknown capacity can be easily obtained since its ratio to C_0 is equal to the ratio of the voltage on Tap 1 to the voltage on Tap 2. Similarly, the ratio R_x/R_0 is equal to the ratio of the voltage on Tap 2 to the voltage on Tap 1. Thus, the bridge provides the values of C_x and R_x.
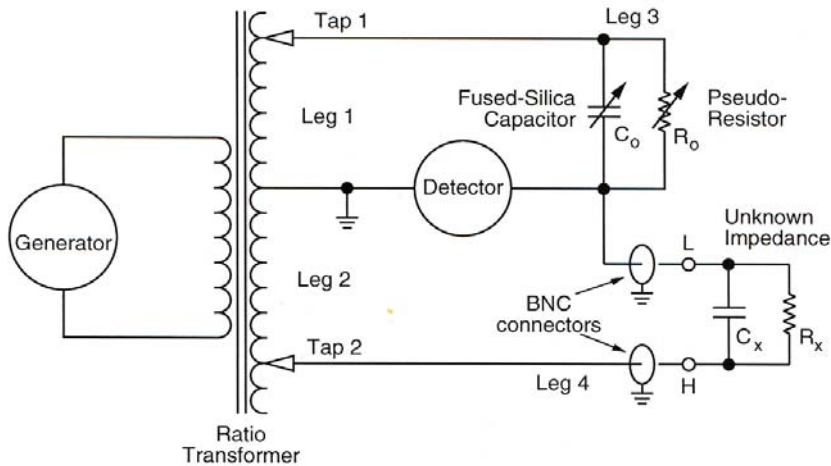
Fig. II.4 The basic electrical circuit of the AH 2700 A bridge.

Since the sample is modeled as a parallel circuit of a pure capacitor C_x and a pure resistive element R_x, the complex admittance of the circuit is given by:

$$Y^* = \frac{1}{Z^*} = R_x + i\omega C_x = i\omega C^* = i\omega C_g (\varepsilon' - i\omega\varepsilon'') \tag{II.15}$$

The real and imaginary parts of the sample permittivity can be then related to C_x and R_x:

$$\varepsilon' = \frac{C_x}{C_g}$$
$$\varepsilon'' = \frac{1}{\omega R_x C_g}$$

(II.16)

II.2.2 Time domain measurements

Though the principle of a time domain experiment may seem quite simple, the experimental details involved are rather complicated. In this kind of experiment the dielectric relaxation function $\Phi(t)$ is directly recorded. The relation between $\Phi(t)$ and time dependent permittivity is given by:

$$\varepsilon(t) = \varepsilon_\infty + \Delta\varepsilon\Phi(t)$$

(II.17)

When a constant voltage V is applied to a capacitor filled with a molecular dielectric, the charge on the electrodes varies in time due to orientational polarization of the molecular dipoles:

$$Q(t) = VC(t) = VC_g\varepsilon(t)$$

(II.18)

Relations (II.17) and (II.18) relate the relaxation function with the time dependence of the charge on the capacitor electrodes. The measurement of the charge is one of the experimental difficulties to be overcome, since the standard multimeters usually measure the electric current instead. For such reasons, a modified Sawyer-Tower bridge is employed [97]. Details on the experimental setup, its resolution limits and the accessible time/frequency range are presented elsewhere [11]. Here, only a brief description of the physical principle will be given.

In order to directly access the time depending charge on the sample capacitor C_s, a reference capacitor C_{ref} in a serial connection has to be used (see Fig. II.5). A constant voltage V is applied to this serial connection. The value of the reference capacitor C_{ref} is chosen to be roughly *1000* times greater that the maximum value of the sample capacity during the experiment (the static permittivity ε_s of the material under investigation can be estimated from the frequency domain measurements). Since the charge on both capacitors has the same value, the potential on the reference capacitor V_{ref} is in the order of *1000* times smaller than V. This small potential drop assures that the potential on the sample capacitor $V-V_{ref}$ stays

essentially constant during the experiment. The change in time of the $V_{ref}(t)$ is recorded and since it is directly related to the charge on the electrodes of the sample capacitor $Q_s(t)=V_{ref}(t)C_{ref}$, the relaxation function $\Phi(t)$ is implicitly accessed, cf. (II.18).
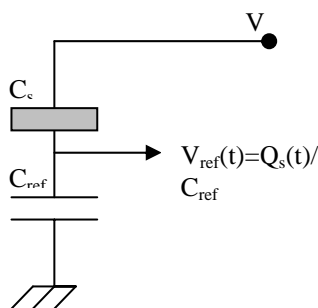
Fig. II.5 The basic electrical circuit of the modified Sawyer-Tower Bridge

II.2.3 Low temperature measurements

In order to access the tunneling regime for molecular glasses, glycerol was investigated down to *0.03 K* by using the Oxford CF1200 dynamic cryostat. For this purpose, a dielectric capacitor consisting of two plates made from annealed copper, separated by few silica fibers each with a *50 μm* diameter, was build and inserted in the ultra-low temperature cryostat [14]. The investigations were carried out in collaboration with Experimentalphysik V, the low-temperature experimental group of Prof. G. Eska at University of Bayreuth. In the temperature range *4.2 K – 1.2 K*, cooling was done by the standard technique of pumping *^{4}He*, and for lower temperatures a *^{3}He - ^{4}He* dilution refrigerator (1000 E from Oxford Instruments) was used. Due to its higher stability, an Andeen Hagerling 2500 precision bridge operating at single frequency (*1 kHz)* was applied, rather than the multifrequency bridge AH2700 A in the temperature range below *4 K*.

II.3 Phenomenological Description of the Dielectric Response

In this Paragraph we will discuss a number of functions used for the interpolation of the complex dielectric permittivity, response function and the distribution function of correlation times, as suggested in the literature [2,11].

II.3.1 The Debye function

The simplest relaxation process is described by an exponential decay of the step response function,

$$\Phi(t) = \exp(-t/\tau) \tag{II.19}$$

where τ is called *the relaxation time*. Accordingly, Eq. (II.10) transforms for this case into the *Debye equation*:

$$\frac{\varepsilon^*(\omega) - \varepsilon_\infty}{\Delta\varepsilon} = \frac{1}{1 + i\omega\tau} \tag{II.20}$$

The real and imaginary parts of the complex permittivity $\varepsilon^*(\omega)$ can be separated as:

$$\varepsilon' = \varepsilon_\infty + \Delta\varepsilon\frac{1}{1 + (\omega\tau)^2}$$

$$\varepsilon'' = \Delta\varepsilon\frac{\omega\tau}{1 + (\omega\tau)^2} \tag{II.21}$$

These quantities are represented in Fig. II.6 as functions of frequency:
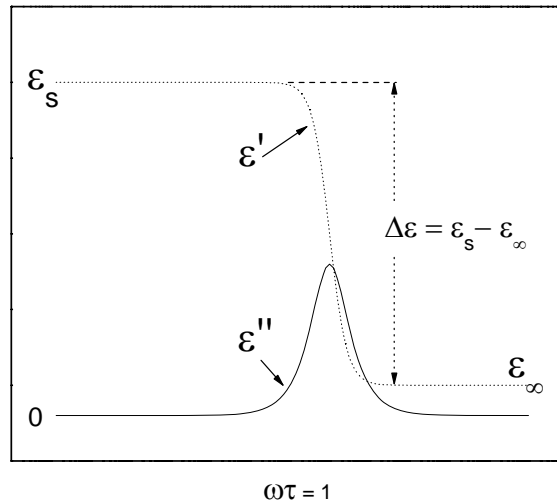
Fig. II.6 The real (dotted line) and imaginary part (line) of the complex permittivity in the Debye model.

As seen, the real part is a monotonous function of frequency and decays from the value ε_s at low frequencies to the value ε_∞ far above the relaxation frequency defined by $\omega\tau = 1$. On the other hand, the imaginary part is a Lorentzian function with the maximum at $\omega\tau = 1$. The dielectric response of molecular systems is commonly presented by the frequency dependence of the imaginary part $\varepsilon''(\omega)$ (*spectrum*) due to its peak structure and large variation range in contrast to $\varepsilon'(\omega)$. As an alternative, the tangent of the loss angle can be also used:

$$\tan\delta(\omega) = \frac{\varepsilon''(\omega)}{\varepsilon'(\omega)} \qquad (\textit{dielectric loss}) \tag{II.22}$$

18

Derived within certain models for molecular reorientation, *e.g.,* isotropic rotational diffusion [3], the Debye relaxation is not suited to describe the dielectric response of glass-forming liquids. For this purpose, some empirical expressions were introduced and some of them are presented in the following. They allow for an additional stretching parameter to interpolate the relaxation peaks as*, e.g.*, the α-peak observed in the spectra of glass-forming systems, discussed in the next Chapter.

II.3.2 The Cole-Davidson (CD) function

In 1950, Davidson and Cole [15] proposed a generalization of Eq. (II.19):

$$\frac{\varepsilon^*(\omega) - \varepsilon_\infty}{\Delta\varepsilon} = \frac{1}{(1 + i\omega\tau_0)^\beta} \tag{II.23}$$

The expression reduces to Eq. (II.20) for $\beta = 1$. The real and imaginary parts of the complex permittivity can be separated as:

$$\begin{aligned}
\varepsilon'(\omega) &= \varepsilon_\infty + \Delta\varepsilon(\cos\varphi)^\beta \cos(\beta\varphi) \\
\varepsilon''(\omega) &= \Delta\varepsilon(\cos\varphi)^\beta \sin(\beta\varphi)
\end{aligned} \tag{II.24}$$

where $\varphi = arctg(\omega\tau_0)$.

The CD function produces an asymmetrically broadened peak for the imaginary part $\varepsilon''(\omega)$ with a power-law proportional with ω on the low frequency side and another proportional with $\omega^{-\beta}$ on the high frequency side.

This function plays an important role in the analysis presented in this Thesis. Other empirical expressions used for the interpolation of spectra in the frequency domain as, *e.g.*, the Cole-Cole and Havriliak-Negami equation are described in [2].

II.3.3 The Kohlrausch function

In time domain the Kohlrausch relation (sometimes mentioned as the Kohlrausch-Williams-Watts or, simply *KWW equation*) assumes a stretched exponential decay for the relaxation function [2,3]:

$$\Phi(t) = \exp[-(t/\tau)^{\beta_{KWW}}] \, , \; 0 < \beta_{KWW} \leq 1 \tag{II.25}$$

The average relaxation time is given by:

$$\langle\tau\rangle = \frac{\tau_{KWW}}{\beta_{KWW}} \Gamma\left(\frac{1}{\beta_{KWW}}\right) \tag{II.26}$$

with Γ denoting the gamma function. The KWW function has no analytic Fourier transform.

II.3.4 Distributions of relaxation times

An alternative for interpolating the dielectric spectra is the direct use of an appropriate *distribution of relaxation times*. This idea goes together with assuming a distribution of subensembles, each relaxing in a Debye-like manner, allowing for the presence of dynamic *heterogeneities*. The distribution of relaxation times G(lnτ) describes both relaxation function and permittivity and can be extracted from both time and frequency domain data:

$$\Phi(t) = \int_{-\infty}^{\infty} \exp(-t/\tau)G(\ln\tau)d\ln\tau$$

$$\frac{\varepsilon^*(\omega) - \varepsilon_\infty}{\Delta\varepsilon} = \int_{-\infty}^{\infty} \frac{1}{1 + i\omega\tau}G(\ln\tau)d\ln\tau \tag{II.27}$$

The *mean relaxation time* is given by the integral over the relaxation function:

$$\langle\tau\rangle = \int_{0}^{\infty} \Phi(t)dt \equiv \tau \tag{II.28}$$

In the case of a Debye relaxation *G(lnτ)* reduces to a delta-function. For CD equation the corresponding distribution of relaxation times is given by (cf. Eq. II.27):

$$G_{CD}(\ln\tau) = \begin{cases} 0, for\, \tau > \tau_0 \\ \frac{1}{\pi}\left(\frac{\tau}{\tau_0 - \tau}\right)^\beta \sin(\pi\beta), for\, \tau < \tau_0 \end{cases} \tag{II.29}$$

The average relaxation time is for this case:

$$\tau = \tau_0\beta_{CD} \tag{II.30}$$

The distribution G_{CD} is plotted in Fig. II.7.

The Generalized Gamma distribution function

In some cases three parameters ($\Delta\varepsilon, \tau, \beta$) seem insufficient to describe the evolution of the spectra in a large frequency and temperature range. In order to overcome this, further functions were introduced by our group. Here the approach introduced by Kudlik *et al.* and Blochowicz *et al.* will be shortly described [11,13]. This analysis

uses the so-called *generalized gamma (GG) distribution of relaxation times* (see Fig. II.7):

$$G_{GG}(\ln\tau) = N_{GG}(\alpha,\beta)\left(\frac{\tau}{\tau_0}\right)^{\beta}\exp\left(-\frac{\beta}{\alpha}\left(\frac{\tau}{\tau_0}\right)^{\alpha}\right) \tag{II.31}$$

that yields a relaxation function $\Phi(t)$ and a complex permittivity $\varepsilon''(\omega)$ via Eq. (II.27). The normalization factor $N_{GG}(\alpha,\beta)$ assures that the integral of the distribution over all relaxation times equals *1*. The maximum of the distribution is at $\tau = \tau_0$. The broadening of the peak is controlled by the parameters α and β, that can assume values between *0* and ∞. For *0 < β < 1* there appears a power law ω^{β} in $\varepsilon''(\omega)$ on the high frequency flank of the α-peak. If β > *1* the high frequency exponent stays always *−1* and the peak resembles more and more a Debye shape as β increases towards ∞. The α parameter controls the shape of the GG distribution at long relaxation times, respectively low frequencies. The broader is the peak the smaller is the value of α. For a stable interpolation routine, the values of α cannot exceed the interval of 0.3 – 50. The mean relaxation time is given by:

$$\tau = \tau_0 \left(\frac{\alpha}{\beta}\right)^{\frac{1}{\alpha}} \frac{\Gamma\left(\frac{\beta+1}{\alpha}\right)}{\Gamma\left(\frac{\beta}{\alpha}\right)} \tag{II.32}$$

The Extended Generalized Gamma distribution function

For some molecular systems an additional power-law appears in the spectra on the high frequency side of the main relaxation peak (cf. Fig. III.3 a, discussed in the next Chapter). Therefore Blochowicz *et al.* extended the GG function to account for this so-called excess wing (EW) [11]:

$$G_{GGE}(\ln\tau) = N_{GGE}(\alpha,\beta,\gamma,\sigma)\left(\frac{\tau}{\tau_0}\right)^{\beta}\exp\left(-\frac{\beta}{\alpha}\left(\frac{\tau}{\tau_0}\right)^{\alpha}\right)\left(1+\left(\frac{\tau\sigma}{\tau_0}\right)^{\gamma-\beta}\right) \tag{II.33}$$

where N_{GGE} is the normalization factor. Two additional parameters are introduced to describe the evolution of the EW: γ is the exponent of the high frequency power law $\omega^{-\gamma}$ that appears in the spectrum at highest frequencies and σ marks the crossover between the $\omega^{-\beta}$ and $\omega^{-\gamma}$ regimes (the "onset" of the excess wing).

For the average relaxation time we now have:

$$\langle \tau \rangle = \tau_0 \left(\frac{\alpha}{\beta} \right)^{\frac{1}{\alpha}} \frac{\Gamma\left(\frac{\beta+1}{\alpha} \right) + \sigma^{\gamma-\beta}\left(\frac{\alpha}{\beta} \right)^{\gamma-\beta} \Gamma\left(\frac{\gamma+1}{\alpha} \right)}{\Gamma\left(\frac{\beta}{\alpha} \right) + \sigma^{\gamma-\beta}\left(\frac{\alpha}{\beta} \right)^{\gamma-\beta} \Gamma\left(\frac{\gamma}{\alpha} \right)} \tag{II.34}$$

The single peak distribution described by Eq. (II.31) is obtained for $\beta \cong \gamma$ or $\sigma \cong 0$.

A distribution for thermally activated processes

As shown in the next Chapter, the dielectric spectra of most of the molecular glass-forming systems exhibit in the glassy state an additional symmetric (with some exceptions) peak that is much broader than a Debye. To account for this relaxation peak, usually a thermally activated process is assumed (also discussed in the next Chapter), and Blochowicz *et al.* [11] introduced a suitable distribution of relaxation times $G_\beta(ln\tau)$:

$$G_\beta(\ln \tau) = N_\beta(a,b) \frac{1}{b\left(\frac{\tau}{\tau_0} \right)^a + \left(\frac{\tau}{\tau_0} \right)^{-ab}} \tag{II.35}$$

where $N_\beta(a, b)$ is the normalization factor.

The position of the maximum of the distribution is at τ_0 and the parameters *a* and *b* control the broadening and asymmetry of the β-peak: for a<1 and ab<1 the peak is defined between the two power laws ω^a and ω^{-ab}. The peak is symmetric for b = 1 and its broadening while cooling is controlled solely by parameter *a*. This distribution is also shown in Fig. II.7 below.
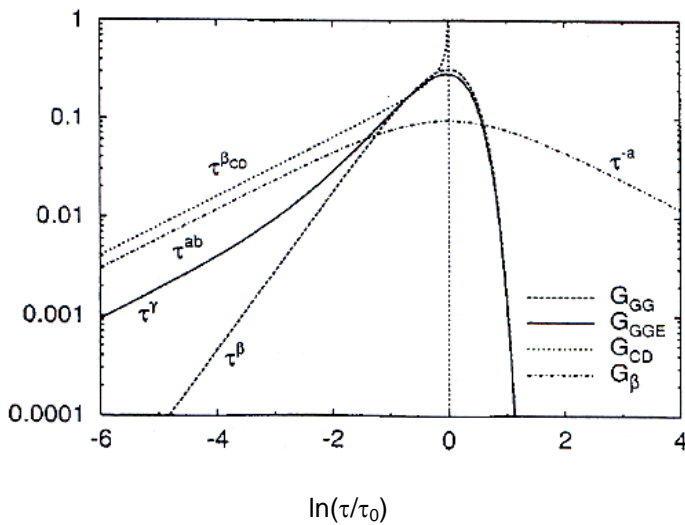
Fig. II.7 Distributions of relaxation times discussed above. Picture from [11].

III. The evolution of the dynamic susceptibility of simple glass formers from the liquid state to the tunneling regime; overview

In the following it will be presented an overview concerning the temperature evolution of the various relaxation phenomena for molecular systems upon cooling from the boiling point down to cryogenic temperatures.

III.1 The high-temperature regime ($T \gg T_g$)

The investigation of the low viscosity glass forming liquids became an important experimental task due to the impact of the Mode Coupling Theory (*MCT*). This model is, at the moment, the most discussed theoretical approach aiming to describe the glass transition phenomenon [10,33]. This theory triggered an important experimental effort and new techniques were developed in order to confirm or disprove its predictions.

A close inspection of the glycerol spectra at highest temperatures in Fig. I.3 (a) indicates that their shape is not changing with temperature. In order to verify this, the high temperature spectra of glycerol are scaled in Fig. III.1 (a) by their minimum according to:

$$\varepsilon''(\omega) / \Delta\varepsilon(T) = \chi''(\omega) = \frac{\chi''_{min}}{a+b}(b(\frac{\omega}{\omega_{min}})^a + a(\frac{\omega}{\omega_{min}})^b) \qquad (III.1)$$

where the exponents *a* and *b* define the power laws exponents at the high and, respectively, the low frequency side of the minimum observed in the GHz range; ω_{min} and χ''_{min} are the frequency and the amplitude of the minimum. This "minimum scaling", inspired by the *MCT*, works nicely for all the spectra above some temperature $T_x = 300\ K$ and fails below, as it will be proven in the next paragraph. The exponents *a* and *b* were obtained by interpolating the scaled minimum as a sum of two power-laws and they values are indicated in the figure below [35,37].

Providing that the *FTS* applies, a collapse of the spectra scaled by height and position of the α-peak (*i.e.* the "α-peak scaling"), should work. This is indeed the case, as indicated by Fig. III.1 (b) where the same spectra of glycerol

above T_x are scaled accordingly. Both the minimum and the α-peak scaling characterize the high temperature regime above T_x.
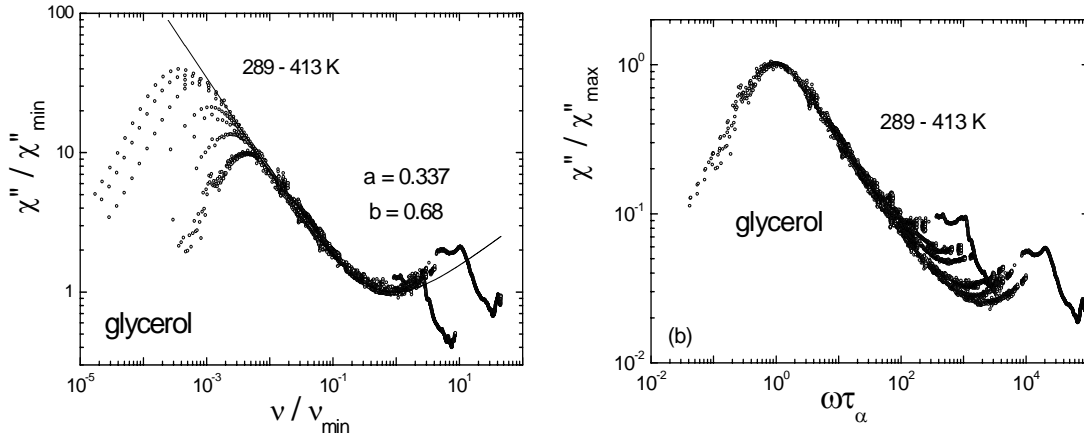
Fig. III.1 (a) The "minimum scaling" for dielectric spectra of glycerol at high temperatures. (b) The same data in (a) collapsed by the "α-peak scaling".

III.2 The intermediate temperature range ($T_g < T < T_x$)

As mentioned above, the dynamics of molecular glass formers in the intermediate temperature range close to T_g is characterized by the emergence of slow secondary relaxation processes, namely the excess wing (*EW*) and the β–process. In order to distinguish between different glass formers, a classification was proposed by *Kudlik et al.* [26]: systems showing a clearly distinguishable secondary relaxation β-peak belong to the "Type B" class (*e.g. m-FAN*) while those not showing a secondary peak, but only the *EW* are referred to as "Type A" (*e.g.* glycerol). Though purely phenomenological, this classification implies that the *EW* has a different physical nature than the β-process. Some experimental investigations support this idea [11,30], while others, for example the aging experiments, indicates that the *EW* might be just the high-frequency flank of a "special" β-peak submerged under the α-peak [31]. The situation is far from being clear since for some systems both features may appear simultaneously, *e.g.*, for *m-FAN* (see Fig. I.3 b). The physical origins of the EW and of the β-process are still a matter of debate.

For the sake of simplicity we will discuss the temperature evolution of these relaxation features separately. As will be shown, the central properties of the relaxation in the high temperature regime, namely α–peak scaling and

minimum scaling fail upon cooling, implying that below the crossover temperature T_x the evolution of the dynamic susceptibility changes [35, 36].

III.2.1 Glass formers with excess wing

In order to demonstrate that the evolution of the susceptibility spectra qualitatively changes from the high temperature scenario to a behavior determined by the emergence of the EW at temperatures close to T_g, we present in Fig. III.2 (a) the minimum scaling of the full glycerol dataset including now temperatures down to T_g. Clearly, below *290 K* the minimum scaling fails, as the susceptibility minimum continuously flattens upon cooling. This observation may be taken as an indication for the emergence of the excess wing recognized in the spectra of glycerol (cf. Fig. I.3 a). As indicated in Fig. III.2 (b) for propylene carbonate (*PC*) [25], also the α-peak scaling fails below a certain temperature (around 200 K), and the scaling breaking down coincides with the appearance of the *EW*.
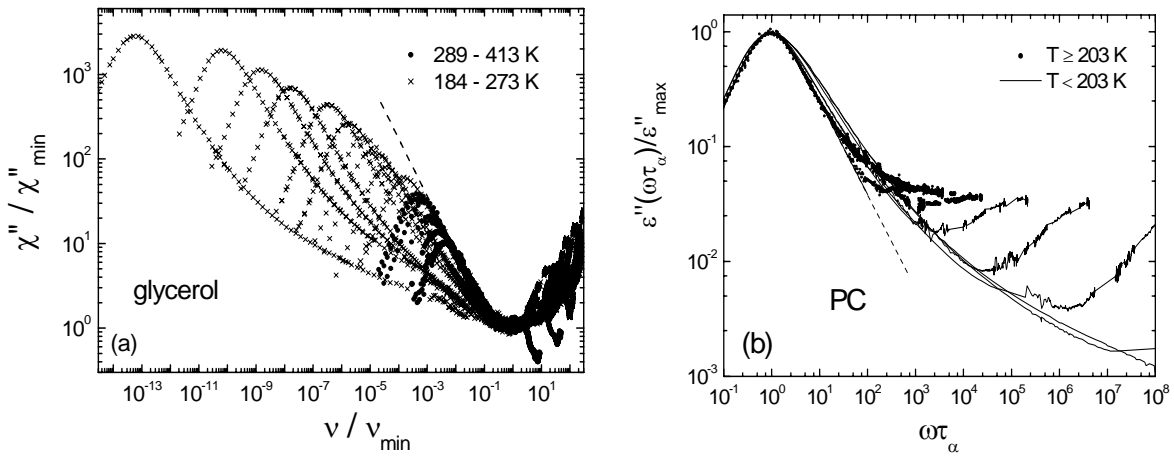
Fig. III.2 (a) Scaling of the susceptibility minimum for the dielectric spectra of glycerol; dashed line: interpolation of the minimum at high temperatures applying Eq. (III.4), cf. [37]. (b) Dielectric spectra of propylene carbonate (PC, $T_g = 158$ K) measured by Lunkenheimer *et al.* [25], scaled by the α-peak height and position. Dashed line: a *CD* function with $\beta_{CD} = 0.78$.

Davidson and Cole first identified the EW in the dielectric spectra of glycerol in 1951 [15]. Disregarded until the beginning of 90's, it focused the attention of scientific community since the so-called Nagel scaling was introduced [38]. Nagel and coworkers found a way to collapse the dielectric spectra measured for various systems, at different temperatures and containing both α-peak and

EW, on a universal master curve. As a consequence of this scaling, the exponent of the EW (γ) and that of the high frequency flank of the α-peak (β) are connected, *i.e.* $\frac{\beta(T)+1}{\gamma(T)+1}=1.3$. The authors claimed that the high frequency wing is an intrinsic feature of the α-process, universal for all glass formers and, therefore, even in the case of a well-resolved β-peak any analysis should employ an EW contribution [92]. Though Kudlik *et al.* proved that the Nagel scaling is mathematically not well defined [39], the latter attracted many theoreticians and physical models were proposed to explain the EW [40].

On the other hand, based on the aging experiments of Schneider e*t al.* [31], Lunkenheimer and Ngai suggested that the EW is just the high frequency flank of a slow β-process [41]. This may justify why the dielectric spectra of type A glasses appears as curving on the EW side while aging towards the equilibrium at temperatures slightly below T_g. Consequently, the authors analyzed the spectra of type A glass formers above T_g using a two-peak approach. Though the number of the fitting parameters was quite high, the interpolation of the data was not perfect (as seen in Fig. III.3 (a) for temperatures close to T_g).

Blochowicz *et al.* [11,42] obtained better fits for the α-peak including the EW contribution by using the extended generalized gamma (GGE) distribution of relaxation times described in Paragraph II.3.5. In fact, this approach is similar with the one above in the sense that it involves also a two-peak description of the overall spectral shape [11]. However, here the time constants of the two processes are chosen as identical $\tau_\alpha = \tau_{EW}$ as observed in Fig. III.3 (b). By this, one reduces the number of fitting parameters, and the temperature evolution of the spectra can be parameterized by the change of the stretching parameters β and γ and the onset σ of the EW (see II.3.5).

This analysis was applied to several type A glass formers, indicating that the EW parameters show similar behavior when plotted as functions of the time constant τ_α, *i.e.* independent of fragility [42,43]. According to this approach the EW contribution vanishes at a crossover temperature T_x (associated with a characteristic time constant $\tau_\alpha \cong 10^{-8}$ *s*) [30,42,43]. At higher temperatures $T > T_x$ the overall (slow dynamics) spectrum reduces to a single peak with a

constant stretching exponent. This crossover temperature ($T_x \cong 1.2 \cdot T_g$ for fragile systems) turned out to be similar with the Stickel temperature T_S [43] and with the temperature at which the decoupling of translational and rotational diffusion coefficients is discussed [93].
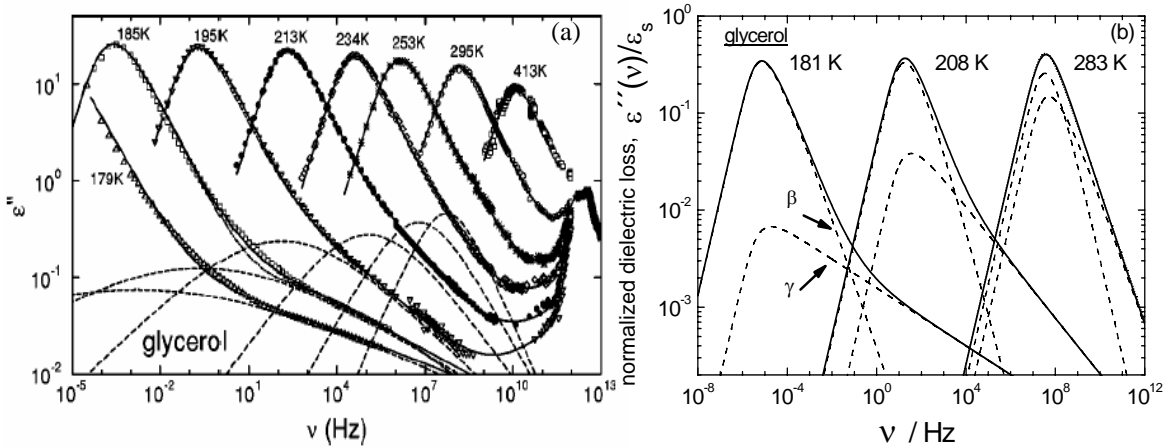
Fig. III.3 Dielectric spectra of glycerol with interpolations of the α-peak and excess wing by a two-peak function according to (a) Ngai and (b) Blochowitz. Figures taken from [41] and, respectively, [84].

Though different in detail all the approaches aiming to describe the evolution of the dynamic susceptibility agree that the width parameter of both α–peak and excess wing exhibit a pronounced temperature dependence below the crossover temperature T_x. In other words, the models suggest that below T_x the FTS fails for the spectra of the slow dynamics.

III.2.2 Glass formers with β-process

The β-process is identified in a large variety of glass forming compounds, and it shares a number of common features. Most of them are recognized in Fig. I.3 (b) where the dielectric spectra of m-fluoroaniline (m-FAN) are presented. First of all, the β-peak emerges in the supercooled state upon cooling close to T_g, and persists in the glass at $T < T_g$. Here, it is a thermally activated process and the temperature dependence of the characteristic time constant follows an Arrhenius law, as shown in Fig. III.4 (a) for three type B systems. An important empirical observation is that the mean activation energy is directly related to T_g. With some exceptions $E_a \cong 24 \, k_B T_g$ was found to hold for simple

molecular glasses, but also for polymers [26,45,49,51]. This indicates that the β-process is intimately related to the glass transition phenomenon. Moreover, its relaxation strength is virtually temperature independent below T_g, and it strongly increases with temperature above, cf. Fig III.4 (b). It is worth noting that the dielectric strength of β- relative to α-process $\Delta\varepsilon_\beta/\Delta\varepsilon_\alpha$ largely differs from material to material.
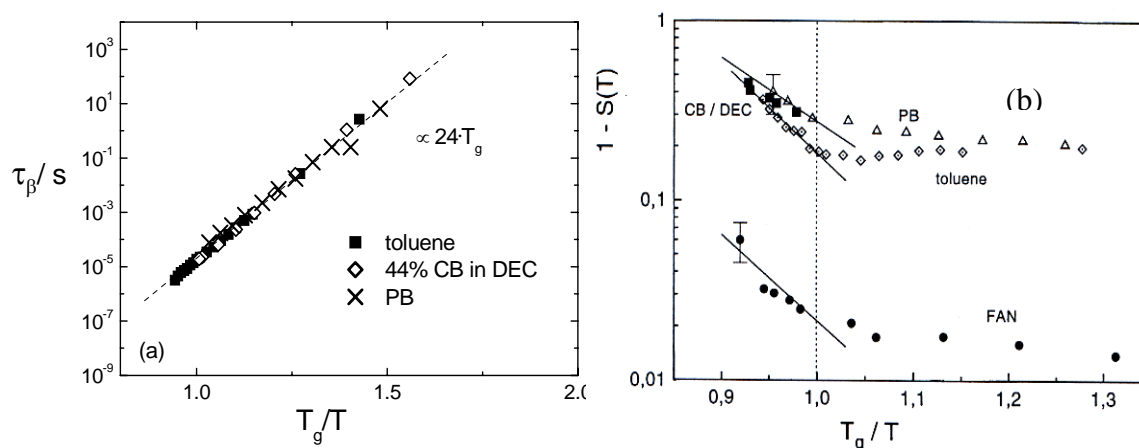
Fig. III.4 (a) Time constants of the β–process obtained from dielectric spectroscopy as a function of the reduced reciprocal temperature T_g/T for a series of glasses. (b) the relative relaxation strength of the β-process plotted against T_g/T for few type B systems. Pictures taken from [26].

The β-peak is much broader than the α-peak and usually it appears as being symmetric. The most used expression to interpolate it is the *Cole-Cole function* [2,3]. However, as most of other empirical functions it is not suitable to describe the temperature evolution of a thermally activated process [2,11]. Nevertheless, this condition is fulfilled by a log-Gauss distribution or by the distribution described in II.3.4 [11].

There exist two scenarios concerning the molecular origin of the β-process. The first one, introduced by Johari, states that only a small number of molecules confined in some low-density sites called "islands of mobility" participate in this process [52]. The second scenario is based on the Williams and Watts considerations, *i.e.*, essentially all molecules participate in this process [53]. This is experimentally supported by NMR [54,55,56] and solvation [94] experiments.

Within the Williams-Watts approach, the same molecular dipole vector participates in both relaxation processes, yielding a correlation function that

partially decays at short times via the β-process and at long time decays to zero due to the α-process. Assuming the two processes to be statistically independent, the complete relaxation function is given by:

$$\Phi(t) = \Phi_\alpha(t)\left[(1 - \lambda(T)) + \lambda(T)\Phi_\beta(t)\right] \tag{III.2}$$

where λ is the temperature dependent fraction of correlation lost via the β-process. This approach will be used in this Thesis for the analysis of dielectric spectra containing both α and β-peaks.

According to the NMR studies, the β-process in the glass is a highly hindered motion, that can be modeled by reorientation of the molecule within a cone with a small fixed opening around $\theta_\beta \approx 4^0$ below T_g in the case of toluene [56]. Based on such considerations, Döß et al. [78] and Benkhof et al. [27] proposed that the relative dielectric strength $\Delta\varepsilon_\beta/\Delta\varepsilon_\alpha$ is determined by the amplitude of the reorientational angle θ_β. Thus the decrease in $\Delta\varepsilon_\beta/\Delta\varepsilon_\alpha(T)$ upon cooling can be explained by the decrease of the average reorientational angle θ_β with T. Accordingly, if θ_β is very small, the dielectric intensity of the β-process should be very weak.

III.3. The glassy state $(T < T_g)$

III.3.1 The secondary relaxation processes

As discussed above, the spectra of molecular glass formers in the deep supercooled state are characterized by the presence of the secondary relaxation processes (EW and β-process) in addition to the α-process. Both the EW and the β-process survive in the glass (cf. Fig. I.3), and they give the main contribution to the spectra in the moderate temperature range below T_g down to, say, 50 K [26].

As the β-process manifests itself in a widespread variety (amplitude and temperature dependence) among different glass formers, it renders a system dependent glassy behavior. Due to this complex relaxation pattern governed by the secondary relaxation peaks there are no conclusive studies of type B systems in the temperature range below T_g down to the cryogenic temperatures. Figure III.5 gives an example of such relaxation response.

Clearly, the situation here is quite puzzling as internal degrees of freedom may be involved for some systems showing secondary relaxation peaks.
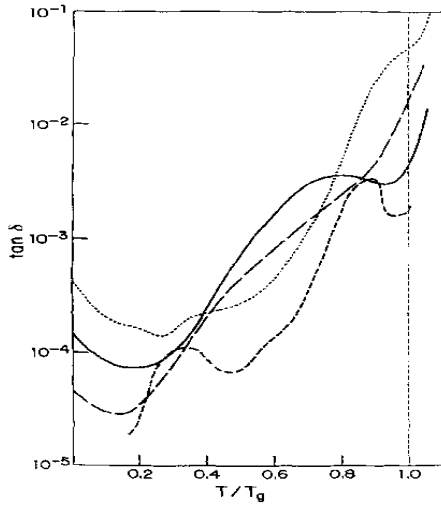
Fig. III.5 Dielectric loss for a series of alcohols measured at 10 kHz below T_g. Picture from [73]

On the other hand, as discussed next, type A systems appear to exhibit a more uniform evolution in the glassy state. There exist some dielectric investigations of type A systems focusing below T_g down to say *20 - 50 K.* As an example we present in Fig. III.6 (a) the dielectric response of glycerol measured down to *57 K* [11,42].

The figure contains spectra measured both in supercooled ($T > T_g$) and glassy state ($T < T_g$). For temperatures above T_g, in addition to the α-peak the EW can be identified as an additional power-law $\varepsilon''(\nu) \propto \nu^{-\gamma}$. Extracting the exponent γ, the latter appears to decrease with the temperature in the supercooled state and to freeze below T_g to a small value around *0.1*, cf. Fig. III.6 (b). This flat dielectric response below T_g is usually referred to as the Nearly Constant Loss (*NCL*).

For several molecular glass formers the *NCL* extends over several decades in frequency and it was observed for temperatures down to *50 K* [11,13,26,42]. The temperature dependence of the loss in this temperature range was found to be exponential $\varepsilon''(T) \propto exp(T/T_f)$ with a quite similar exponent $T_f \cong 34$ for the type A systems compiled in our group [26]. Hansen and Richert obtained similar results using a high precision bridge operating at single frequency of 1 kHz [75]. In addition, their study revealed that some glasses display an increase of the dielectric loss in the range *25 K < T < 50 K* indicating a crossover from *NCL* to another relaxation mechanism.
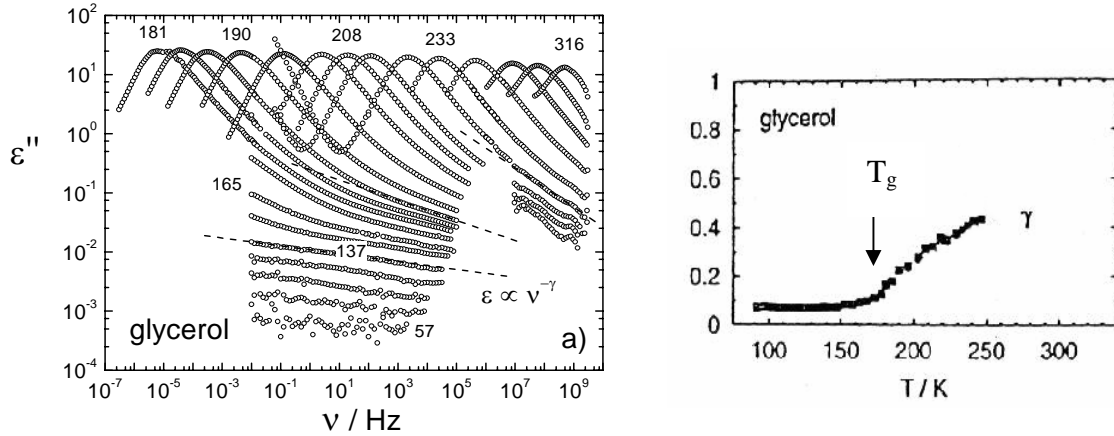
Fig. III.6 (a) Dielectric spectra of glycerol (picture from [11]); at frequencies higher than the α-peak the high-frequency wing can be recognized. (b) the power-law exponent γ as a function of temperature; T_g is indicated (figure from [26]).

The extension of the above mentioned studies towards lower T was limited (until recently) by the resolution of the dielectric spectrometers. Up to our knowledge, it is not yet clear how and whether at all the crossover to the Asymmetric Double Well Potential (*ADWP*) dynamics (intensively discussed for the inorganic glasses at lowest temperatures) takes places in molecular systems.

III.3.2. The Asymmetric Double Well Potential dynamics

The low temperature anomalies of glasses

In the search for universal relaxation properties, the amorphous systems are well investigated in the supercooled regime $T > T_g$ (the molecular systems) as well as in the very low temperature regime, say below *10 K* [58-62]. This low temperature regime is well studied for inorganic glasses, but information on molecular glasses is poor. The reasons may be their high tendency to crystallize and their low viscosity at room temperature, experimental drawbacks for their investigation in ultra low-temperature equipments. All the cryogenic measurements on molecular systems consider, to our knowledge, only some alcohols and polymers [73,74].

At sufficiently low temperatures the behavior of crystalline materials is well explained by the Debye theory of harmonic oscillations [63]. Accordingly, the collective lattice vibrations are propagating through the crystal viewed as an

elastic continuum, insensitive to the spatial arrangement of the lattice. This model explains the temperature dependence of the specific heat exhibiting the famous T^3 law at low temperatures.

Until the end of the 60's it was believed that the theory of Debye could be easily extended also to non-metallic amorphous solids since the wavelength of the contributing phonons at low temperatures is much larger as compared with the scale of atomic or molecular disorder. However, in 1971, Zeller and Pohl proved unambiguously that the low temperature properties of amorphous materials are very different from those of crystals [64]. In particular, they showed that thermal properties such as the specific heat or the thermal conductivity of the vitreous solids below *1 K* indicate the presence of low energy excitation in addition to those from phonons.
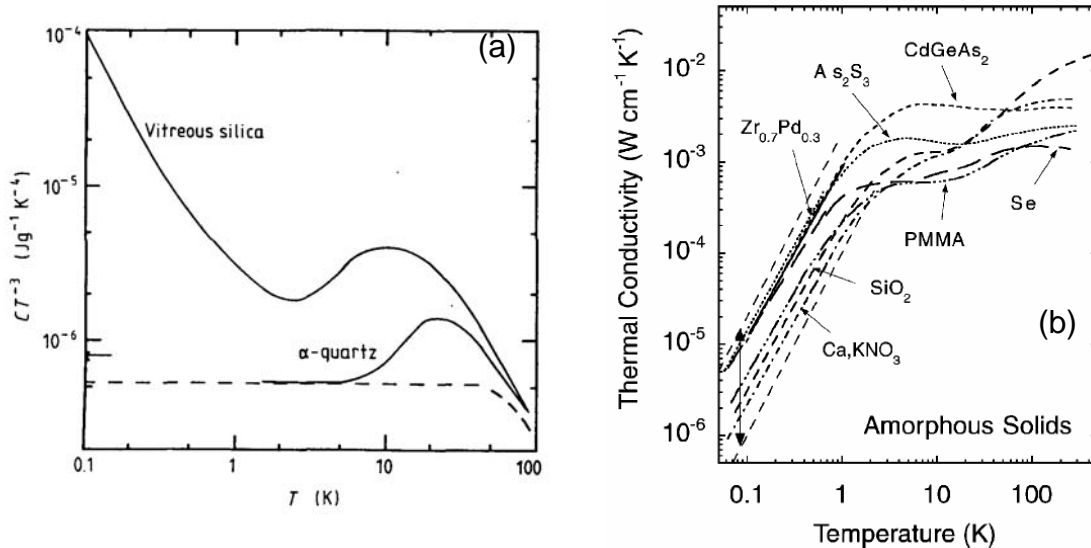
Fig. III.7 (a) Specific heat of crystalline *SiO₂* and vitreous silica below 1 K (from [58]). (b) Thermal conductivity of several amorphous solids as a function of temperature; the arrow indicates the variation interval (about 20). For crystal a linear dependence is expected here according to Debye's theory. Picture from [62].

For example, in Fig. III.7 (a) the temperature dependences of the specific heat (*C*) of *SiO₂* for the amorphous and crystalline states, respectively, are compared. Below *1 K* the crystal shows the Debye behavior ($C \propto T^3$), however, for glassy *SiO₂* the specific heat is a few orders of magnitude higher and depends roughly linearly on temperature. As another example, in Fig. III.7 (b) the thermal conductivity *Λ* of several amorphous materials is displayed for temperatures below room temperature. For all glasses the thermal

conductivity below 1 K depends quadratically on temperature, and between 2 and 20 K Λ is almost temperature independent. Above *20 K* the thermal conductivity increases again with temperature. Such a behavior was proved to be specific for a large variety of amorphous materials pointing to the fact that the presence of the additional excitations is an intrinsic characteristic of glasses.

Another important finding is that the thermal parameters of glasses below *1 K* not only qualitatively strongly differ from those of crystals, but their values are very similar for a large number of systems, independent of the material. This is also shown in Fig. III.7 (b) were the values of the thermal conductivity Λ obtained for network glasses, ionic glasses and organic polymers vary within a factor of only *20* below a few *K*.
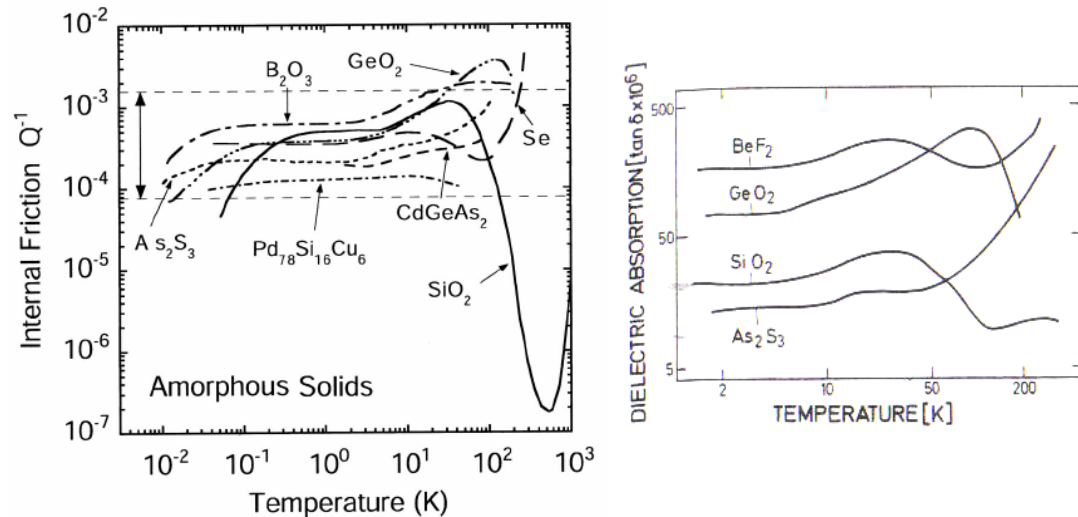
Fig. III.8 (a) Temperature dependence of the internal friction coefficient Q^{-1} for several glasses; the arrow indicates the same variation interval as in Fig. III.10 (b). Picture from [62]. (b) Dielectric loss below room temperature for several glasses; measurements performed at the frequency of 1 kHz. Picture from [65].

Besides the thermal properties, also the relaxation behavior of glasses in the low temperature range shows a peculiar behavior. Figure III.8 (a) presents the internal friction coefficient Q^{-1} (the acoustic attenuation) obtained from mechanical relaxation measurements as a function of temperature for a large variety of glasses. The acoustic attenuation displays a temperature independent "plateau" in the temperature range between *100 mK* and *10 K*, with a similar absorption level. Thermal conductivity as well as acoustic attenuation data, allows the extraction of the ratio between the dominating

phonons wave length and their mean free path, showing similar values for all the glasses studied so far [62]. Dielectric measurements at *kHz* frequencies [65] show a similar relaxation pattern, cf. Fig. III.8 (b).

All these findings indicate that in the low temperature range amorphous solids exhibit low temperature "anomalies" with quite universal properties. The low-temperature relaxational behaviour of glasses can be fairly well explained by the standard tunneling model (*STM*) as discussed in the next paragraph.

The Standard Tunneling Model (STM)

Soon after the results of Zeller and Pohl were published, Phillips and, independently, Anderson *et al.* introduced in 1972 the Tunneling Model (*TM*) [66,67]. This is the most widely accepted model to describe the low temperature properties of the non-crystalline solids. The *TM* assumes that the additional low energy excitations in glasses are related to the existence of some atoms or groups of atoms that can tunnel between two configurations with similar energy. The tunneling particles are located within asymmetric double well potentials (*ADWP*), schematically presented in Fig. III.9. At lowest temperatures, due to the tunneling two-level systems (*TLS*) are formed. *TM* is a phenomenological model and the microscopic nature of the *TLS* systems is not yet fully understood.

The main ingredients of the "standard" tunneling model (*STM*) are:

- a broad distribution of *ADWP* parameters (due to the structural disorder of glasses);

- when perturbed by an external field the *TLS* relax via the absorption or emission of a single thermal phonon (so-called "one phonon process" or "direct process");

- any interaction between the *TLS* are neglected.

The *TLS* may interact with external fields (*e.g.* electric field) via relaxation or resonance processes depending on the temperature and probing frequency. The resonance takes place when the energy is absorbed or emitted within the *TLS*. As the resonances appears for frequencies in the *kHz* range at extremely low temperatures below *1 mK*, while the measurements for this

Thesis were performed in the temperature range above *10 mK*, the discussion here will concern only the relaxation phenomenon.
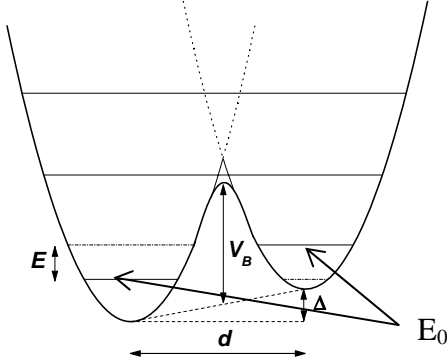
Fig.III.9 Schematic representation of an asymmetric double well potential (ADWP) characterized by the barrier *V*, the asymmetry Δ, the distance between minima *d* and by the ground state of the single wells E_0; note that the difference between the lowest energy levels *E* is due to the tunneling (schematic shown here by the dashed horizontal lines) but also to the asymmetry Δ.

At the lowest temperatures only the ground vibrational states of the *ADWP* can be occupied. The energy difference *E* between the lowest energy levels within the *ADWP* results from both the asymmetry Δ and the tunneling splitting Δ_0. Following the quantum mechanics description, $E = \sqrt{\Delta^2 + \Delta_0^{\,2}}$ [60].

For a given *ADWP*, the applied electric field modulates the asymmetry Δ and consequently the energy difference *E*. The equilibrium is established by the absorption or emission of one thermal phonon. The relaxation rate τ^{-1} for such "one-phonon process" is given by [68]:

$$\tau^{-1} = A\Delta_0 E \coth(E/2k_B T) \tag{III.3}$$

where A is a constant characteristic of the glass:

$$A = \left(\frac{\gamma_l^2}{v_l^5} + 2\frac{\gamma_t^2}{v_t^5} \right) \frac{1}{2\pi\rho\hbar^4} \tag{III.4}$$

The indices *l, t* refer to the longitudinal and transversal phonons, ρ is the mass density and $\gamma_{l,t}$ are the coupling constants between the phonons and the TLS. The tunnel splitting Δ_0 is related to the ADWP parameters by:

$$\Delta_0 \approx E_0 \exp(d\sqrt{2mV}/\hbar) \tag{III.5}$$

m is the mass of the tunneling "particle" and E_0 is the ground-state energy of the single well potential.

An important quantity in the following discussion is the minimal relaxation time τ_{min}, characteristic for symmetric *TLS ($\Delta = 0$)* with energy splitting matching thermal energy ($E = \Delta_0 = k_B T$). The minimum condition of Eq. (III.3) gives:

$$\tau^{-1}{}_{min} = A k_b{}^3 T^3 \tag{III.6}$$

Two limiting situations should be considered for the analysis of the dielectric (or acoustic) loss caused by the relaxation process:

(a) for $\omega\tau_{min} \gg 1$ (high frequencies, low temperature) even the fastest TLS with the relaxation time τ_{min} are unable to relax towards equilibrium within a period of the external electric field and they give the main contribution to the loss. From Eq. (III.6) a cubic temperature dependence is expected for the loss:

$$\tan\delta = \frac{\varepsilon''}{\varepsilon'} \approx \frac{CT^3}{\omega} \qquad \text{high } \omega, \text{ low T} \tag{III.7}$$

where C is a constant reflecting the coupling strength between the external field and the TLS. For electric interaction one finds [60,68]:

$$C = \frac{\bar{P}\mu_{eff}^2}{3\varepsilon_0\varepsilon'} \tag{III.8}$$

with the assumption that the *TLS* dipole moments are randomly orientated. The expression may need corrections for including the effects of the local field. $\bar{P}$ is the density of tunneling systems (number of *TLS* / unit volume / unit energy) and μ_{eff} is the effective dipole moment of the *TLS*. ε_0 is the dielectric permittivity of the vacuum and ε' is the dielectric constant of the material under investigation.

(b) for $\omega\tau_{min} \ll 1$ (low frequencies, high temperature) the main contribution to the loss is given by the systems for which $\omega\tau \approx 1$. The calculations lead to a plateau of the loss [68]:

$$\tan\delta = \frac{\varepsilon''}{\varepsilon'} = \frac{\pi}{2}C \qquad \text{low } \omega, \text{ high T} \tag{III.9}$$

The real part of the permittivity $\varepsilon' = \Delta\varepsilon + \varepsilon_\infty$ also appears in the above equations via C (see Eq. III.8). The dielectric strength $\Delta\varepsilon$ associated with such relaxation processes is very small, thus yielding an almost temperature independent $\varepsilon' \cong \varepsilon_\infty$ originating mainly from the high frequency resonance processes. The tiny change of the overall $\varepsilon'(T)$ is insignificant for the temperature dependence of the loss, $tan\delta \propto \varepsilon''$. However, for the *relative* change $\delta\varepsilon'/\varepsilon' = (\varepsilon'-\varepsilon_{ref})/\varepsilon'$ due only to the contribution of the *TLS*, the transition from the regime *(b)* to *(a)* is

marked by the change of the slope in the semilogarithmic representation at a function of T/T_{ref} [60,68].

(a) $\omega \tau_{min} \gg 1$ $\qquad \dfrac{\delta \varepsilon'}{\varepsilon'} = -C \ln\left(\dfrac{T}{T_{ref}}\right)$ $\qquad$ *high ω, low T*

(b) $\omega \tau_{min} \ll 1$ $\qquad \dfrac{\delta \varepsilon'}{\varepsilon'} = \dfrac{C}{2} \ln\left(\dfrac{T}{T_{ref}}\right)$ $\qquad$ *low ω, high T* $\qquad$ (III.10)

Here T_{ref} is the reference temperature where ε'_{ref} is measured; usually it is chosen to be the lowest accessed temperature in the measurements.
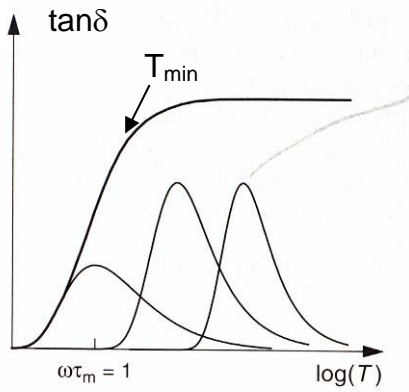
Fig III.10. The predictions of the STM for the dielectric loss as function of temperature. Picture adapted from [98].

Summarizing, the *STM* predicts a plateau of the dielectric loss for temperatures below some *K*. This plateau height is expected to be frequency independent. At lower temperatures the loss is expected to decrease, cf. Fig. III.10, and the crossover temperature for which this decrease starts is given by (according with Eq. III.6):

$$T_m = \sqrt{\frac{\omega}{Ak^3}}$$ (III.11)

In this regime ending the relaxation, a cubic temperature dependence is expected for *tanδ*.

The thermally activated ADWP dynamics

Above *10 K* the relaxation behavior of the investigated (inorganic) glasses is less universal and less understood. Depending on the probing frequency, a more or less pronounced relaxation peak appears when internal friction or dielectric loss data are plotted as functions of temperature. For example, in Figs. III.8 the mechanic and the dielectric absorption above *10 K* increases to a maximum, and the position of the maximum depends on the material. In order to account for this behavior, Gilroy and Phillips extended the *STM* to higher temperatures where thermally activated transitions over the barrier of the ADWP's are expected [69,95].

The important parameters for a given *ADWP* in this temperature range (see Fig. III.11) are the barrier height *V* and the asymmetry Δ.

The jump rates ν over the barrier V_B between the minima are given by:

$$\nu_{12} = \tau_0^{-1} \exp\left(\frac{V - \Delta/2}{kT}\right)$$
$$\nu_{21} = \tau_0^{-1} \exp\left(\frac{V + \Delta/2}{kT}\right)$$

(III.12)

where $\tau_0 \sim 10^{-12} - 10^{-13}$ sec is a typical molecular attempt time. The overall rate $\nu = \nu_{12} + \nu_{21}$ yields a relaxation time

$$\tau = \frac{1}{\nu} = \tau_0 \frac{\exp\left(\frac{V}{kT}\right)}{\exp\left(\frac{-\Delta}{2kT}\right) + \exp\left(\frac{\Delta}{2kT}\right)} = \tau_0 \exp\left(\frac{V}{kT}\right) \sec h\left(\frac{\Delta}{2kT}\right)$$

(III.13)

The dynamic susceptibility is expressed by integrating over the ADWP's parameters [69,70]:

$$\chi''(\nu) = \frac{C}{T} \int_0^\infty \int_0^\infty \frac{2\pi\nu\tau(\Delta,T)}{1 + (2\pi\nu\tau(\Delta,T))^2} \operatorname{sech}^2\left(\frac{\Delta}{2T}\right) f(\Delta) g(V) d\Delta dV$$

(III.14)

where *C* is a constant determined by the specific experiment (dielectric or acoustic), *g(V)* is the distribution of barrier heights *V*, *f(Δ)* is the distribution of the asymmetry parameter Δ. For the dielectric case

$$C = \frac{\mu_{eff}^2}{3\varepsilon_0}$$

(III.15)

where μ_{eff} is now the effective dipole moment relaxing via thermally activated *ADWP* dynamics.

If the thermal energy is high enough with respect to the asymmetry parameter Δ, *i.e.*, $\Delta < 2kT$, and the distribution function for Δ is flat, $f(\Delta) = f_0$ Eq. (III.14) reduces to:

$$\chi''(v) = 2Af_0 \int_0^\infty \frac{2\pi v\tau}{1 + (2\pi v\tau)^2} g(V)dV , \tag{III.16}$$

where now $\tau = \tau_0 exp(V/kT)$ and A is a material constant. An important consequence of the linear temperature cut-off is that the prefactor of the integral in (III.16), *i.e.* the area under the spectra becomes temperature independent.

Gilroy and Phillips assumed an exponential distribution of the barrier heights with no low-energy cut-off:

$$g(V) = \frac{1}{V_0} \exp(-V/V_0) \tag{III.17}$$

V_0 has the meaning of the mean activation energy. With this $g(V)$, Eq. (III.16) transforms to:

$$\chi''(v) = 2Af_0\alpha(2\pi v\tau_0)^\alpha \int_{2\pi v\tau_0}^\infty \frac{x^{-\alpha}dx}{1 + x^2} \tag{III.18}$$

where $x = 2\pi v\tau$ and $\alpha = kT/V_0$.

According to this model, for frequencies $\omega \ll 1/\tau_0$, where $1/\tau_0$ is the attempt frequency on the order of $10^{13} - 10^{14}$ Hz, the loss is given by [69]:

$$\varepsilon''(\omega,T) \propto \alpha(\omega\tau_0)^\alpha \tag{III.19}$$

Power-law spectra are expected with a characteristic exponent α being proportional to temperature. The dependence $\alpha = \alpha(T)$ gives directly the mean activation energy V_0.

Using this model Gilroy and Phillips were able to interpolate for the first time the acoustic attenuation data for silica [69]. In several cases an exponential distribution cannot reproduce the data, and different distributions (*e.g.*, a Gaussian) were discussed [71]. Nevertheless, the distribution $g(V)$ can be extracted directly from the frequency dependent measurements of

susceptibility covering several decades [70,71,72], as it will be demonstrated in Chapter V. Accordingly, recent quasi-elastic light scattering experiments on silica and calcium potassium nitrate (*CKN*) revealed a distribution g(V) that is essentially an exponential with barrier heights in the range *0 – 1500 K* [70,71].

IV. Results; Relaxation properties of molecular glass formers at T ≥ 100 K

The following Chapter considers the evolution of the three relaxation features, α-process, excess wing (EW) and β-process. Above the glass transition temperature T_g the spectra are dominated by the α-relaxation peak and, in addition, the secondary processes (EW and/or β-process) emerge. These secondary processes survive in the glass ($T < T_g$) and give the main contribution to the dielectric response down to, say, 100 K. As the main experimental effort of this Thesis is spent on investigations at even lower temperatures, only few molecular glass-formers are newly investigated in the temperature range considered in this Chapter. Some of the previous investigations are extended to a broader frequency and temperature range and aging experiments are performed. Having at hand a huge collection of data, this work tries to consistently describe the temperature evolution of the different spectral contributions (α-process, EW and β-process). Since there are no generally accepted theoretical approaches to account for the relaxation behavior in this temperature range, the spectral evolution is purely phenomenologicaly described.

A new approach is introduced here, called in the following approach II. This scenario stands for the applicability of the frequency temperature superposition (FTS) for the α-peak in whole temperature range down to T_g. This is in contrast with previous analyses, as *e.g.*, the one introduced by Blochowicz et al. (referred to in the following as approach I), concluding a considerable temperature dependence of all individual spectral contributions, including the α-peak itself. As it allows almost perfect interpolation of the data, the proposed scenario offers a quite different picture for the relaxation pattern of molecular systems.

IV.1 Experimental results

In the following are presented the dielectric spectra of propylene glycol (PG) and trimethyl phosphate (TMP), both measured within this work. The samples were purchased from Sigma-Aldrich and investigated as received. The experimental details are given in II.2. The data, measured above and slightly below T_g, are presented in Fig. IV.1.
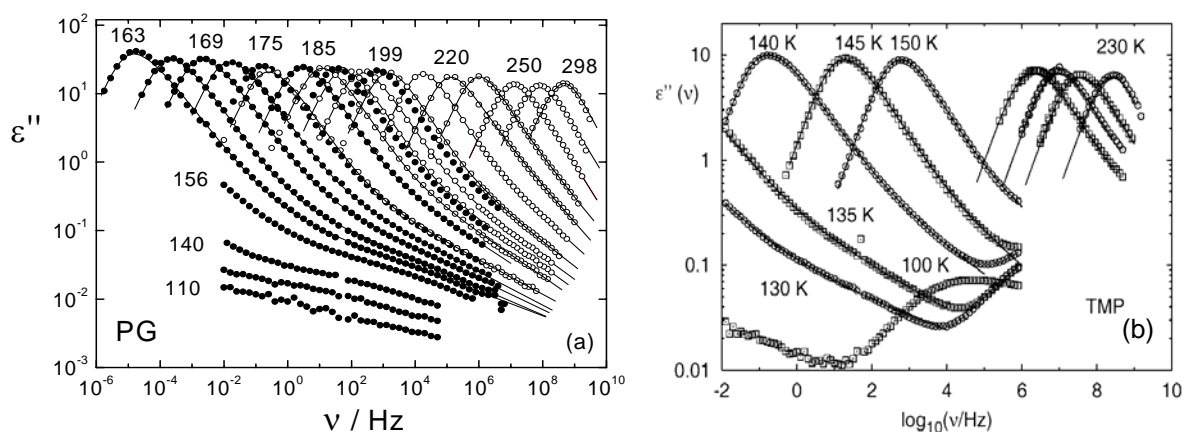
Fig. IV.1 Dielectric spectra of (a) propylene glycol PG, $T_g = 168$ K and (b) trimetyl phosphate TMP, $T_g = 136$ K. Few temperatures (in K) are indicated. The solid lines are fits using Approach I.

In Fig. IV.1. (a), in addition to the spectra measured with the time domain and the frequency domain broadband spectrometer (plotted as dots), the high frequency data by Lunkenheimer et al. [41] (open circles) are included for PG. A good agreement between the different datasets is observed in the common temperature range. By including the high frequency results the dielectric spectra are monitored over 15 decades in frequency above T_g. Here, besides the shift of the α-peak, the EW emerges and gets more pronounced while approaching T_g, thus type A characteristics are revealed for this system. Below T_g the spectra get very flat and, apparently, only their amplitude changes with temperature here.

For TMP a β process can be identified in the spectra, cf. Fig IV.1 (b). This process is quite fast and the β-peak can be clearly observed only at the lowest temperature presented here (T = 100 K), well below T_g. At higher temperatures one recognizes an EW contribution between the reminiscence

of the α- and the β-peak. Due to the high tendency to crystallize of this system, a gap appears between the spectra measured while heating, after fast quenching into the glass and those measured above the melting point T_m.

IV.2. Spectra analysis using approach I

As already mentioned in III.2.1, the approach introduced by Kudlik *et al.* [26] and Blochowicz *et al.* [11,42] describes both the α–peak and the EW in type A systems by using a special distribution of relaxation times being an extension of the generalized gamma distribution (see II.3.4). This so-called GGE function has the advantage to interpolate the spectra close to T_g showing a well-pronounced EW but also to reduce to a single peak for a certain constellation of its parameters, as typically observed for the spectra measured at high temperatures.

The newly measured systems are analyzed here using this approach, and the results of the analysis are discussed together with those previously obtained for glycerol, propylene carbonate (PC), 2-picoline, ethylene glycol (EG), m-tricresyl phosphate (m-TCP), 4-tertbutyl pyridine (4-TBP) and m-fluoroaniline (m-FAN) [11,30,42,43]. For every system, the investigated temperature range, the glass transition temperature T_g and the corresponding abbreviation used in this Thesis are posted in Appendix A.

The dielectric spectra of 2-methyl tetrahydrofuran (MTHF) [80] are included in the present analysis. As for TMP and m-FAN, a β-contribution appears in the MTHF spectra close to T_g, however well separated from the α-peak (cf. Appendix B). Between the two relaxation features an EW is well resolved, allowing an analysis with the GGE function. In such cases when the spectra contain all three spectral contributions (α-process, EW and β-process) the fits are performed in accordance with the Williams-Watts approach (see III.2.2), using $G_{GGE}(\ln\tau)$ distribution for the α-peak and the EW, together with $G_\beta(\ln\tau)$ for the β-process.

To remind the reader, the GGE distribution was introduced by Eq. (II.33):

$$G_{GGE}(\ln\tau) = N_{GGE}(\alpha,\beta,\gamma,\sigma)\left(\frac{\tau}{\tau_0}\right)^\beta \exp\left(-\frac{\beta}{\alpha}\left(\frac{\tau}{\tau_0}\right)^\alpha\right)\left(1+\left(\frac{\tau\sigma}{\tau_0}\right)^{\gamma-\beta}\right) \quad \text{(II.33)}$$

As mentioned in III.2.1, the maximum of the distribution is at $\tau = \tau_0$. The broadening of the distribution peak is controlled by the parameters α and β. The parameter α controls the shape of the distribution at long relaxation times while β defines the slope of the distribution peak at short times. The EW is described by two additional parameters: γ is its exponent and σ marks the crossover between the $\nu^{-\beta}$ and $\nu^{-\gamma}$ regimes (the "onset" of the EW). The connection between the distribution and the measured permittivity is given by Eq. (II.27).

To illustrate the quality of the GGE fits, the interpolations of the spectra measured above T_g for glycerol, 2-picoline, m-TCP and 4-TBP are presented in Fig. IV.2. For the newly measured systems the fits using approach I are previously shown in Fig. IV.1. Using this approach, very good interpolations are obtained for the data spreading up to 15 decades in frequency, as observed for glycerol, 4-TBP and PG.
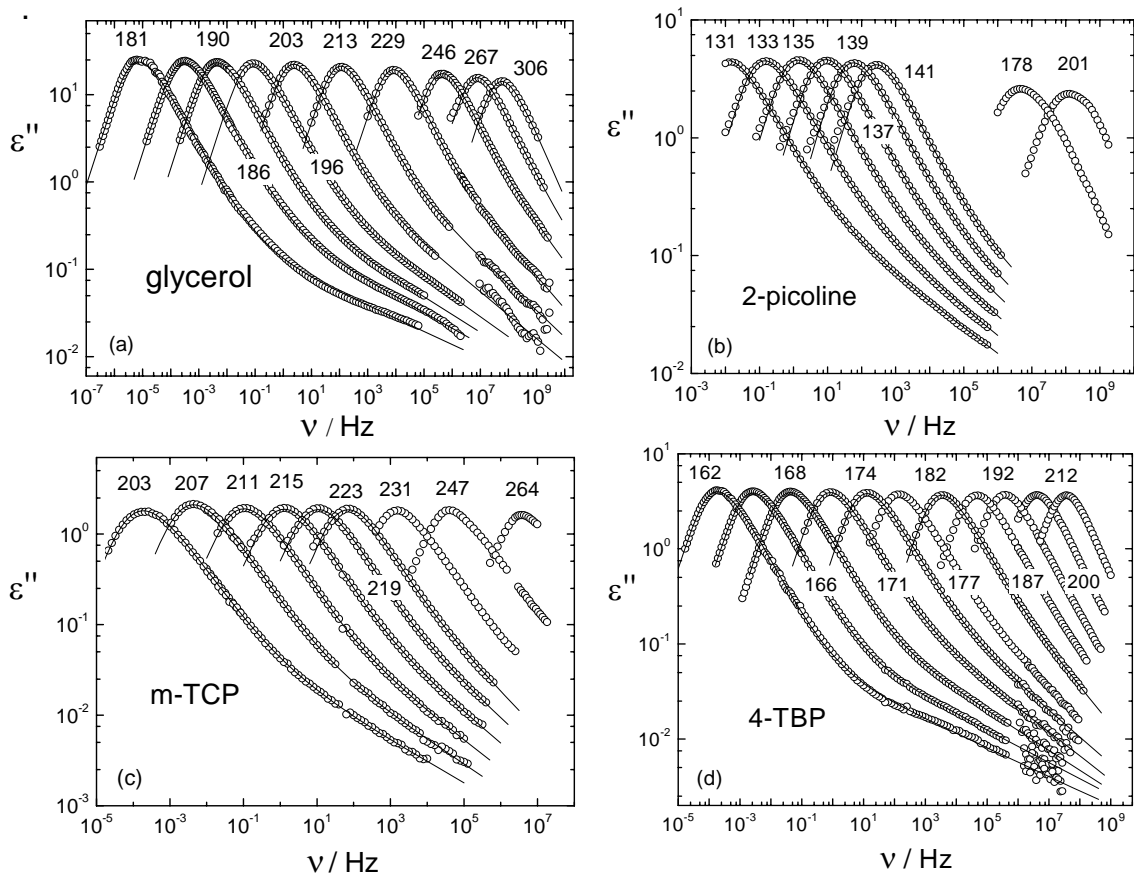
Fig. IV.2. Dielectric spectra of (a) glycerol, (b) 2-picoline, (c) m-TCP and (d) 4-TBP, measured above T_g. Temperatures (in K) are indicated. The solid lines are fits applying the GGE distribution, according to Eq. (II.33).

For some systems the fit quality is slightly spoiled at temperatures close to T_g due to the presence of a small curvature at the highest frequencies in the spectra. This feature may indicate the presence of an additional weak β-process, not well resolved.

For all systems the presumably temperature independent width parameter α of the α-peak is obtained by the interpolation of the spectra close to T_g. The α values for all systems investigated here are given in Table C.1 in Appendix C. The fitting parameters for describing the overall spectral evolution are the overall relaxation strength $\Delta\varepsilon$, and τ_0, β, γ and σ of the GGE function.
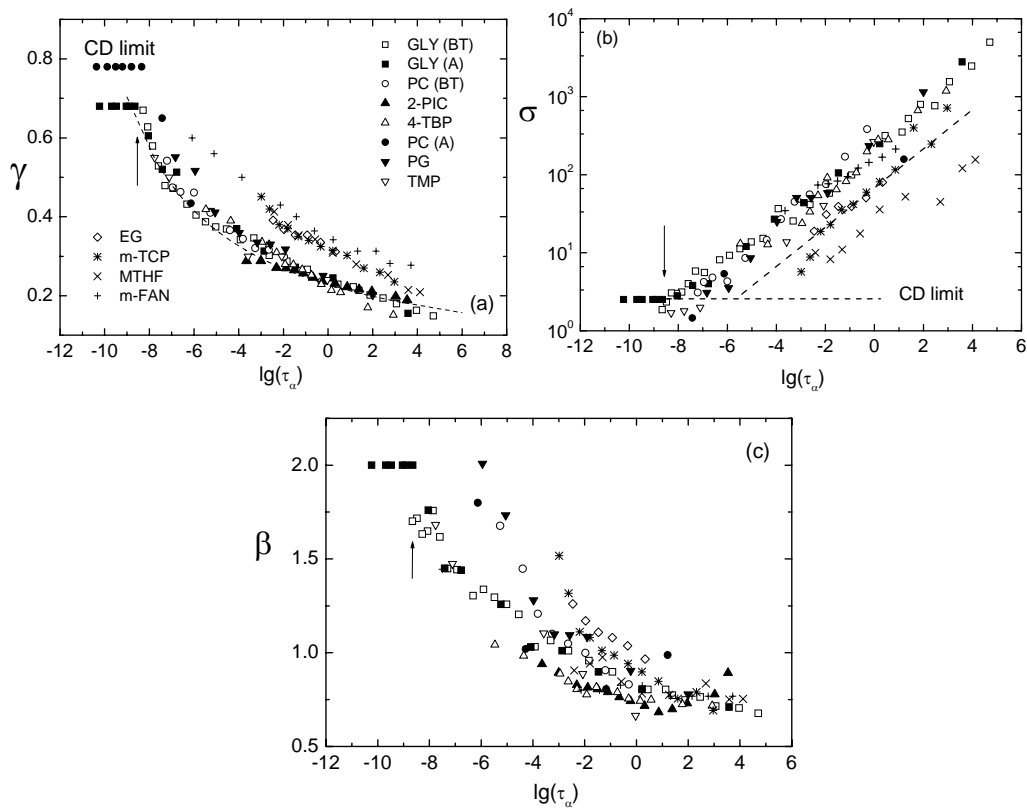
Fig. IV.3 The GGE parameters γ in (a), σ in (b) and β in (c) as functions of the time constant of the α–process (τ_α); the arrow indicate the crossover from a susceptibility with EW (low temperature regime) to the one without EW (high-temperature regime, "CD limit"). In the case of two data sets of glycerol and PC, A refers to dielectric spectra measured by the Augsburg dielectric group and BT by the Bayreuth group. Dashed lines: guides for the eye.

In Fig. IV.3 the results for β, γ and σ, quantifying the changes of the spectral shape, are plotted as functions of the relaxation time τ_α. This representation allows the direct comparison of the susceptibility evolution for different systems independent of their fragility. As seen, the parameters are found to

be quite similar for all investigated glass formers, suggesting that the shape of the α-peak together with the EW is essentially controlled by τ_α.

Starting at T_g (*i.e.* $\tau_\alpha \cong 100$ s), the exponent γ increases nonlinearly with decreasing $\lg\tau_\alpha$. The type A systems EG and m-TCP, as well as the type B m-FAN and MTHF show small, but systematic deviations from the common behavior. For the same systems deviations are found also in the evolution of $\beta = \beta(\lg\tau_\alpha)$ and $\sigma = \sigma(\lg\tau_\alpha)$. While the $\beta(\lg\tau_\alpha)$ parameter show similar changes as $\gamma(\lg\tau_\alpha)$, the EW onset $\lg\sigma$ appears as a linear function of $\lg(\tau_\alpha)$. As observed in Fig. IV.3 (b), σ increases with τ_α and implicitly, decreases with temperature. This indicates that the onset of the EW approaches the α-peak at high temperatures.

A single peak susceptibility is expected for $\sigma \approx 1$, and for few systems this relation is reached at short relaxation times [43]. According to Figs IV.1 and IV.2, at highest temperatures single peak spectra are indeed experimentally observed and, as discussed in III.1, this behavior is characteristic for the slow dynamics above T_x, *i.e.* in the high-temperature regime. As demonstrated in ref. [42], the GGE function with $\sigma \cong 2$ and $\gamma = \beta_{CD}$ can well interpolate a Cole Davidson (CD) distribution of relaxation times. Thus, the GGE function allows to identify a crossover time constant τ_x (associated with T_x) between the low temperature regime characterized by the presence of the additional EW and high-temperature regime with a CD susceptibility ("CD limit"). As indicated in Fig. IV.3 (a) and (b) a value of $\tau_x \approx 10^{-8}...10^{-9}$ can be estimated for glycerol and PC, systems investigated by Lunkenheimer et al. [25] at such short relaxation times. For these two systems the fitting results in the high temperature regime ($T > T_x$), where the exponent $\gamma = \beta_{CD}$ is virtually not changing with τ_α, are added in Fig. IV.3 (a). This is an indication that the FTS applies in good approximation in the high-temperature limit.

Assuming a linear dependence for $\lg\sigma = \lg\sigma(\lg(\tau_\alpha))$ one can estimate a crossover time constant for any system by extrapolating this dependency to $\lg\sigma \approx 1$. As indicated by the intersection of the dashed lines in Fig. IV.3 (b), it appears that the crossover time constant τ_x is not universal.

The two temperature regimes are even better recognized when the GGE parameters β and γ for glycerol and PC are discussed as functions of temperature, cf. Fig. IV.4 (a). Whereas γ does not change at high temperatures, a linear decrease with T is recognized below T_x. Note that both the EW exponent γ, as well as the exponent β for the α-process change by a factor 4 from T_g to T_x, indicating that FTS strongly fails here for both processes.
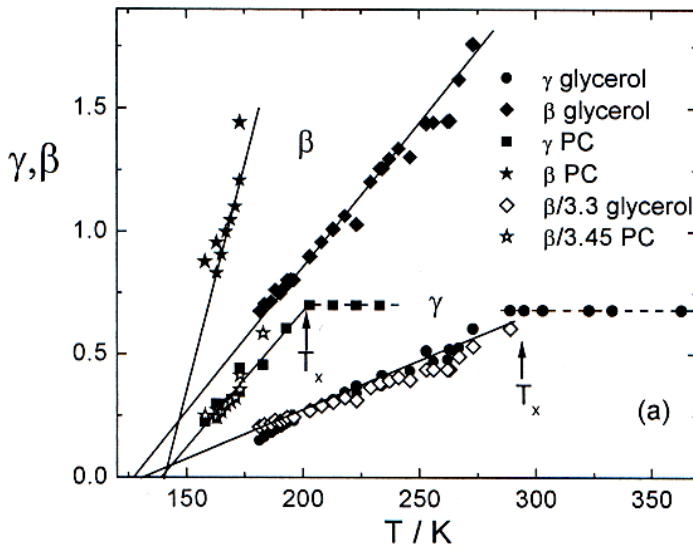
Fig. IV.4 (a) The parameters β and γ for glycerol and PC as functions of temperature; β is divided by a factor c demonstrating that it is proportional to γ in the low temperature regime; data of high-temperature regime from analyzing the spectra measured by Lunkenheimer et al. [25] are included and the crossover temperature T_x is indicated.

More consequences of the approach I analysis are discussed in Appendix C. As shown there, the temperature dependence of the GGE parameters may be connected with the VFT law (see I.1), and the temperature T_x is found to be similar with the crossover temperature T_S reported from the Stickel analysis [23], *i.e.*, as revealed by the failure of the low temperature Vogel-Fulcher-Tammann (VFT) law.

To summarize, the parameters β, γ and σ mapping the evolution of the susceptibility including α-process and EW are strongly temperature dependent. Within approach I the parameters are linked among each other and the spectral shape is controlled by the time constant of the structural relaxation τ_α. This latter result of the model is confirmed by recent isothermal dielectric measurements using pressure as variable [86], indicating that both α-process and the EW are intimately connected. Within this approach the relaxation strength of the EW strongly increases while heating above T_g,

resembling the behavior of the β-process in this respect. This point of the analysis is not discussed here, but treated in ref. [84].

A critical assessment

The above analysis, as well as the others mentioned in Chapter III, agree in the sense that the width parameters of α–peak and EW exhibit a strong temperature dependence in type A systems, *i.e.* the FTS principle is strongly violated below the crossover temperature T_x even for the α–process alone.
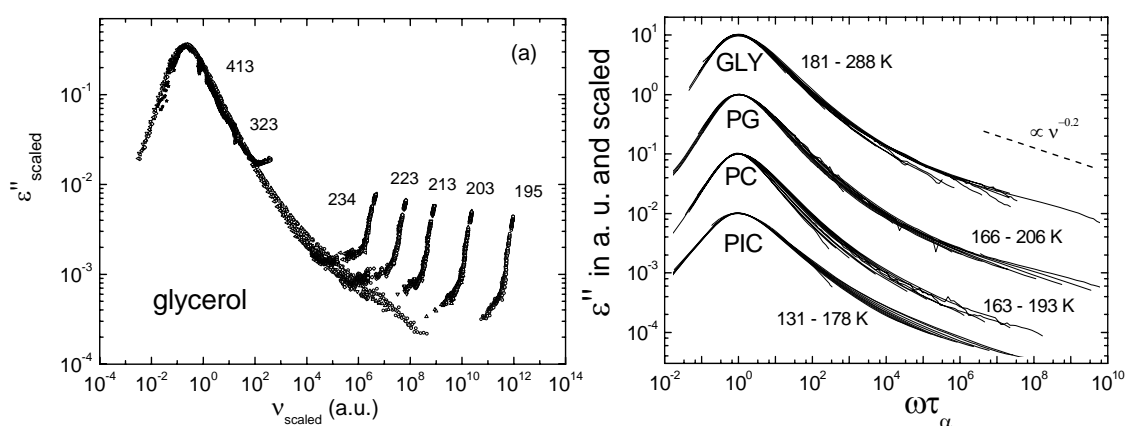
Fig. IV.5 Dielectric spectra scaled by the α-peak maximum and position for (a) glycerol measured by Lunkenheimer et al.[25], (b) glycerol (GLY), propylene glycol (PG), propylene carbonate (PC) and 2-picoline (PIC) measured in Bayreuth group [26,42,43].

However, simple "α-peak scaling" (cf. III.1) of the spectra measured above T_g, as done in Fig. IV.5 (a) for glycerol measured by Lunkenheimer et al. and in (b) for other type A systems measured in Bayreuth, clearly show that the shape of both α-process and EW are not changing so drastically with temperature. In other words, the strong change of $\gamma(T)$ and $\beta(T)$ parameters as revealed, *e.g.*, by approach I, is not at all obvious from a mere inspection of the spectra at different temperatures. Moreover, for a given system measured at different temperatures, the high-frequency flanks constituting the EW appear as parallel in the double logarithmic plot in Fig. IV.5 (b), and their apparent exponents are very similar among different systems (close to 0.2). This is best seen when the data are measured close to T_g, as the EW is most pronounced here.

Furthermore, when inspecting the derivatives $dlg(\varepsilon''(\nu))/dlg(\nu)$ of the glycerol spectra in Fig. IV.6, the minimal value of the derivative, *i.e.* the maximum negative slope in spectrum, appears to be almost temperature independent (see the horizontal dashed line), pointing to the validity of FTS. The exponent γ of the EW is directly given by the level of the derivatives plateau at highest frequencies [11,42,43]. However, it is almost impossible to identify any plateau at all, as the data are strongly scattered above 10^5 Hz.
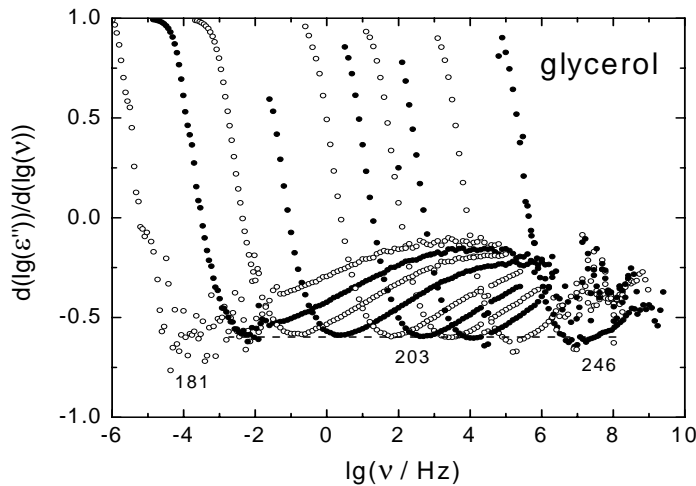
Fig. IV.6 Double logarithmic derivative of the glycerol data above T_g; the spectra are presented in Fig. V.2. The dashed line is a horizontal.

Indications for the validity of FTS may be obtained also by using the optical Kerr effect (OKE) data compiled recently by Fayer and co-workers [113]. In an OKE experiment the pulse-response function $\phi_{OKE}(t)$ is measured which is related to the usually obtained step-response $F_{LS}(t)$ by $\phi_{OKE}(t) = - dF_{LS}(t)/dt$. The index stands for "Light Scattering". The OKE decay curves measured for benzophenone ($T_g = 213$ K) exhibit an interesting property [114]: in the full temperature range covered a master curve can be obtained when the time scale is scaled by t/τ_α and the ordinate is scaled by the value of ϕ_{OKE} at τ_α (cf. Fig. IV.7 a). Moreover, comparing the dielectric data of type A systems measured close to T_g in the pulse-response representation similar decay curves are obtained, cf. Fig. IV.7 (b), thus, essentially, both techniques probe the same spectral features [114,115]. In particular, the first power-law regime (nothing else than the EW) exhibits a quite similar exponent γ as in the case of the OKE data of benzophenone.

49

Providing that the EW is present also in the OKE data, these results indicate that not only the shape of the α-decay (at longest times), but also the EW exponent γ may be considered as temperature independent.
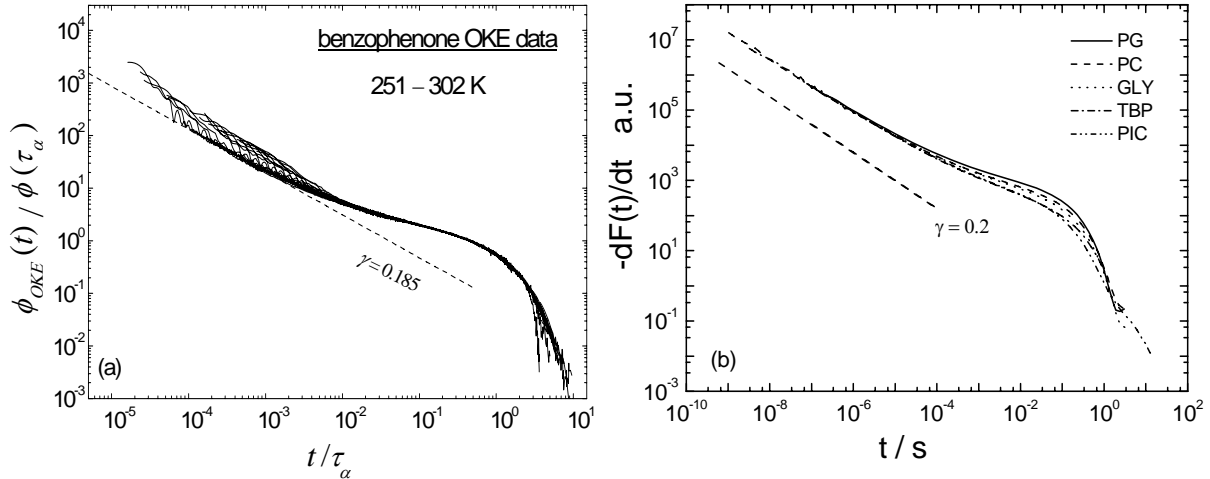
Fig.IV.7 (a) Optical Kerr effect data of benzophenone compiled by Cang et al. [113] as a function of the scaled time t/τ_α providing a master curve (b) Pulse-response representation of the dielectric data close to T_g scaled to achieve agreement at short times for five glass formers: PG, PC, glycerol, 4-TBP and PIC; the time constant τ_α are chosen to be similar. In both (a) and (b) the dashed lines correspond to power laws in susceptibility representation with exponent γ.

One may ask whether it is possible that the conclusion that the FTS principle strongly fails is a mere artifact of the interpolations covering in most cases only a restricted frequency window. The strong temperature variation for the stretching parameter of the α-process itself may appear as a result of interpolating the overall slow dynamics (resembling more and more a single peak susceptibility at high temperatures) with a two-peak function, as, *e.g.,* provided by approach I.

Independent of any considerations, it is a fact that the FTS for the *overall slow dynamics* (α-peak + EW) fails, though not strongly cf. Fig. IV.5 (b), in all type A systems. The best example may be the behavior of PC below T_x, cf. Fig. III.2 (b) also. However, as discussed in III.2.1, the broadening of the relaxation peak for PC is accompanied by the appearance of the EW that gets more pronounced while approaching T_g. Since the exponent γ of the EW appears not to change with temperature (cf. Fig. IV.5 b), one may ask whether the FTS failure or, more precisely, the overall peak broadening is due to a smooth increase of the EW amplitude (relative to the α-process) while cooling. If true,

the temperature change of the EW is opposite to the behavior observed for β-processes.

Next the α-relaxation is discussed for type B glass formers, systems exhibiting a discernible β-peak in their spectra above T_g. In Fig. IV.8 (a) the spectra measured at $T \approx T_g$ for various systems (previously measured) are plotted together with the results for newly investigated TMP.

At a first inspection of the data one observes a large variation in the amplitude of the α-process among different systems, reflecting large differences between the corresponding molecular dipole moments (cf. II.1). It appears that the lower is the relaxation strength $\Delta\varepsilon_\alpha$ the broader is the α-peak.
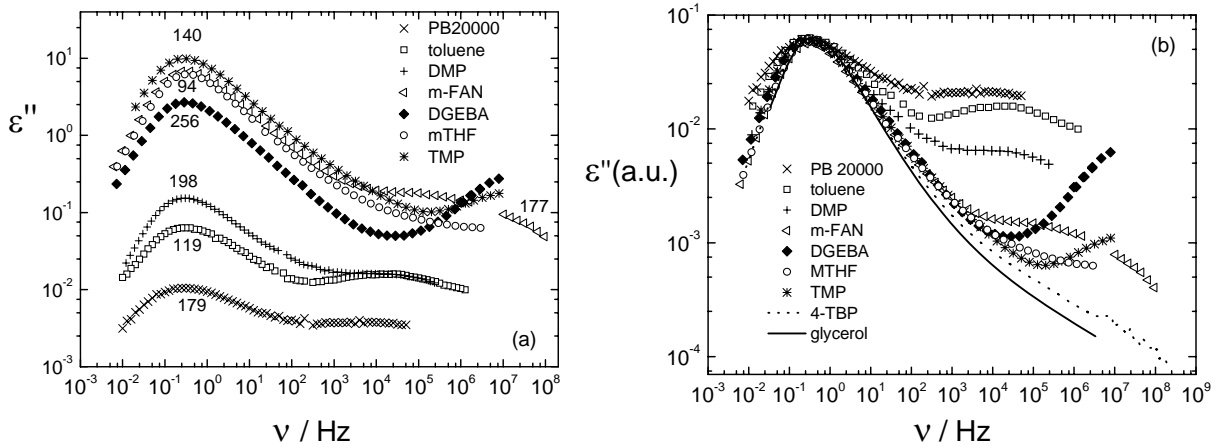
Fig. IV.8 Dielectric spectra of the type B systems measured at temperatures close to T_g. (b) The spectra in (a) are vertically shifted to coincide at the relaxation maximum; for comparison, the data of type A glycerol (measured at 196 K) and 4-TBP (measured at 166 K) are added.

In Fig. IV.8 (b) all the spectra in (a) are rescaled by the α-peak maximum. In this way one may clearly reveal a strong variation among the systems for the relative amplitude of the β- with respect to the α-contribution. For comparison, the spectra measured close to T_g for type A glycerol and 4-TBP are included. A general picture emerges: the smaller or faster is the relative β-contribution, the more the EW is revealed on the right flank of the α-peak. This suggests that the EW may be present even in the case of a strong β-relaxation that may obscure its contribution. An example in this sense is the behavior of the glass former PGE, for which the EW is revealed only at lowest frequencies when measurements are performed very close to T_g, cf. Fig. IV.9 (c). On the other hand, as most of type A systems reveal a curvature in their spectra close to

T_g, this may also suggest that in such cases the β-peak is obscured by the overwhelming EW. As for 4-TBP this curvature is the strongest, its spectra well fits in the smooth crossover between of type A and type B spectral shapes, cf. Fig. IV.8 (b). Upon such considerations one may assume that both secondary processes EW and β-process are always present in the spectra close to T_g.

In type B systems the α-peak appears usually as broad, with a stretching exponent β ≤ 0.5, that may hide the EW. However, if the β- and α-process are sufficiently separated (as for triphenyl phosphate-TPP, phenyl glycid ether-PGE and diglycyl ether of bisphenol A-DGEBA) one finds indications that the α-peak itself obeys FTS, according to the peak scalings presented in Fig. IV.9. The applicability of FTS for such systems was previously noticed by Olsen [34].
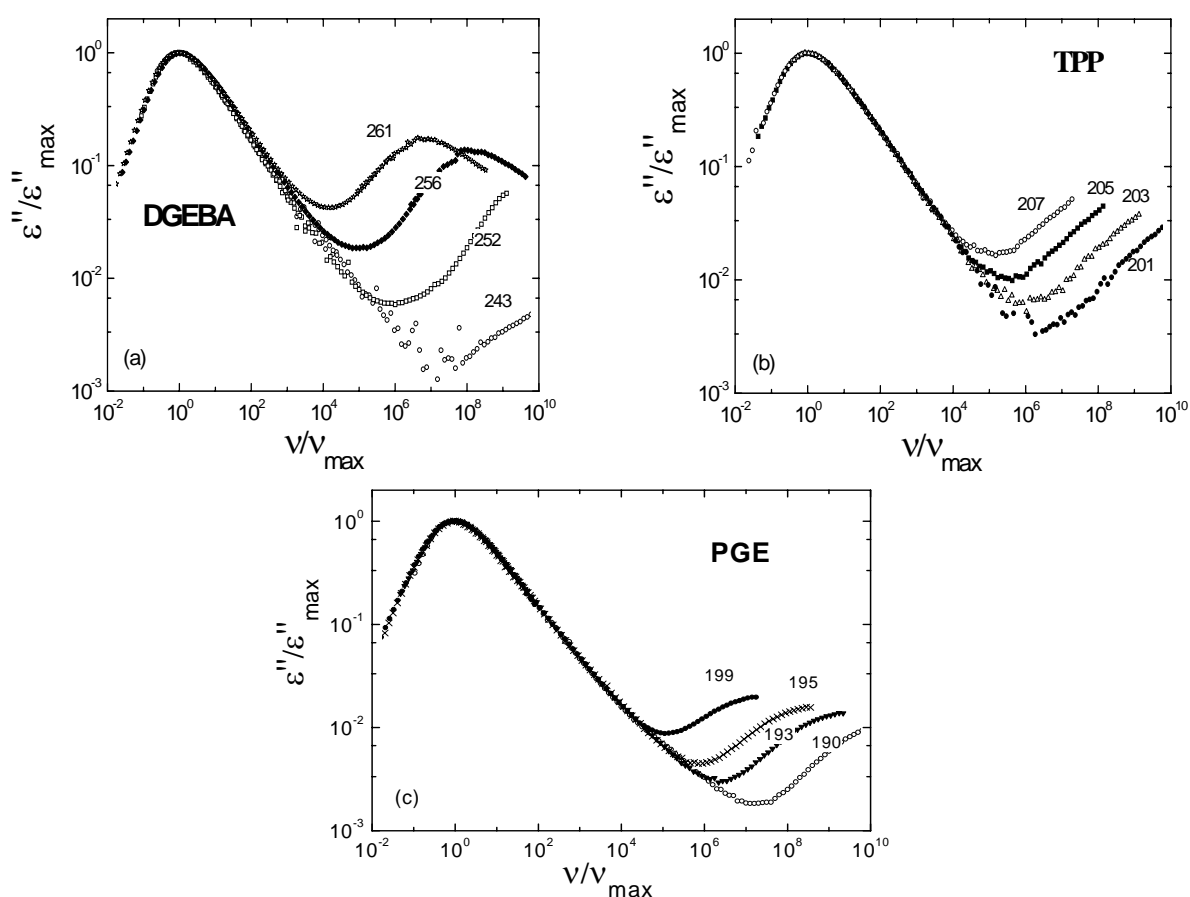
Fig.IV.9 Selected dielectric spectra of DGEBA [115], TPP [115] and PGE [116] scaled by the α-peak position and amplitude. The systems exhibit a strong β-peak, however the α-peaks superimpose well, demonstrating FTS.

IV.3. Spectra analysis using approach II

The model independent findings discussed above can be used as arguments in favor of an alternative description. This so-called in the following approach II will be consequently applied in the rest of the Thesis. Guided by the idea that FTS holds for the α-peak itself, this analysis suggests that the latter can be described by a susceptibility function with a stretching exponent not changing over the entire temperature range relevant for the glass transition. A change of the relative weight of the EW with respect to that of the α-peak is allowed to account for the minor changes of the overall slow dynamics spectra (α-peak + EW).

IV.3.1 Analysis of type A systems

Glycerol, T > T$_g$

In order to introduce the analysis one should resort to the best dielectric data currently available, *i.e.*, spectra of glycerol measured by Lunkenheimer *et al*. [25]. The spectra are plotted in Fig. IV.10, where, in addition, the spectrum at the lowest temperature T = 181 K measured within this work, is included.

To interpolate the data we describe the relaxation function as a product of two terms, explicitly $F(t) = \phi_{ex}(t)\phi_{\alpha}(t)$. The function $\phi_{ex}(t)$ denote the partial loss due to the EW and $\phi_{\alpha}(t)$ due to the α–process. Introducing the normalized relaxation functions with their corresponding relaxation strengths, one may write, in accordance with Williams-Watts (see III.2.2):

$$F(t) = [(1 - S_{ex})\Phi_{ex} + S_{ex}]\Phi_{\alpha}(t) \tag{IV.1}$$

Thus, the EW is interpreted as a secondary relaxation process that relaxes (statistically independent) a certain fraction of the total polarization. From F(t) the dielectric spectrum is calculated via $\varepsilon'' = \Delta\varepsilon\,\omega\,\mathrm{Re}\big[FT(F(t))\big]$ (cf. Eq. II.10), where FT denotes the Fourier transform. The α-peak is usually well described by the CD function, while the EW power-law spectrum can be equally well described by the high frequency power-law asymptote of an additional CD function. Accordingly, the relaxation functions $\Phi_{\alpha}(t)$ and $\Phi_{ex}(t)$ are

expressed by the corresponding time-domain equivalents of CD function, *i.e.* the incomplete gamma function [90].

One should mention here that a convolution of a simple power-law (for EW) with a Fourier transform of a CD (for the α-process) provides similar fitting results. The choice for a CD function accounting for the EW contribution is motivated by the sake of clarity in attributing an individual spectral area to this process. The time constants of the two processes are fixed to each other, *i.e.*, $\tau_\alpha = \tau_{ex}$. The high-frequency exponents are denoted β and γ for the α–process and the EW contribution, respectively. The resulting fits are nearly perfect (see Fig. IV.10), and supports the choice of the CD functions. The same analysis but using the KWW function, more natural for the time domain was tested and could not provided such good fits. Thus, the parameters of this model are: τ_α and β for the α-process, γ and S_{ex} for the EW and the overall relaxation strength $\Delta\varepsilon$.
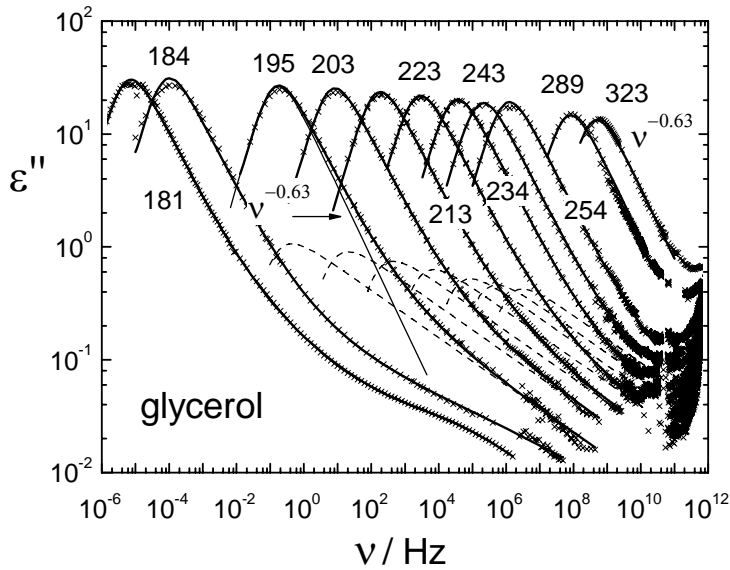
Fig. IV.10 Dielectric loss of glycerol at indicated temperature with fits according to approach I; dashed line are EW contributions according with Approach II and the solid line indicated by arrow is a CD function with $\beta_{CD} = 0.63$.

First the high-temperature data was analyzed demonstrating that the α-peak above 289 K is well interpolated by a CD function with $\beta_{CD} = 0.63$ ($S_{ex} = 1$ in Eq. IV.1). This value is close to the one obtained by the "minimum scaling" and "peak scaling" above T_x, discussed in III.1. Next it is assumed that the high-temperature value of β is appropriate for all temperatures down to T_g, and kept fixed accordingly. This leaves some freedom in the choice of the EW exponent γ, and fits constrained with $\beta = 0.63$ lead to values of $\gamma = 0.2 - 0.23$

in the temperature range 195 K < T < 289 K. A similar value was already foreseen from the model independent α-peak scaling (see Fig. IV.5 b). Due to its small interval of variation, it is tempting to assume that the EW exponent γ is also temperature independent, in order to further reduce the number of fitting variables.

The exact value of γ was extracted to consistently interpret the aging experiments at T $\approx$ T$_g$, discussed in the next section. As shown there, the aging analysis yields γ = 0.21. Thus γ = 0.21 is assumed for all temperatures, and the interpolations above 195 K are repeated with only three parameters, *i.e.* the relative relaxation strength of the excess wing 1-S$_{ex}$, the time constant τ_α, and the overall amplitude $\Delta\varepsilon$. The resulting fits, shown in Fig. IV.10, are nearly perfect and indistinguishable from those obtained using approach I (cf. Fig. IV.2). Note that the evolution of the spectral shape for T > T$_g$ is now described by the variation of a single parameter 1-S$_{ex}$(T), and any contribution from a secondary β-peak can be disregarded here. The evolution of 1-S$_{ex}$(T) for glycerol is discussed in IV.3.3 together with the results obtained for other glass formers.

In Fig. IV.10 the individual contributions of the EW at several temperatures as obtained from the above fitting procedure are presented as dashed lines. These contributions grow with decreasing temperature, opposite to the behavior expected for a β-process.

As commonly observed for other type A systems, at temperatures very close to T$_g$ a curvature appears in the spectra of glycerol measured at 181 K and 184 K, indicative for a small β-contribution, cf. Fig. IV.10. In accordance with the previous discussion, both EW and β-process may be present in the spectra of molecular glasses at T$_g$. However, within the present interpretation, in type A systems the weak β-contribution manifests itself only as a small curvature in the spectra measured at temperatures close to T$_g$, when *both the α-process and the EW* become well separated from the latter. Since within approach II the EW amplitude behaves differently with respect to the one of β-process, this may offer the possibility to disentangle the two spectral contributions at temperatures close to T$_g$ and even below. Thus, it becomes a

challenge to reinterpret the aging experiments of Schneider et al. [31] accordingly.

Aging experiments described by approach II

When a glass former is cooled rapidly below its glass transition temperature T_g, it freezes into a non equilibrium state, *i.e.* the glass. Physical aging describes the relaxation of the out-of-equilibrium glass towards the equilibrium liquid state under isothermal conditions. During aging the structural relaxation time τ_α grows in time towards the equilibrium value that can be estimated from the extrapolation of the VFT law at temperatures above T_g. Depending on temperature, the equilibrium state may not be reached even over a time scale of years, thus aging experiments are done at temperatures below, but very close to calorimetric T_g.

In the case of molecular glassformers, that are usually fragile systems, there are strong changes of τ_α while aging. On the other hand, studies of type B systems at $T > T_g$ [24,47] showed that the temperature dependence of the time constants of the β-process τ_β is much weaker with respect to $\tau_\alpha(T)$, thus the two processes continuously separate while cooling towards T_g. The results reported by Schneider et al. [31] for glycerol, aged at 179 K, are presented in Fig. IV.11.
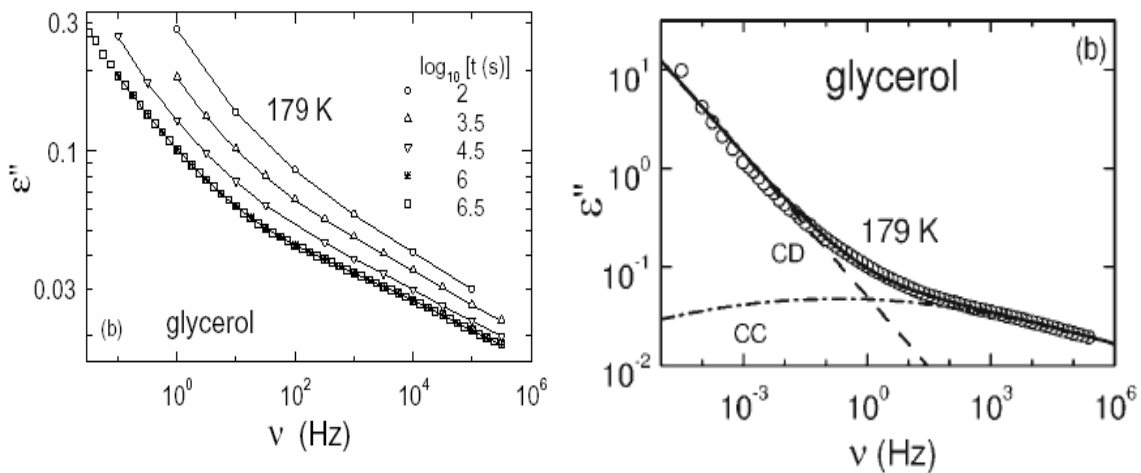
Fig. IV.11 Dielectric spectrum of (a) glycerol (T_g = 186 K) measured at 179 K at different aging times and (b) The equilibrium spectrum at 179 K interpolated by a sum of a power-law and a Cole-Cole function. Figures taken from [31].

During the experiments (extending up to five weeks!) the spectrum at highest frequencies (attributed to the EW) develops into a shoulder and its curvature becomes more pronounced as the system equilibrates. The authors concluded that the EW is just the high-frequency flank of a submerged β-peak, and fitted the equilibrium spectrum by adding a power-law and a Cole – Cole contribution. Deviations between the experimental results and the corresponding interpolation can be observed for low frequencies, cf. Fig. IV.11 (b).

Figure IV.12 (a) presents the results for glycerol annealed at 181 K, obtained within this work. The lower spectrum (dots) is measured 70 h later than the upper one (open circles). The invariance of the loss after this aging time indicated that the equilibrium was established. Both spectra recorded in the non-equilibrium and the equilibrium state, respectively, show a similar curvature at highest frequencies, as the aging appears to affect mainly the low frequencies.
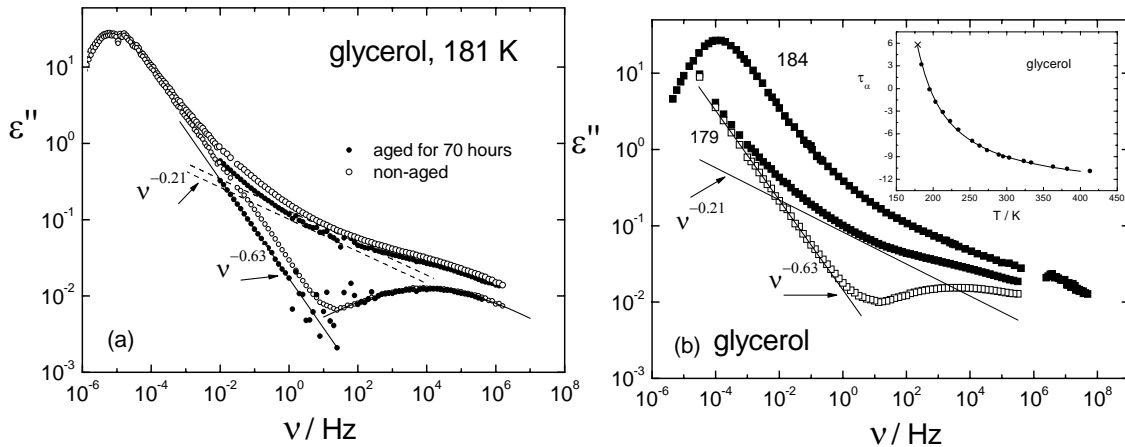
Fig. IV.12 Aging analysis of two different data sets of glycerol: (a) data measured within this work; (b) data at 179 K reported by Schneider et al [31]; spectrum at 184 K was added for comparison. Inset: time constants of glycerol measured by Lunkenheimer et al. (dots), interpolated by a VFT function (line). The point at lowest temperatures (cross) is obtained from the aging analysis with approach II. See text for details.

According to approach II, a fine-tuning of the EW exponent γ is essential for a further characterization of the β-process in the glass, due to the relatively small amplitude of this process with respect with the α-process (roughly a factor of thousand cf. Fig. IV.12). In order to extract a value for the exponent γ the EW is subtracted from the overall spectra, aged and non-aged, as a

power-law $A\nu^{-\gamma}$ to reveal the presumably *temperature invariable high-frequency flank of the α-process* with exponent $\beta = 0.63$, as determined at highest temperatures. The second constraint used to refine γ is that a *symmetric β-peak* results after the subtraction of $A\nu^{-\gamma}$. Both conditions are fulfilled for $\gamma = 0.21 \pm 0.005$. This value is in good agreement with the analysis at higher temperatures (T > 195 K), where the EW exponent is determined as a fit parameter under the constraint of $\beta = 0.63$. There are extremely small differences between the aged and non-aged β-peaks, which implies that the β-process virtually does not change in the course of the aging experiment.

In Fig. IV.12 (b), a similar analysis is applied for the glycerol spectrum aged by Schneider et al. [31]. As this experiment is performed at a lower temperature, T = 179 K, the aging effects are significantly larger. Subtracting the EW contribution as a power-law $A\nu^{-0.21}$ from the equilibrium spectrum one rediscovers the high frequency flank of the α-peak that extends as $\nu^{-0.63}$ for 3 decades in amplitude. Assuming that the α-peak height does not change significantly from 184 K to 179 K, one can estimate a time constant for the α-process $\tau_{\alpha} \approx 10^6$ s for the equilibrium spectrum measured at 179 K. This time constant agrees well with the others measured at higher temperatures, as indicated by the Inset of Fig. IV.12 (b).

Both the Schneider et al. and the current approach can interpolate the aging data. Both agree that a β-process is observed in the spectra, however this process appears significantly different within the two scenarios: in the former one it is partially submerged under the α-peak and it is identified with the EW, in the later is an additional relaxation feature. One should admit that the Schneider et al. interpretation appears somehow simpler, as their aging description involves only two processes. However, as we will try to demonstrate next, within the Schneider interpretation the β-process in type A systems must be of a "special" kind, different from the one typically observed in type B glasses.

Assuming an Arrhenius behavior for the time constants of the β-process ($\tau_{\beta} = \tau_0\exp(E_a/T)$ with a typical value for the attempt time $\tau_0 \approx 10^{-13}$ s, one can estimate a mean activation energy E_a from the position of the predicted β-

peak in the aged spectrum. From the Schneider et al. analysis the β-maximum at 179 K appears around 1 Hz (cf. Fig. IV.11 b), thus E_a (in K) must be on the order of 30·T_g. On the other hand, approach II predicts a β-peak that is by roughly four orders of magnitude faster, cf. Fig. IV.11 (a). From a simple fit of the peak using, *e.g.*, G_β function [11], one obtains $\tau_\beta \approx 1.6 * 10^{-5}$ s and, following the above considerations $E_a \cong 19 \cdot T_g$. This value appears much closer to those observed in type B systems [26], where E_a varies between 12·T_g and 24·T_g.

Further experiments are needed to clarify whether any of the two above analyses predicts the "true" position for the β-peak, *i.e.* to really identify its maximum position after aging. An attempt is made within this work for 4-TBP, a system that reveals in its spectra close to T_g the strongest high frequency curvature among all type A systems (cf. Fig. IV.2). The experiment is performed at 155 K, *i.e.* 10 K below T_g (165 K), where the structure relaxes within 150 hours. The aging analysis within the current approach is discussed in Appendix D. As in the case of glycerol, the high temperature stretching exponent of the α-peak and a symmetric β-peak with $E_a \approx 22 \cdot T_g$ are revealed after the subtraction of an EW power-law with an exponent $\gamma = 0.21$ from the overall equilibrium spectrum. Though the high frequency curvature gets more pronounced upon aging, we fail to reveal any peak maximum. Nevertheless, the author believes that this system remains a good candidate for separating a β-peak by aging at even lower temperatures, for longer times.

Following these considerations, to quantitatively interpolate the glycerol spectra close to T_g, the relaxation function is described as a three-step function and written as a product of three terms, explicitly $F(t) = F_\beta(t) F_{ex}(t) \phi_\alpha(t)$ in which F_β(t) and F_{ex}(t) denote the partial loss due to the β–process and the EW, respectively, and $\phi_\alpha(t)$ the overall relaxation due to the α–process. Introducing the corresponding relaxation strengths S_i one may write:

$$F(t) = [(1 - S_\beta)\phi_\beta(t) + S_\beta][(1 - S_{ex})\phi_{ex} + S_{ex}]\phi_\alpha(t) \qquad (IV.2)$$

For the β–process the symmetric distribution of relaxation times G_β discussed in Paragraph II.3.4 is applied. The parameters of the model are: τ_α and β for

the α-process, γ and S_{ex} for the EW and τ_β, S_β and the shape parameter *a* for β-process. The relative amplitudes of the processes are $1-S_\beta$ for the β-process, $S_\beta(1-S_{ex})$ for the EW and $S_\beta S_{ex}$ for the α-process. The stretching parameter of the α-process and the EW are kept constant $\beta = 0.63$ and $\gamma = 0.21$. As seen in Fig. IV.10 the fitting of the spectra at 181 K and 184 K works very well in the whole frequency range, as the β-process is additionally accounted.

The present approach has the advantage to consider the stretching parameters of the α-process and the EW as temperature independent, even though it allows for the presence of both secondary processes (EW+β-process). These constraints reduce considerably the number of free parameters in the analysis. Moreover, it offers the possibility to extend the investigations also below T_g, where for the first time "typical" β-processes can be identified and characterized also in type A systems, as discussed next.

Glycerol, $T < T_g$

The above analysis can be extended to temperatures below T_g where the α-peak exits the accessible frequency window. Assuming that the exponent of the EW is not changing even below T_g, one can isolate the symmetric β-peak and even some residual contribution from the α-process by subtracting the EW power-law contribution $A\nu^{-0.21}$.
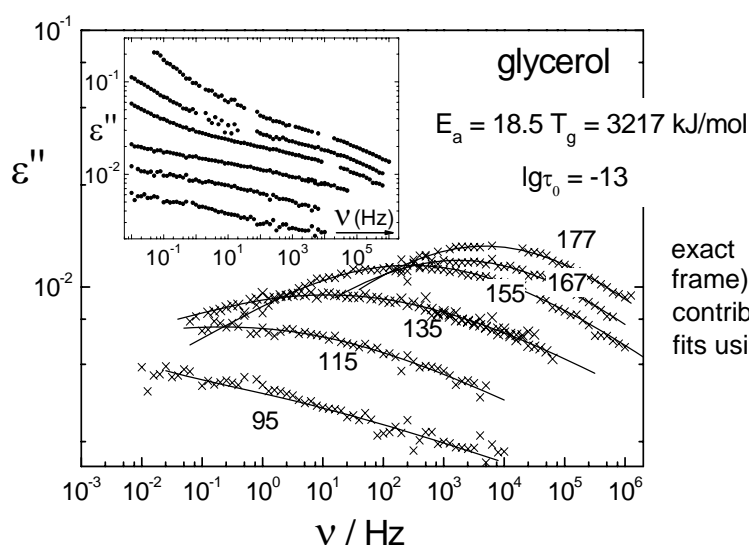
Fig. IV.13 The β-peaks of glycerol extracted from the dielectric spectra below T_g (shown in the Inset for the exact temperatures given in the main frame) by subtracting the EW contribution as $A\nu^{-0.21}$. The solid lines are fits using $G_\beta(\ln\tau)$, cf. II.3.4.

The same procedure as the one done for the aged spectrum is applied at T <

T_g. As demonstrated in Fig. IV.13, using approach II a typical β–peak is found for the first time for glycerol below T_g. In order to reveal the β-contribution at temperatures where one cannot access its maximum (below 115 K), the temperature dependence of A is extrapolated from above. The evolution of A(T), the time constants and the relaxation strength of the β-process are discussed in IV.4.2, where the results obtained within the same analysis for m-FAN are included.

Other type A systems

Next we analyze in the same spirit the dielectric spectra of propylene carbonate ($T_g \approx 158$ K) in the temperature range between 163 K and 179 K. Fig IV.14 contains datasets measured by Lunkenheimer et al. [25] (dots) and by Kudlik et al. [26] (circles). The dataset measured by Lunkenheimer et al. in the high-temperature regime is used here for defining the width of the α-peak. By this means we justified the choice of β = 0.78. This value is also indicated in Fig III.2 (b) where the α-peak scaling for PC is presented
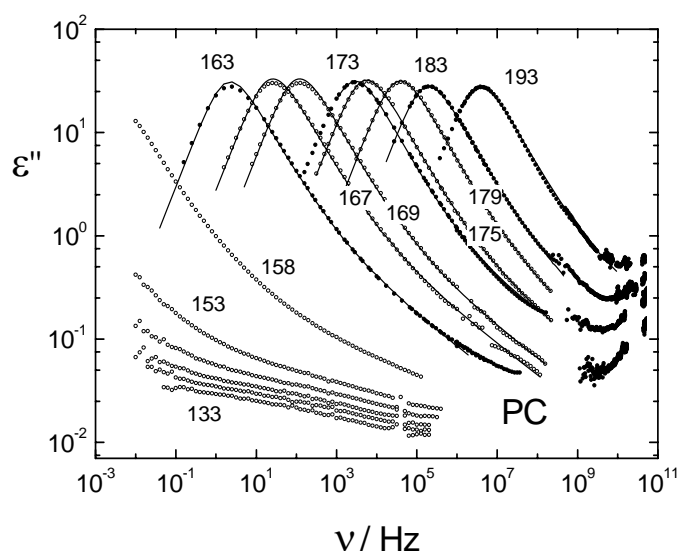
Fig. IV.14 (a) Selected dielectric spectra of PC as presented by Lunkenheimer et al. [25] (dots) and Kudlik et al. [26] (circles) at indicated temperatures (in K) with approach II fits (lines).

In order to identify the γ parameter of the EW one interpolates the spectra at 167 K and 169 K (where the EW is best defined) using a fixed β = 0.78. From these constrained fits a value for γ = 0.2 is obtained. Having now both stretching parameters β and γ, we keep them fixed for the analysis of all spectra above 163 K. Again, only three parameters are free: $1-S_{ex}$, τ_α and $\Delta\varepsilon$. The interpolations are good again, as seen in Fig. IV.14.

Unfortunately only two dielectric datasets (glycerol and PC) are measured in such a large frequency range allowing to identify in the high-temperature regime (above T_x) the stretching parameter of the α-process. In order to demonstrate that approach II can be also applied for datasets acquired in a more limited frequency range, the 2-picoline interpolations, plotted in Fig. IV.15, are discussed next. The gap in the 2-picoline experimental data is due to the unavoidable crystallization of this system [30].
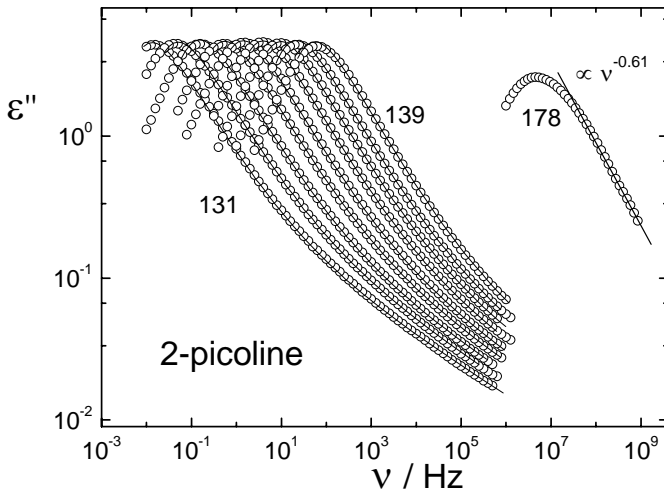
Fig. IV.15 Dielectric spectra of 2-picoline [42] together with approach II fits. Between 131 K and 139 K spectra are measured every 1 K.

Even though the high temperature regime may not be experimentally reached in this case, one may tentatively consider the single peak limit (where the EW contribution is negligible) to be the spectrum at the highest temperature here, T = 178 K. From a CD interpolation of this spectrum $\beta = 0.61$ is obtained. We then fit the spectrum at the lowest temperature around T_g (131 K), where the EW is best defined constraining $\beta = 0.61$. This strategy returns a value for $\gamma = 0.2$, as for glycerol and PC. Finally, all the spectra are interpolated keeping β and γ unchanged, thus the temperature variance of the overall spectral shape is mapped solely by the optimized $1-S_{ex}$. The interpolations are again close to perfect, cf. Fig. IV.15. The $1-S_{ex}$ results are discussed in IV.3.3, together with those obtained the other systems.

IV.3.2. Analysis of type B systems with EW contribution

m-FAN, T > T$_g$

In order to extend the approach II considerations to systems with well-resolved β-peak, previously classified as type B, the dielectric spectra of the glass former m-FAN are analyzed next in the temperature range 162 K – 182 K. This system shows a clearly discernible β–process and an EW close to T$_g$ (cf. Fig. IV.16). In order to account for the β-peak contribution, Eq. (IV.2) is used, as done above for the analysis of glycerol at T ≈ T$_g$.
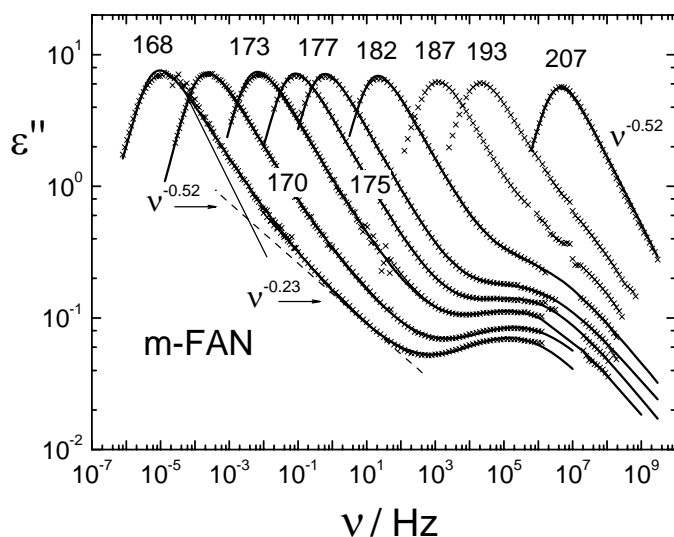
Fig. IV.16 Dielectric loss of m-FAN at indicated temperatures (in K) with approach II fits.

Again β is fixed at highest temperature, β = 0.52, as obtained from a CD fit of the spectrum at 207 K. The exponent of the EW, obtained from the fit of the spectrum at 168 K, where the wing is best resolved, is also fixed to γ = 0.23. The EW contribution at 168 K is indicated as the dashed line in Figure IV.16, where the fits with the three contributions (α-process, EW and β-process) are also included. No systematic deviation between fits and data is observed.

The parameters for the β-process of m-FAN above T$_g$ are plotted in Fig. IV.17. In this temperature range the β-peak shape appears to be temperature independent, as indicated by the evolution of the width parameter a(T) of the distribution G$_β$(lnτ). According to the inset (a) of Fig IV.17, a = 0.32 ± 0.02 in the whole temperature range above T$_g$. The temperature dependence of the time constant τ$_β$ can be interpolated by an Arrhenius law (see I.1), as shown

in the inset (b). The time constants display a weaker temperature dependence than in glass $T < T_g$ [11]. The only parameter that shows a significant change with temperature (as compared with its evolution in the glass) is the relative amplitude $1-S_\beta$. As previously mentioned in III.2.2, this strong increase of its amplitude is as characteristic for β-process above T_g.
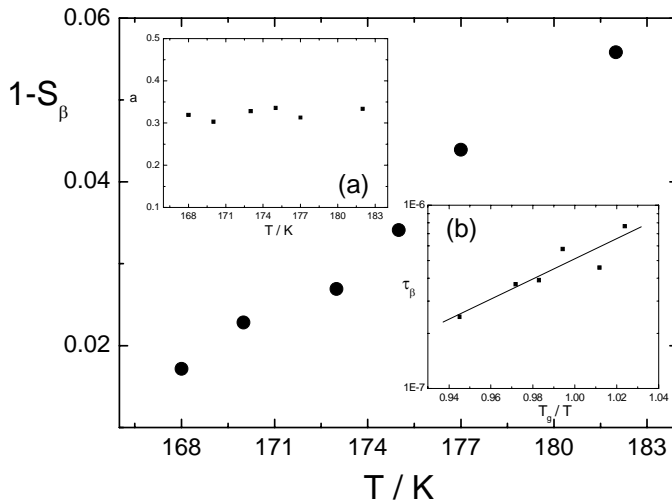
Fig. IV.17
Parameters of the β-process for m-FAN above T_g as obtained with approach II: in the main frame the temperature dependence of the relative amplitude $1-S_\beta$, and in the insets: (a) stretching parameter a(T); (b) time constant $\tau_\beta(T_g/T)$.

m-FAN, T < T_g

Below T_g the above analysis is not further possible due to the shift of the α-process out of the frequency window. However, the analysis is extended in the same manner as done for glycerol at $T < T_g$. In order to separate the individual spectral contributions, we assume that the exponent β of the remaining α-contribution is not changing below T_g. According to the Figure IV.18 (a) the EW is subtracted from the spectrum measured at 162 K as a power-law to reveal the α-contribution as proportional with $\nu^{-0.52}$ and a symmetric β-peak. The two conditions are fulfilled for $\gamma = 0.22$.

The β-peaks can be extracted in this manner for the temperature range down to say 130 K. As discussed for the case of glycerol, the temperature dependence of the EW prefactor *A* close to T_g was extrapolated at lowest temperatures. The parameter A for glycerol and m-FAN is plotted in Fig. IV.19 (a) as a function of temperature and in (b) as a function of the reduced temperature T/T_g. The temperature dependence A(T) is very similar for both systems and A even appears as identical in the reduced temperature

representation. Note that A increases with temperature above T_g, though the relative contribution $1-S_{ex}$ of the EW with respect to the α-process decreases instead.
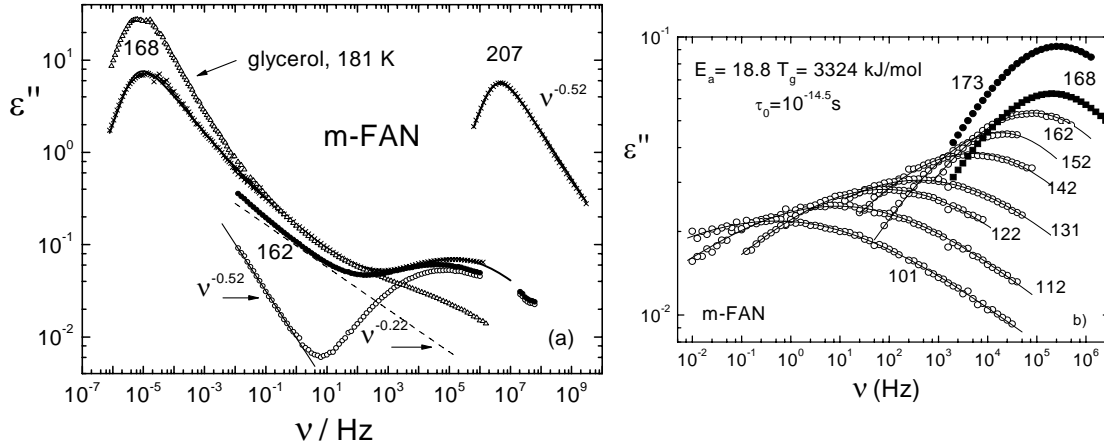
Fig. IV.18 (a) The dielectric spectra of m-FAN at 207 K, 168 K and 162 K together with the resulting spectrum after subtraction of the EW contribution at 162 K. The spectrum of glycerol measured at 181 K is added for comparison. (b) β-peaks of m-FAN extracted from the dielectric spectra at $T \leq 162$ K with fits. Data at 168 and 173 K are generated from the fits with Eq.(IV.2).

The extracted β-peaks are plotted in Fig. V.18 (b), together with their interpolations using the G_β distribution [11]. We included the individual β-contribution extracted from the fits for two spectra measured above T_g. For these two β-peaks it appears that only their amplitude changes with T.
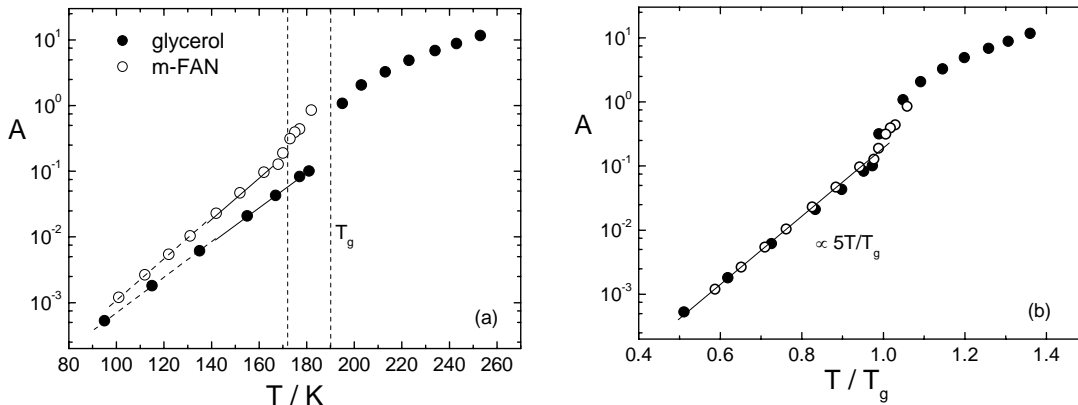
Fig. IV.19 (a) The prefactor A of the EW power- law $A\nu^{-\gamma}$ for glycerol, and m-FAN as function of temperature T_g are indicated by the dashed lines. (b) Same results in (a) now as a function of the reduced temperature T/T_g.

The exponent γ for m-FAN is close to 0.2, as for the other systems investigated here. We added in Fig V.18 (a), for comparison, the spectrum of

glycerol measured at 181 K. One can recognize that in the intermediate frequency range (attributed to the EW) the two spectra appear similar, pointing to a common exponent γ.

The time constants τ_β for m-FAN are compared in Fig V.20 with those extracted for glycerol. From the Arrhenius temperature dependence the activation energy of the β-process for m-FAN can be estimated to $E_a = 18.8$ T_g. E_a appears similar for the two systems. For glycerol the value of $E_a = 18.5$ T_g is close to the one estimated from the aging interpretation.

Regarding the residual contribution of the α–process, its "isostructural" relaxation time below T_g can be estimated assuming that its relaxation strength stays temperature independent in the glass. The data points fall below the equilibrium liquid line of $\tau_\alpha(T)$ but are expected to converge on it upon sufficiently, yet inaccessibly long aging, cf. Fig. IV.20.
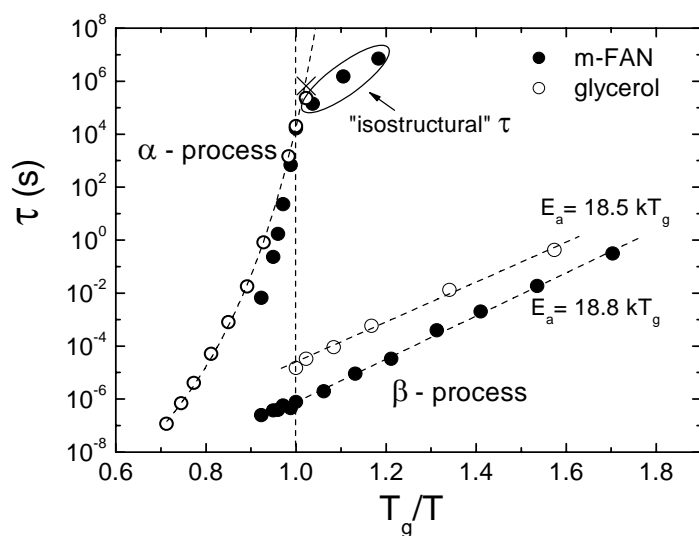
Fig. IV.20. The relaxation times of glycerol and m-FAN in the temperature activation plot.

To conclude, the approach II can be extended also for type B systems that exhibit a well-defined EW in their spectra above T_g. The good interpolations demonstrate that the spectra above T_g consist of the α-peak obeying FTS, a β-process with characteristics in accordance with previous investigations and an EW with a temperature independent exponent close to 0.2. From the evolution of the approach II parameters, it appears that the differences observed between the spectra of the type A glycerol and type B m-FAN (introduced in I.1) appear only due to a different amplitude of the β-process.

IV.3.3. The excess wing at $T > T_g$

The temperature dependence of the EW amplitude ($1-S_{ex}$) for all the systems analyzed above is presented in Fig. IV.21 (a). The relaxation strength of the EW decreases with temperature, as previously mentioned. Assuming a linear temperature dependence, $1-S_{ex}$ extrapolates to zero at a certain temperature. For glycerol and PC this crossover temperature is close to (slightly above) T_x determined from approach I, and also to the Stickel temperature [32].
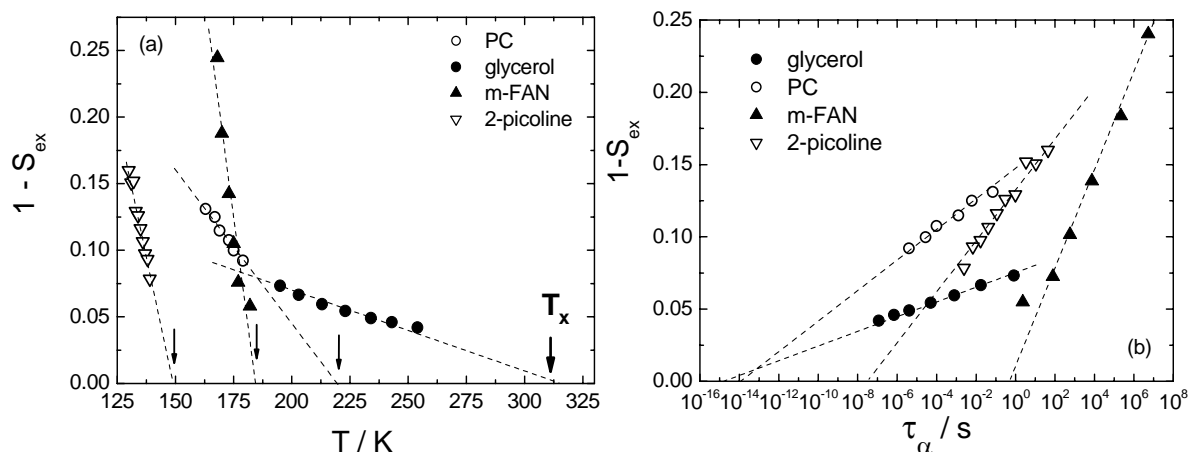
Fig.IV.21 (a) Temperature dependence of the relative relaxation strength $1-S_{ex}$ of the EW for m-FAN, glycerol, PC and 2-picoline. Linear extrapolation yields crossover temperature T_x (indicated by arrows); (b) $1-S_{ex}$ data from (a) now as a function of τ_α.

However, if the results for $1-S_{ex}$ are plotted as functions of the time constants of the α-process, as done in Fig. IV.21 (b), one can estimate an approximately linear dependence also in this case. According to this extrapolation, the EW contribution for m-FAN becomes negligible in this analysis already at high τ_α due to the dominant β-contribution here. For this system the vanishing of the EW cannot be identified with the crossover to the high-temperature regime, since in this case the β-process still contribute to the spectral shape of the slow dynamics. On the other hand, one may speculate that for glycerol and PC the EW may be present in the spectra measured up to highest temperatures, as it seems to vanish at a time constant in the vibration limit. Accordingly, the fast dynamics may obscure the relative small EW contribution here. This point of the analysis will be readdressed in Chapter VI.

Independent of any representation, we note that for type A glycerol, PC and 2-picoline the small parameter $1-S_{ex}$ changes within a factor 2 in the whole temperature range above T_g, reflecting the minor changes in the peak scalings shown in Fig. IV.5 (b).

IV.4. Consequences of approach II

IV.4.1. Unperturbed type A characteristics

It is interesting that the EW exponent appears to be not only temperature independent, but also system independent, *i.e.* $\gamma \approx 0.2$. In order to further check this non-trivial result of the analysis, we focus next on glass-formers for which the β-contribution is minimal or, alternatively, fast and well separated from the α-peak. For these systems the type A characteristics should be less affected by the β-contribution and, within the light of the above results, the unspoiled EW exponent should appear as $\gamma \approx 0.2$ in the temperature range below T_g.
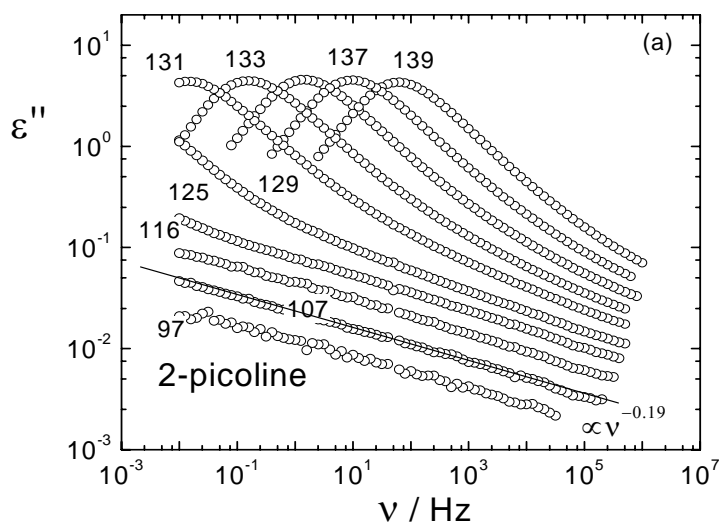
Fig. IV.22 Dielectric spectra of 2-picoline in the temperature range 139 K– 97 K from [26]. The solid line is a power law $A\nu^{-0.19}$.

The glass forming 2-picoline is a system which appears, at first glance, to show no curvature in its spectra close to and below T_g, cf. Fig. IV.22. This is easily proved by the good interpolation of the spectrum at 107 K extending over eight decades in frequency by using a simple power-low $A\nu^{-\gamma}$. The exponent γ of the power-law is in this case $\gamma = 0.19$, close to the one discussed above, and it appears as not changing with temperature below T_g.

Next we present in Fig. IV.23 the results for m-TCP investigated at temperatures close and below T_g. The measurements between 200 K and 160 K and are obtained as part of this work by employing an Alpha Analyzer[*] from Novocontrol [149]. The lower resolution limit of the Alpha spectrometer (almost one decade below the one of the Schlumberger spectrometer, cf. II.2) allows to monitor the evolution of the EW in the glass. In a broad (low) frequency range the spectra below 200 K can be interpolated by power-laws $A\nu^{-\gamma}$ with a temperature independent exponent γ. The value of γ is again 0.2. This system shows no β-peak in the spectra above T_g (cf. Fig. IV.2), however, a secondary peak appears at much lower temperatures, cf. Fig. IV.28. The maximum of the peak is revealed only if the AH2700 high precision bridge is applied, as shown later.
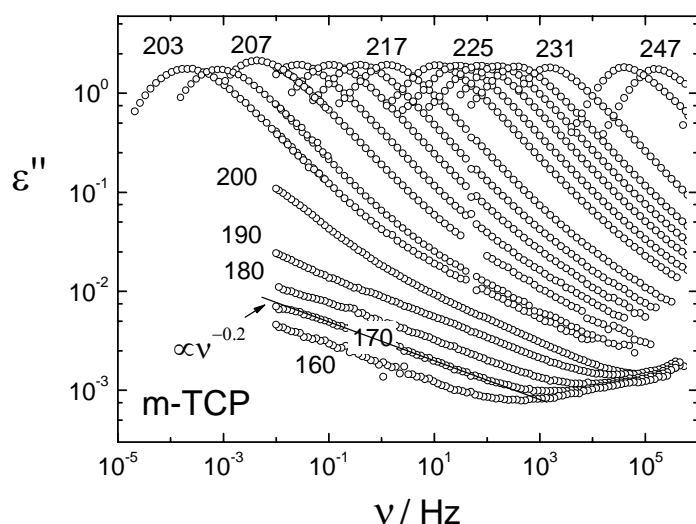
Fig. IV.23 Dielectric spectra of m-TCP as obtained using the Schlumberger spectrometer for 247 K > T > 203 K from [43] and the Alpha spectrometer (this work) for 190 K > T > 160 K . Above T_g, few temperatures (in K) are indicated. Solid line: a power-law with exponent -0.2.

We finally present the TMP spectra measured below T_g. This system was already introduced in IV.I. For the intermediate temperature range below T_g down to say 100 K the spectra contains two contributions. As seen in Figure IV.24 (a), one arises from the EW as a power-law $A\nu^{-\gamma}$ exponent $\gamma = 0.19$ that does not change from 130 K to 100 K, and the second one from a fast β-process. Below 100 K the β-peak can be analyzed with the distribution G_β (cf. II.3.4). The resulting time constants τ_β are plotted together with the results for the α-process in Fig. IV.24 (b). The β-process in TMP is fast, well separated

---

[*] This spectrometer was only recently acquired by our group and used in this work only for m-TCP investigations.

from the α-peak ($E_a = 15.5 \cdot T_g$), thus favoring the investigation of the resolved EW.
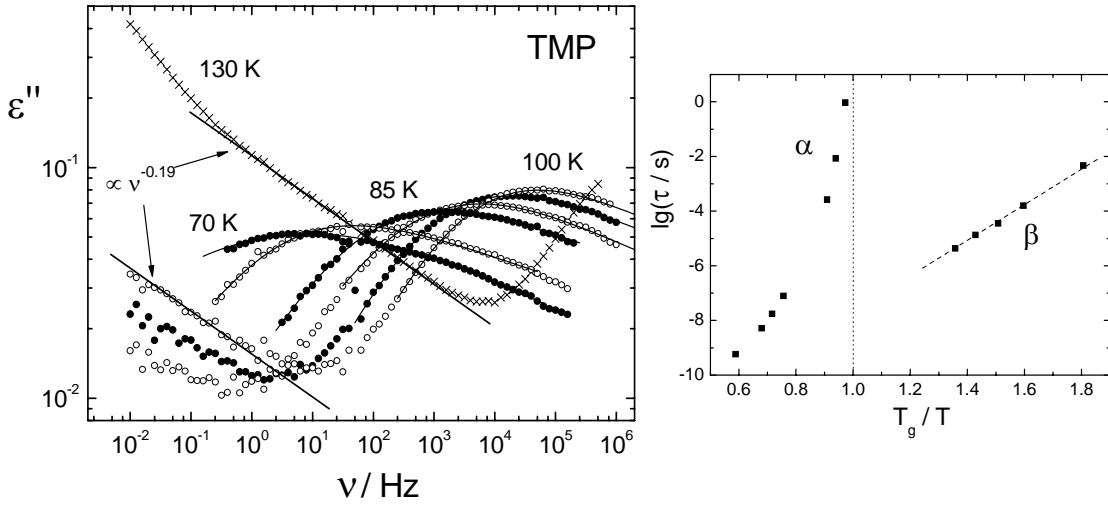
Fig. IV.24 (a) Dielectric spectra of TMP in the temperature range below T_g down to 70 K together with G_β fits for the β-process. Solid lines are power laws $A\nu^{-0.2}$ (b) Time constants for the α- and β-processes as function of the reduced temperature T_g/T. The dotted line indicates T_g and the dashed line is an Arrhenius fit.

In order to compare the temperature dependence of the EW amplitude for the systems discussed above, namely 2-picoline, m-TCP and 4-TBP, the prefactor *A* of the power-law $\varepsilon''_{EW} = A\nu^{-\gamma}$ is plotted in Fig. IV.25 as function of the reduced temperature T/T_g. Note that the parameter A is just the value of ε''_{EW} at 1 Hz. Here are also included the results for glycerol and m-FAN from Fig. IV.19, obtained within approach II analysis (model dependent).
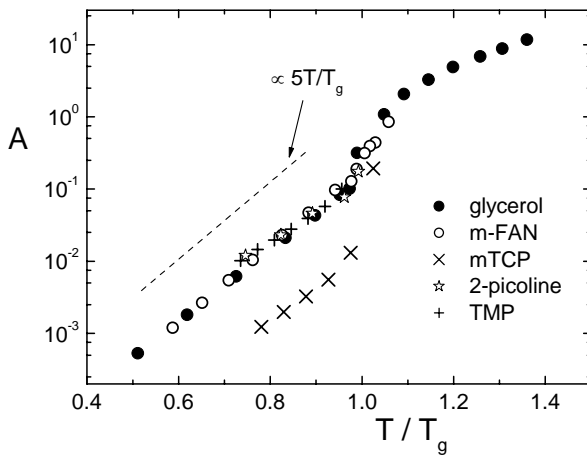
Fig. IV.25 The prefactor A of the EW power-law $A\nu^{-\gamma}$ as function of the reduced temperature T/T_g.

For all systems an exponential temperature dependence for $A(T/T_g)$ is observed and, with the exception of m-TCP, the parameter A appears as

identical in this representation. As it will be shown later, this is a consequence of a similar molecular dipole moment of these systems.

As suggested by the dashed line, the slope of lgA(T/T_g) is close to 5 for all systems, thus one may write for the EW below T_g:

$$\varepsilon''_{EW}(\nu, T) \propto \nu^{-0.2} exp(5T/T_g) \tag{IV.3}$$

Further systems with fast β-process should be investigated to check if they reveal the same behavior as m-TCP or TMP: for temperatures below T_g, the spectra should consist of both the β-contribution and an EW with a power law exponent $\gamma = 0.2 \pm 0.01$.

IV.4.2. The Nearly Constant Loss

According to previous investigations, type A glass-formers show similar relaxation features in the supercooled regime but also in the intermediate temperature range below T_g [26,75]. Here, the extremely broad spectra can be interpolated, in the first approximation, by a simple power-law, *i.e.* $\varepsilon''(\nu) = A\nu^{-\gamma}$ with an small exponent $\gamma \approx 0.1$ - 0.2, resembling the previously called nearly constant loss (NCL). In the previous investigated temperature range from T_g down to say, 50 – 70 K, exponent γ was found almost material and temperature independent, and the prefactor A revealed a similar exponential temperature dependence, *i.e.* $A \propto exp(T/T_{NCL})$ with $T_{NCL} \cong 34$ K for most of type A glass-formers investigated in the kHz regime. This relaxation behavior is revealed not only by dielectric data, but also by NMR and acoustic attenuation measurements [26].

Examples of NCL spectra can be depicted from Fig. IV.13 (Inset) for glycerol, Fig. IV.14 for PC, Fig. IV.22 for 2-picoline and Fig. IV.23 for m-TCP. According to the discussion above, for 2-picoline and m-TCP this NCL is nothing else than the pure EW with the exponent $\gamma \approx 0.2$. On the other hand, for glycerol or 4-TBP the NCL results from the interplay the overwhelming EW contribution and a weak β-process. For these systems the weak β-contribution may change the apparent exponent α from $\gamma \approx 0.2$, as commonly observed at $T \approx T_g$, to lower values ($\gamma \approx 0.1$) in the glass, cf. Fig. IV.26 (a). For m-TCP the

power-law analysis at low temperatures is hampered by the presence of the fast β-process.
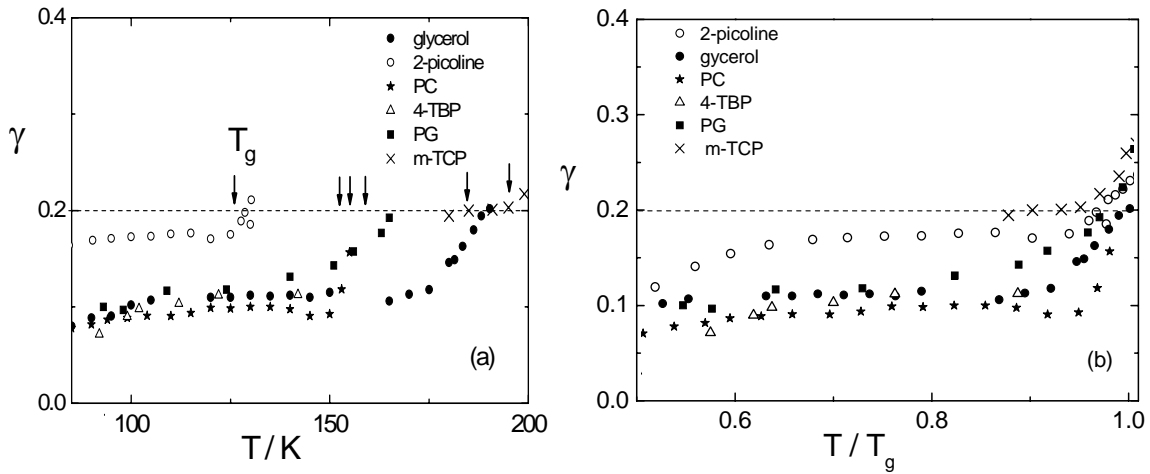
Fig. IV.26 (a) Power law exponent γ at temperatures close to and below T_g (indicated by an arrow for every system). (b) γ from (a) vs. reduced temperature T/T_g.

According to approach II, one expects a common exponent for all systems at T_g. In order to demonstrate this, γ is displayed as a function of T/T_g in Fig. IV.26 (b). As observed here, γ at $T/T_g = 1$ appears as universal.
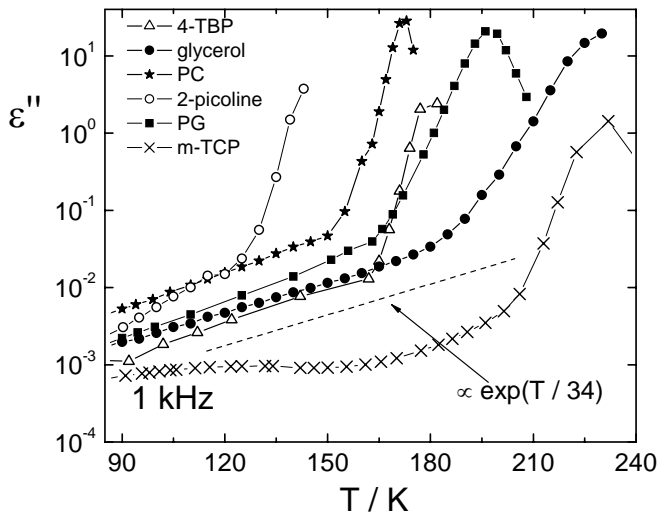
Fig. IV. 27 Temperature dependence of ε'' at 1 kHz; the dashed lines corresponds to an exponential dependence $\varepsilon''(T) \propto \exp(T/T_{NCL})$ with $T_{NCL} = 34$.

In type A systems the EW contribution is larger than the one of the β-process at temperatures above, as well below T_g, where the NCL is discussed. This difference in the amplitudes of the two processes can be depicted from the aging analysis for glycerol and 4-TBP (cf. IV.3.1 and Appendix D). As the EW dominates here, the temperature dependence of its amplitude below T_g (see Fig. IV.25), $A \propto \exp(5T/T_g)$ is in agreement with the previous observed

exponential temperature dependence for the NCL. _i.e._ A $\propto$ exp(T/T$_{NCL}$) with T$_{NCL}$ $\cong$ 34 K. This is justified by the fact that for most of the systems considered here T$_g$ $\approx$ 5T$_{NCL}$.

The amplitude of the EW decreases faster than the one of the β-process and the latter dominates the spectra at temperatures far below T$_g$: for example, the EW amplitude A (ε''_{EW} at 1 Hz) in the glycerol spectrum at 95 K is below 10^{-3} (cf. Fig. IV.19 a), while the amplitude of the β-process at 1 Hz is clearly above, cf. Fig. IV.13. If this is true, one should be able to scale the spectra attributed to the thermally activated β-process at such low temperatures, ending the NCL regime. As demonstrated later in V.3.2 this is indeed the case for glycerol.

IV.4.3 The influence of the molecular dipole moment on the amplitude of secondary processes

For glass formers with very small β-contribution (type A) the dielectric response in the glass appears quite uniform, cf. Fig. IV.27. According to this figure, the amplitude of the dielectric response of type A systems in the glass appears to correlate with the amplitude of the α-peak. This is not the case for type B systems, as discussed next.

For comparison, the temperature dependence of the dielectric loss ε''(T), measured at 1 kHz, is present in Fig. IV.28 for systems with strong β-processes, that may obscure the presence of any EW contribution below T$_g$. The data are obtained as part of this work by applying the high-precision bridge AH 2700. In Fig. IV.28 only single frequency data are presented, while the results obtained within three decades in frequency (covered by the bridge) are analyzed in details in next Chapter.

For type B systems the ε''(T) curves appear as distinctive. At high temperatures, above T$_g$, ε''(T) is dominated by the α-peak, while in the glass by the β-peak. For the high molecular mass PB2000 even two secondary relaxation peaks can be identified in the glass, as discussed in details in Chapter VII. The data for m-TCP are also added here to indicate a β-contribution at low temperatures.
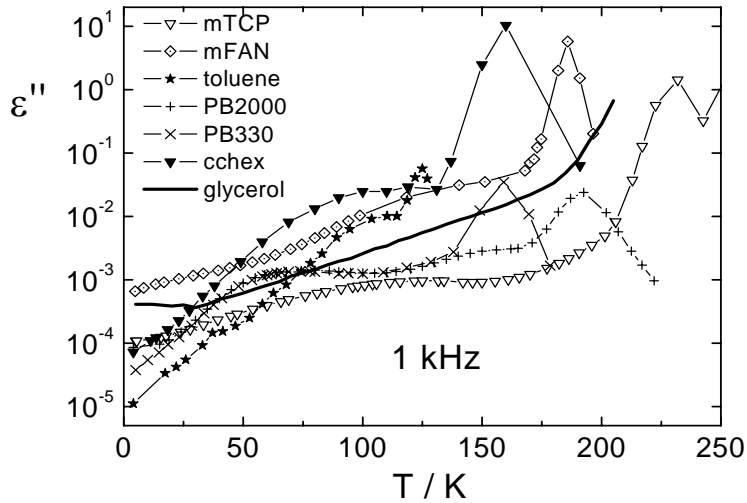
Fig. IV.28 Temperature dependence of ε'' at 1 kHz for the type B systems and glycerol as obtained with the high precision bridge.

As for these systems the β-contribution appears not to correlate with the α-amplitude (cf. also Fig. IV.8.b), it becomes interesting to present all the data (for type A and type B) scaled by the value of the molecular dipole moment that controls the amplitude of the latter.

Up to our knowledge, such a scaling was not done yet. This maybe due to the fact that one cannot find in literature the values for the molecular dipole moments μ_{mol} for many molecular systems. In order to overcome this problem, we estimate μ_{mol} using the Curie law at temperatures well above T_g, as discussed next.

The Curie law (introduced in II.1) relates the dielectric strength $\Delta\varepsilon$ of any relaxation process with the relaxing dipole moment μ, the number density of the dipoles in the dielectric material and the temperature T:

$$\Delta\varepsilon = \frac{n\mu_{mol}^2}{3\varepsilon_0 kT} \tag{II.6}$$

This law was found to interpolate well the data for the α-process for low viscous liquids, however, it usually fails for high viscous liquids close to T_g [117]. In order to access the values of μ_{mol}, we evaluated for most of the systems the dielectric strength of the α-process $\Delta\varepsilon = \varepsilon_s - \varepsilon_\infty$ at the highest accessible temperature (T_{ref}), where the Curie law should hold best. For

74

systems the dielectric strength of the α-process $\Delta\varepsilon = \varepsilon_s - \varepsilon_\infty$ a*t the highest accessible temperature* (T_{ref}), where the Curie law should hold best. For systems with very low dipole moment as, *e.g.* toluene and PB, $\Delta\varepsilon$ could not be evaluated directly from $\varepsilon'(\nu)$ data. Instead, $\Delta\varepsilon$ was obtained as a fitting parameter in the interpolation of the spectra $\varepsilon''(\nu)$ cf. analysis in IV.2. The reference temperatures T_{ref} and the corresponding values of the strength $\Delta\varepsilon_{ref}$ used in the analysis are posted in Table IV.1.

	System	*T_{ref} (K)*	*$\Delta\varepsilon_{ref}$*
	Glycerol	413	23.8
	PC	212	65
Type A	2-picoline	202	6.5
	Salol	245	3.9
	4TBP	187	10.1
	m-TCP	260	4
Type B	m-FAN	198	17.8
	Toluene	127	0.3 (from[26])
	PB330	200	0.06 (from [26])

Table IV.1. The values of T_{ref} and $\Delta\varepsilon_{ref}$ used for the evaluation of the molecular dipole moments μ_{mol} according to the Curie law.

Taking for granted the Curie law at such high temperatures, the following relation should hold:

$$\mu_{mol}^2 = \frac{3\varepsilon_0 k T_{ref} \Delta\varepsilon_{ref}}{n} \tag{V.4}$$

Since the number density for the systems under consideration vary within a factor smaller than 4 (cf. discussion in V.2), one just have to divide ε'' by the product $T_{ref}\Delta\varepsilon_{ref}$ in order to scale out the contribution of the dipole moment.

The result of this scaling is shown in Fig. IV.29. Here $\varepsilon''/(T_{ref}\Delta\varepsilon_{ref})$ is plotted as a function of the reduced temperature T/T_g for all systems investigated in this work down to cryogenic temperatures, around 4 K. Some interesting features are revealed: the systems that do not exhibit secondary relaxation peaks the dielectric loss ε'', above and also below T_g exhibit a quite similar behavior. Among these systems the corresponding amplitudes of the α-process, the NCL, the ADWP peak and the tunneling plateau (the last two are discussed in

the next Chapter) vary within a small factor below 5. For systems with strong β-contribution the scaling works well at the highest and the lowest temperatures, but not in the temperature range dominated by the β-peak, *i.e.* the β-process does not scale with the molecular dipole moment. As suggested by the behavior of the systems with fast β-processes (*e.g.*, 4-TBP or m-TCP) close to T_g, one may speculate that the EW is always present in molecular glasses as a relaxation background that may be obscured in cases of strong β-contribution.
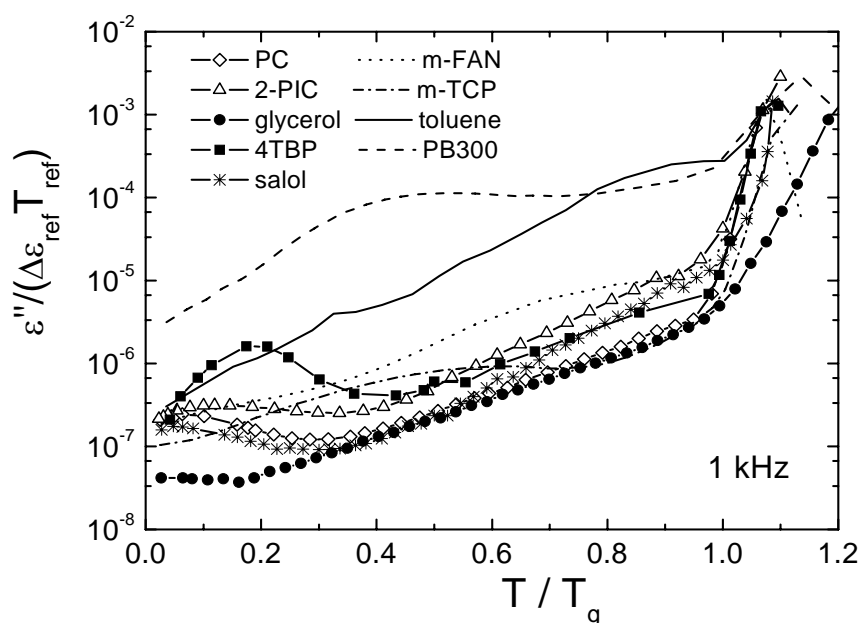
Fig. IV.29 The imaginary part of permittivity ε" for all molecular glasses investigated in this work down to 4 K, scaled by the molecular dipole moment (see text for details) in the reduced T/T_g scale.

Another remarkable fact is that by scaling out the dipole moment, independent from the particularities observed above, the data at lowest temperatures collapse to a system independent constant value for most of the systems. As discussed in the next Chapter, this may be taken as an indication that the tunneling regime is reached for molecular systems at such low temperatures, below, say, 10 K.

IV.5 Conclusions

According to the proposed scenario (approach II), the long-time part of the overall relaxation in molecular systems (α-process) keeps its shape and thus obeys FTS at all temperatures. The corresponding stretching parameter β is taken from the high-temperature spectra; here the analysis is not hampered by the appearance of any secondary relaxation processes thus β can be determined unambiguously.

As demonstrated by the good interpolations, the EW exponent γ can also be chosen as temperature independent. Thus, the overall spectral evolution for systems exhibiting no discernible β-manifestation above T_g (previously introduced as type A), is essentially attributed only to a small variation of the relative weight $1-S_{ex}$ of the EW with respect to the α-peak. At variance with the behavior of the β-process, the EW contribution decreases with temperature. A crossover temperature T_x can be estimated, at which the EW contribution vanishes. The crossover to a single peak susceptibility at high temperatures can be indicated by the linear extrapolation of $1-S_{ex}$ to zero value at $T = T_x$. This crossover temperature T_x is similar with the Stickel temperature or with the one obtained from GGE analysis.

The EW exponent appears also as system independent $\gamma \approx 0.2$. According to this approach, both EW and β-process are always present in the spectra of molecular systems close to T_g. In "type A" systems the weak β-contribution manifests itself only as a small curvature in the spectra close to T_g, when both the α-process and the EW become well separated from the latter. Based on their different temperature evolution, the contributions of both secondary processes (EW and β-process) are disentangled close to T_g, and the corresponding aging experiments are reinterpreted upon such considerations. As shown, typical β-processes can be revealed and analyzed also in type A systems below T_g. Within this scenario, the NCL previously discussed can be interpreted as an interplay of the dominating EW and a weak β-process, both surviving in the glass.

IV. Results; relaxation properties of molecular glass formers

V. Results; Low temperature relaxations in molecular glasses (T << T$_g$)

As discussed in III.3.2, glasses at low temperatures below, say, 10 K, exhibit a peculiar physical behavior with respect to crystals. Thermal properties, as well as acoustic attenuation, show similar values for all (inorganic) glasses studied so far, pointing to universality. In this temperature range the mechanic/dielectric relaxation profile displays a weak temperature and frequency dependence, close to a "plateau". While this relaxation behavior can be interpreted within the standard tunneling model (STM), the theory cannot explain the universality of the phenomena.

Above 10 K the relaxation behavior becomes system dependent and the relaxation response appears as a more or a less pronounced peak when loss is plotted as function of temperature. To describe this behavior the TM was extended to high temperatures at which thermally activated dynamics in asymmetric double well potentials (ADWP) is expected to dominate the relaxation. For a detailed data analysis the distribution of barrier heights g(V) is needed as input, and in most cases an exponential distribution was found to be suitable. However, there are examples when the data cannot be reproduced by the thermally activated ADWP model, even though such an extension of the TM to higher temperatures appears as natural.

The purpose of this work is to extend the previous investigations of the dielectric response of molecular glasses down to cryogenic temperatures by applying the high precision bridge AH2700 (described in II.2.1). By using this bridge, three decades in the frequency dependence of the dielectric loss in molecular glasses can be accessed at such low temperatures. Up to now, a systematic study of the dynamics of such glasses covering the full temperature range below the glass transition temperature T$_g$ down to say, 1 K is missing.

Within the approach II, the nearly constant loss (NCL), experimentally accessed for some molecular systems, is a universal relaxation background, observed only if the β-contribution is small enough. In such cases the NCL is dominated close to T$_g$ by the excess wing (EW) that survives in the glass as a universal power-law $\propto$ exp(5T/T$_g$)$\nu^{-0.2}$. The β-process is perturbing this universality, as its amplitude does not scale with the molecular dipole moment. In order to extend the investigations of the relaxation features not obscured by the presence of a strong β-process towards lower temperatures, the following discussion starts with type A systems. The discussion is extended afterwards for systems with well-resolved β-peaks.

The following questions are addressed in this Chapter: down to what temperatures the dielectric spectra are still dominated by the contribution of the secondary processes, namely excess wing (EW) and β-process, both emerging already above T$_g$ and surviving into the glass? Can the tunneling regime be reached in the accessible temperature range (T > 2 K) for molecular glasses? Do the spectra in the tunneling regime follow the Standard Tunneling Model (STM) predictions? Does one find contributions from thermally activated Asymmetric Double Well Potential (ADWP) dynamics?

V.1 Experimental results and discussion

V.1.1 Systems with weak β-contribution (type A)

The previous dielectric investigations of glycerol, propylene carbonate (PC), salol, 2-picoline, m-tricresyl phosphate (m-TCP) and 4-tertbutyl pyridine (4-TBP) are extended down to cryogenic temperatures close to 2 K. The investigation in the temperature range from 4 K down to 2 K was possible by pumping liquid helium in the cryostat. The measurements for glycerol down to 0.03 K are performed in collaboration with Experimentalphysik V in Bayreuth (Prof. G. Eska); some measurement details are given in II.2.3. The investigated temperature range and the values of T$_g$ for every system are specified in Appendix A.

We present in Fig.V.1 the frequency dependence of the imaginary part of permittivity $\varepsilon''(\nu)$ for the glass formers PC, 2-picoline, salol and glycerol as obtained with the high-precision bridge in the full temperature range down to 2 K. The previously measured broadband data are also included. As seen, both datasets agree well in the common temperature range. Hansen and Richert also investigated salol down to 30 K with a single frequency bridge operating at 1 kHz [75]; their results are in good agreement with those presented here (see Fig. V.9 a).

The bridge measurements cover the frequency range 60 Hz – $2*10^4$ Hz and $\varepsilon''(\nu)$ are monitored to a minimum level of $5*10^{-5}$, as reached for salol. Clearly, the high precision bridge allows the investigation of the dielectric response towards lower temperatures by extending the previous resolution limit, and most important, accessing the frequency dependence of the permittivity.
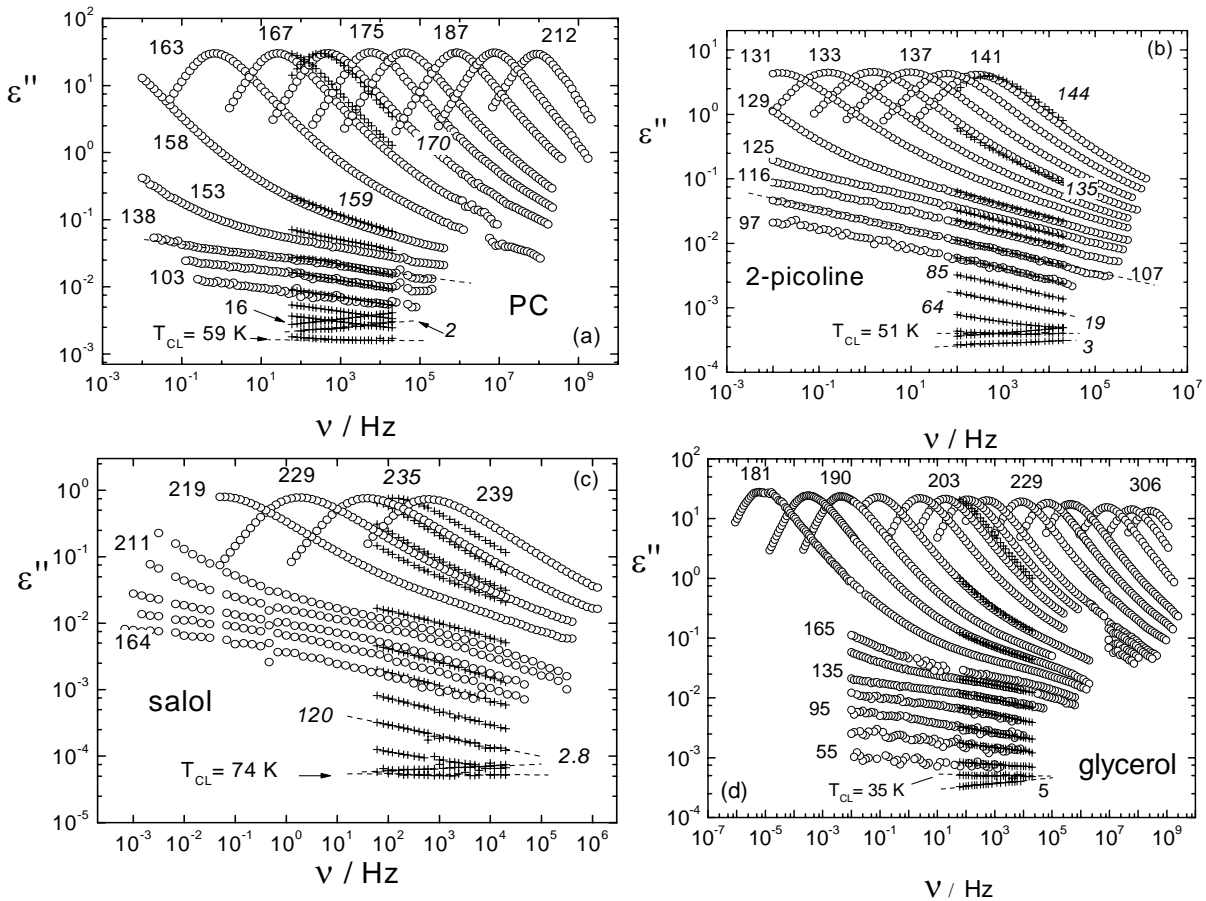
Fig. V.1 Selected dielectric spectra of PC (a), 2-picoline (b), salol (c) and glycerol (d). The data measured with the AH2700 bridge (crosses) are compared with those measured by the broadband technique (open circles), [26,27]; the dashed lines represent power-laws $\varepsilon''(\nu)=A\nu^{-\gamma}$. Few temperatures (in K) are indicated.

The spectra presented here show no indication of a distinct secondary β-relaxation maximum. Besides the shift of the α-peak, one can recognize the EW emerging above T$_g$. In the glass (T < T$_g$) the response gets very flat and the broadband spectra appear as power-laws with constant exponent, since only the amplitude of the signal changes with temperature. However, inspecting the high precision data measured at lower temperatures (below 100 K), one identifies, a crossover range in which the spectra change their slope while further cooling. For every system, at a given temperature (T$_{CL}$), the spectra become completely frequency independent, as a true constant loss is revealed here. The crossover temperature T$_{CL}$ is indicated by an arrow in Figs. V.1 and the values of T$_{CL}$ are posted in Table V.1 for all the systems considered in this Chapter. One example of a spectrum measured at T$_{CL}$ is shown in the Inset of Fig. V.2 (c) for salol.

The crossover is better observed when the results at different frequencies are plotted as function of temperature, as done in Fig. V.2: for all systems the datasets measured at different frequencies intersect at T$_{CL}$. With the exception of glycerol, below T$_{CL}$ ε''(T) develops to a maximum with lowering T, as an indication for the emergence of a different relaxation feature. At even lower temperatures, ε''(T) for 2-picoline, PC and salol exhibits a maximum, cf. Fig. V.2. However, an important observation is that this maximum in ε''(T) does not have an equivalent in the frequency dependence ε''(ν), as discussed later in details. For glycerol neither a minimum nor a maximum is recognized in ε''(T) below T$_{CL}$.

As mentioned above, the spectra measured with the bridge can be well interpolated by power-laws Aν$^{-\gamma}$. The power-law exponent γ at T < T$_g$ is plotted in Fig. V.3 as a function of temperature. In addition, the results for 4-TBP and m-TCP close to T$_g$ are included. As discussed in the next paragraph, these two systems reveal in their spectra a secondary relaxation peak, hampering the power-law analysis at temperatures well below T$_g$. For all systems, the exponent γ below T$_g$ saturates to a small value γ$_{NCL}$ (0.1 − 0.2), cf. also the discussion in IV.4.2. This regime of NCL, *i.e.* within the approach II the joint EW + β-process contribution, expands in a temperature range below T$_g$ down to 40 − 80 K, depending on system. Below this temperature the spectra

further flatten and γ decreases to 0 at T$_{CL}$. The increase of $\varepsilon''(T)$ below T$_{CL}$ correlates with the power-law exponent γ crossing over to a small but positive value, in the current terminology $\gamma < 0$.
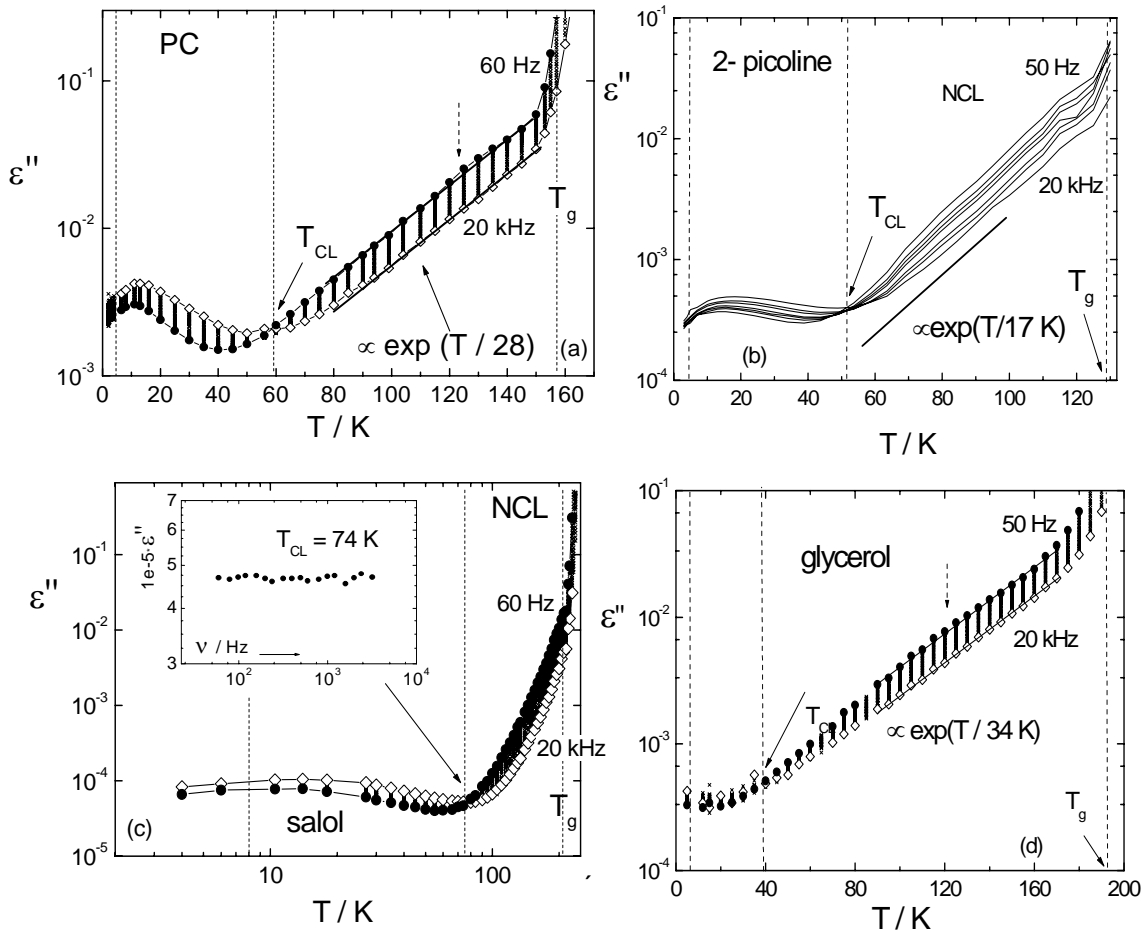
Fig. V.2 Temperature dependence of ε'' for (a) propylene carbonate (PC), (b) 2-picoline, (c) salol – logarithmic scale on T and (d) glycerol, measured with the high precision bridge. In (b) $\varepsilon''(T)$ is plotted for 7 frequencies between 50 Hz and 20 kHz, *i.e.* for every frequency it corresponds a line. For the other systems, data measured at 25 frequencies between 50 Hz and 20 kHz are plotted as small dots; for the sake of clarity, the extreme frequencies are highlighted. The solid lines in represent exponential temperature dependences ($\varepsilon''(T) \propto$ exp(T/T$_{NCL}$)). Inset (c): the spectrum of salol measured at T=T$_{CL}$ (see text for details). The dashed lines suggest different relaxation regimes.

An interesting observation is that independent of any individual details of the curve $\gamma(T)$ in Fig. V.3, it appears that a system independent exponent γ is reached at the lowest temperatures. Here all the spectra can be interpolated by power-laws with small and similar positive exponent (cf. also Fig. V.1). At such lowest temperatures the loss saturates to a plateau (best seen for salol

in Fig. IV.2. (c), where $\varepsilon''(T)$ is plotted in double logarithmic scale), as an indication of a even further relaxation regime below 10 K.
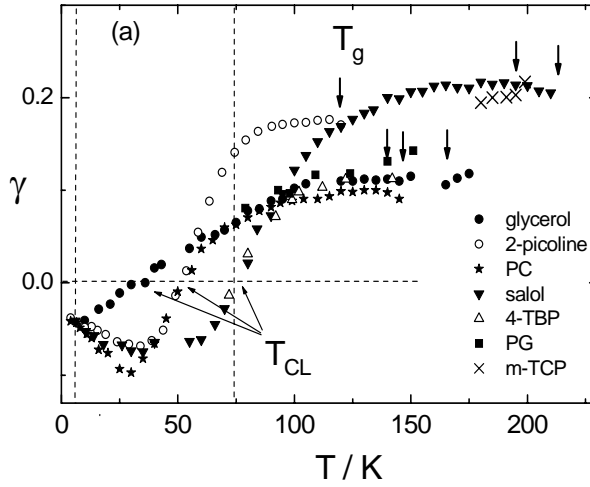
Fig. V.3 Power law exponent γ of the spectra at temperatures below T$_g$ (indicated by an arrow for every system). The dashed lines suggest different relaxation regimes.

In order to compare the results, the temperature dependence $\varepsilon''(T)$ measured at the single frequency of 1 kHz is presented in Fig. V.4 for all the glasses investigated here. The data shown are extensions of those plotted in Fig. IV.27, now down to 2 K. Similar relaxation features are found for all systems. Above T$_g$ the loss is governed by the appearance of the main relaxation (α-process) which leads to a strong increase of $\varepsilon''(T)$ with temperature. Inspecting the temperature dependence of ε'' in the range where γ is essentially temperature invariant, an exponential change is observed for all investigated systems. Explicitly, we rediscover, $\varepsilon''(T) \propto \exp(T/T_{NCL})$ for $v = 1$ kHz holding down to crossover temperature T$_{CL}$.

With the exception of 2-picoline, the parameter T$_{NCL}$ is similar within the different systems (close to 33 K), implying that the curves $\varepsilon''(T)$ in Fig. IV.4 are almost parallel. The values obtained for T$_{NCL}$ and γ_{NCL} are listed in Table V.1, where, for comparison, the results obtained by Kudlik et al. [26] and Hansen and Richert [75] are also included. Just to be remarked, within approach II the NCL close to T$_g$ is dominated by the EW contribution that survives in the glass as a power law $\varepsilon''_{EW}(v,T) \propto v^{-0.2}\exp(5T/T_g)$. Note in Table V.I that for most of the systems T$_g \approx 5\,$T$_{NCL}$ holds, in accordance with the discussion in IV.4.1.
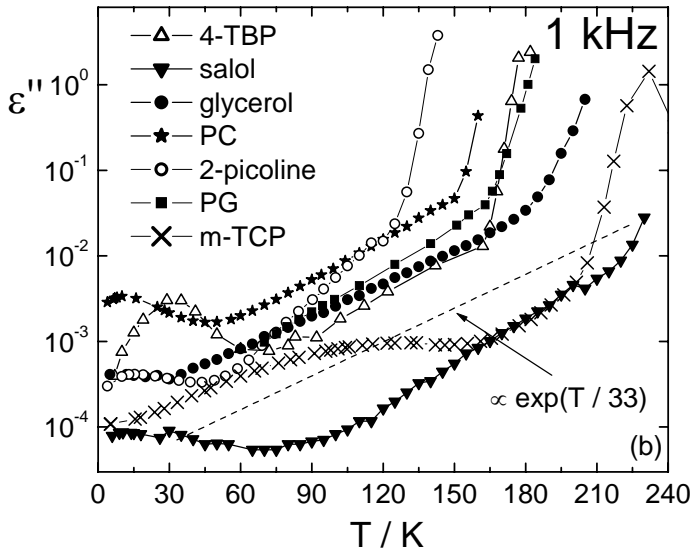
Fig. V.4 Temperature dependence of ε'' at 1 kHz for systems with type A characteristics at $T > T_g$. The dashed line corresponds to an exponential dependence $\varepsilon''(T) \propto \exp(T/33\ K)$.

Peculiarities

Though m-TCP and 4-TBP are type A glass-formers concerning their spectral shape above T_g, one can identify secondary relaxation peaks in their spectra $\varepsilon''(\nu)$ at much lower temperatures around $T_g/2$, as seen in Figs. V.5 (Inset) and V.6. This is at variance with what is observed for other systems at low T, where a peak is recognized in $\varepsilon''(T)$ but not in the spectra $\varepsilon''(\nu)$. The activation energy of these processes (few T_g's) is small as compared to the ones typically found for the β-process and may reflect the presence of internal degrees of freedom of the constituent molecules. Nevertheless, at much lower temperatures, the two systems also show the crossover to the additional relaxation feature marked by the constant loss temperature T_{CL}. Below T_{CL} the spectra changes their slope to positive, and, finally, at the lowest investigated temperature the spectrum can be interpolated by a power-law with a small and similar exponent with the one observed for the other systems discussed above.
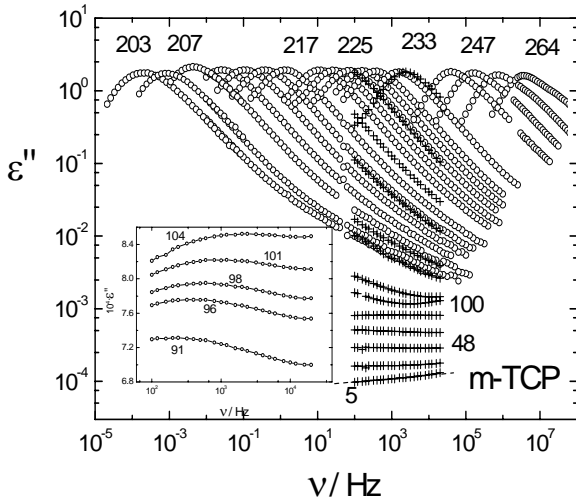
Fig. V.5 Dielectric spectra of m-TCP (T$_g$ = 205 K). Few temperatures (in K) are indicated. Inset: A fast secondary process is recognized as a peak deep in the glass, better recognized when the data are plotted in linear scale. Dashed line is a power-law with exponent 0.04.
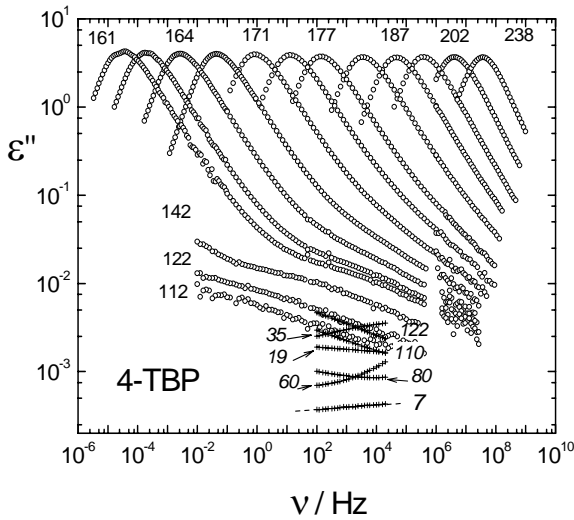
Fig. V.6 Dielectric spectra of 4-TBP (T$_g$ = 163 K). Few temperatures (in K) are indicated. Dashed line is a power-law with exponent 0.04.

	System	T_g (K)	T_{NCL}(K)	γ_{NCL}	T_{CL} (K)	T_{CL}/T_g	T_{NCL}/T_g
Type A	2-PIC	133	17	0.17	51	0.38	0.12
	PC	158	28	0.09	59	0.37	0.18
	4-TBP	163	31	0.11	75	0.46	0.19
	glycerol	189	34, 33[*], 34**	0.11	35	0.19	0.18
	PG	170	30, 34[*]	0.12	-	-	0.2
	salol	220	23, 22.5**	0.21	79	0.36	0.1
	m-TCP	205	-	0.2	48	0.23	-
Type B	m-FAN	172	-	-	54	0.31	-
	toluene	117	-	-	33	0.28	-
	PB 330	140	-	-	19	0.14	-
	CCH	134	-	-	23	0.17	-

Table V.1 Parameters of the "NCL". The numbers with * are obtained by Kudlik et al. [26] and those with ** by Hansen and Richert [75].

V.1.2. Systems with strong β-contribution

In the following we discuss the dielectric response of glasses that reveal already above T$_g$ a distinguishable secondary β-relaxation peak in their spectra. The results of ε''(T) at a single frequency 1 kHz have been already presented and discussed in IV.4.3. However, in order to reveal the frequency dependence of the loss for such systems, we present in Fig. V.7 the spectra of m-FAN, toluene, polybutadiene (PB) with the molecular mass of M$_w$ = 330 and the plastic crystal cyano cyclohexane (CCH), as measured in the whole temperature range down to 3 - 5 K. As observed, the spectra within the different systems appear as similar.
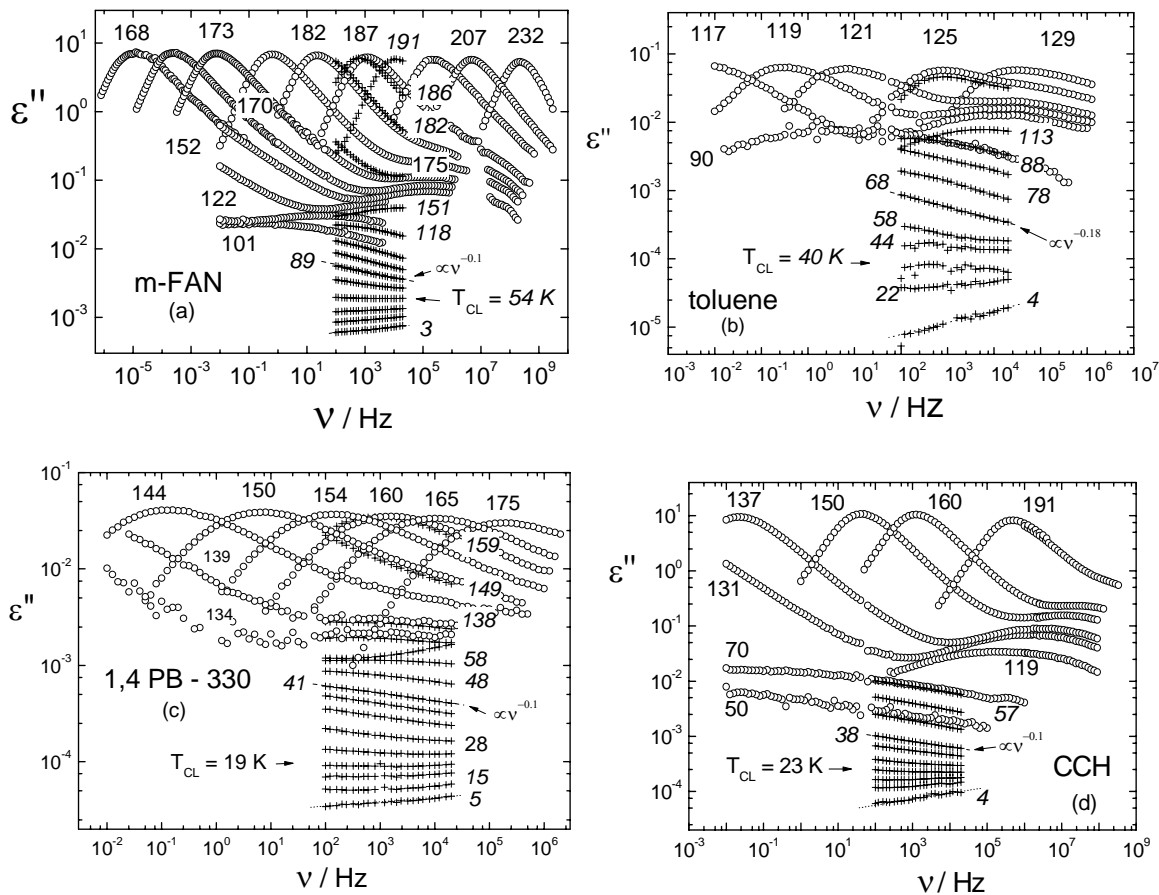
Fig. V.7 Dielectric spectra of m-FAN (a), toluene (b), PB 330 (c) and CCH (d). The new data (crosses) measured with the AH2700 bridge are compared with those measured by the broadband techniques (open circles), previously published in [26,148]; the dashed lines represent power-laws ε''(ν) = Aν$^{-\gamma}$. Few temperatures (in K) are indicated.

At temperatures close and below T$_g$ the relaxation pattern is dominated by the β-process. At lower temperatures the resolution limit of the broadband spectrometer is reached, thus the investigations are further carried out by

applying the high-precision bridge. As the β-peak moves out from the accessible frequency window, the remaining contributions appear as power-laws with a small and temperature independent exponent. As indicated by the power-law interpolations (dashed lines in Fig. V.7), the value of the exponent varies between 0.1 and 0.2 among the systems, resembling the behavior observed in systems with type A characteristics, cf. previous discussion. As generally observed, these (B) systems also exhibit at a given temperature (T_{CL}) a true constant loss that signals the crossover to a further relaxation regime below T_{CL}.

The similarities among A/B systems at such low temperatures are better observed when the exponent γ for m-FAN (extracted in the temperature range where the m-FAN spectra can be interpolated by power-laws) is directly compared with the one for glycerol in Fig. V.8. The main differences appears to be the value of T_{CL} for the two systems.
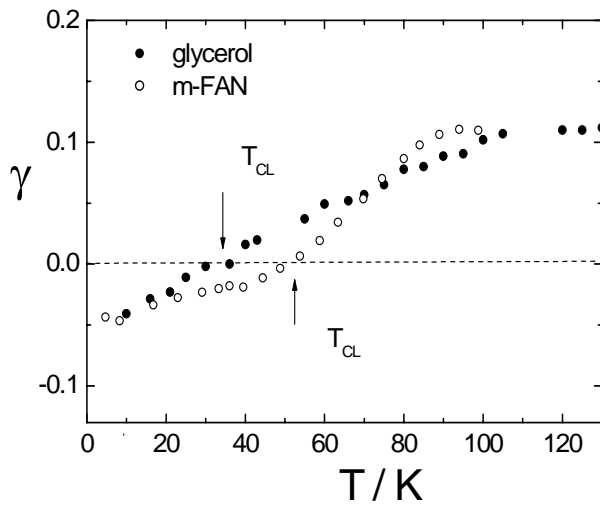
Fig. V.8 The exponent γ of the power-laws $A\nu^{-\gamma}$ interpolating the spectra of m-FAN and glycerol beyond the β-peak and NCL, respectively.

At lowest investigated temperatures the spectra appear similar within all the molecular glasses presented up to now (type A and type B). They can be interpolated by a power-law with a small positive exponent (close to 0.04), pointing to a final distinct relaxation regime that seems to have universal characteristics.

To summarize, for all molecular systems three different relaxation regime can be identified below T_g :

I.   Between T_g and T_{CL} some systems exhibit a behavior resembling the NCL while for others the β-process dominates the relaxation here.

Special cases are m-TCP and 4-TBP that present NCL behavior close to T$_g$ and a fast β-process close to T$_{CL}$.

II.   Below T$_{CL}$ down to say 10 K for all the systems the spectra can be interpolated with power-laws with positive, small and temperature dependent exponent. For salol, PC and 2-picoline there appears a peak in ε''(T) but not in the spectra $\varepsilon''(\nu)$, while for the other glasses no such peak can be recognized.

III.   At lowest temperatures T < 10 K for all systems the relaxation profile is very similar, displaying a weak temperature and frequency dependence.

The first regime was already discussed in IV.4.2 and IV.4.3. In the following the discussion will be focused on regimes II and III, in which the ADWP dynamics is expected to dominate the relaxation behavior.

V.2. The tunneling regime (T < 10 K)

As already mentioned, inspecting Fig. V.3 and Fig. V.8 a remarkable fact is observed: independent of the individual details of the curve γ(T), it appears that a common exponent γ is reached at lowest temperatures. For all molecular systems the spectra exhibit themselves as power-laws with a small, positive exponent, explicitly, γ (2 K – 7 K) = 0.038…0.043. In all (inorganic) glasses studied so far at temperatures below 10 K (in the kHz regime) the tunneling plateau is reached, *i.e.* the dielectric loss becomes independent of temperature and only at much lower temperatures, again a strong decrease is observed [62]. Thus, the system independent small value of the exponent γ at lowest temperatures may be taken as an indication that the tunneling regime is reached, for the first time, also for molecular glasses.

In order to check whether this is indeed the case we extended most of the investigations in the temperature range from 4 K down to 2 K and for glycerol even down to 0.03 K. The results for several systems investigated at single frequency ν = 1 kHz are presented in Fig. V.9 (a) as tanδ(T), and for the others as ε''(T) in Fig. V.11. In order to emphasize the behavior at lowest temperatures, the data are displayed on a logarithmic temperature scale. The

temperature independence of the loss observed in the two figures indicates that indeed a plateau is reached for most of the molecular systems. For glycerol the plateau extends for more than one decade in temperature, cf. Fig. V.9 (a). For comparison, the data of silica measured at 1 kHz [65] are added here, showing a similar behavior to the one observed in molecular systems.

As mentioned, the frequency dependence of $\varepsilon''(\nu)$ or $\tan\delta(\nu)$ in the plateau regime is characterized by a very low exponent γ, common for all glasses investigated here. In Fig. V.9 (b) we compare the present results in the plateau regime with some previously obtained for inorganic glasses (from literature) at somehow lower temperatures and in a broader frequency range. For getting comparable data the spectra are normalized by the plateau value at ν =12 kHz. It turns out that a similar frequency dependence is found for all the glasses including polymers (PMMA [74]), ionic glasses (CKN [74] and LiCl 5H$_2$O [119]) and inorganic network glasses (BK7 [74]). Note that for the type B systems CCH and toluene the spectrum at lowest temperature exhibits a stronger frequency dependence, as the tunneling regime may not be reached here (cf. Fig. V.7). Nevertheless, the general behavior observed in Fig V.9 (b) can be described within the so-called "modified soft atomic potential model", as the dashed line calculated accordingly to this model well interpolate the results [118].
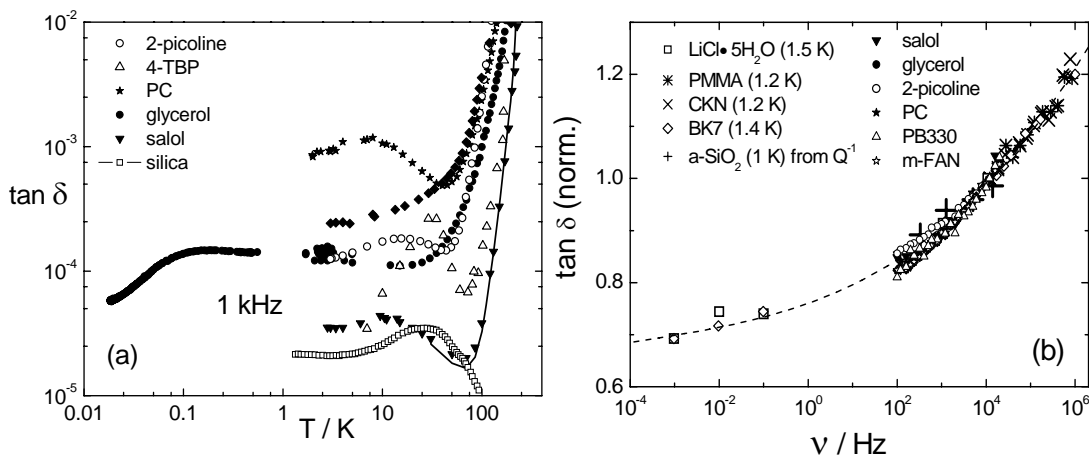
Fig. V.9 (a) tanδ at 1 kHz as function of temperature (logarithmic scale) for some molecular glasses investigated here. For comparison data from ref [75] for salol (solid line) and for silica [65] are added (b) Frequency dependence of tan δ at lowest temperature (2 K – 6 K) as obtained for the molecular glasses studied here and for several other glasses as reported in the literature [74,118,119]. For comparison the internal friction coefficient Q^{-1} estimated from [125] is included (crosses). Data are normalized by the value at 12 kHz. Dashed line is a Soft Potential Model prediction [118,120].

90

Within the STM, at lowest temperatures (below 1 K) the main contribution to the loss is expected to be given by the fastest relaxing TLS (see III.3.2), and the predicted temperature dependence is tanδ $\propto$ T^3. At the same temperatures, a crossover between two power-laws (with exponents in the ratio of (-2):(1) in semilogarithmic plot as function of temperature) is expected for the relative change of real part of permittivity $\delta\varepsilon'/\varepsilon'$ (or the overall capacity). These predictions (Eq. III.7, III.10) are not in accordance with the experimental results for glycerol in this temperature range: the observed ratio of the slopes is close to (-1):(1) for $\delta\varepsilon'/\varepsilon'$ and the temperature dependence of tanδ(T) is much weaker, as observed in Fig V.10. However, similar results with those obtained here are found in literature for many inorganic glasses [121]. Actually, situations when the STM predictions are exactly experimentally confirmed are rather seldom [119]. In order to account for these "exceptions", extensions of the tunneling model were introduced. In particular, incoherent tunneling is suggested to explain results similar with the ones obtained here for glycerol [121].
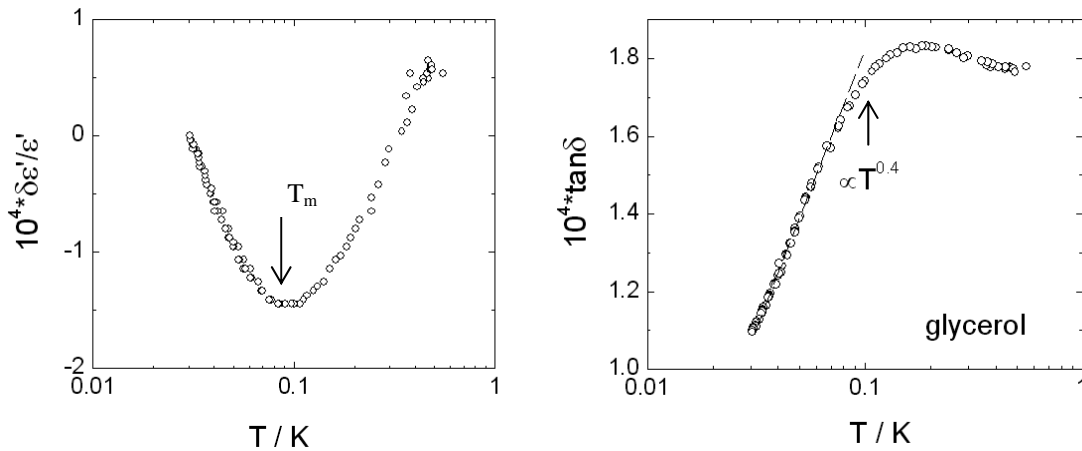
Fig. V.10 Temperature dependence of the capacity and tan δ for glycerol at 1 kHz below 1 K in semilogarithmic plot; the crossover temperature T$_m$ is indicated (see text for details).

As also discussed in III.3.2, in the plateau region the main contribution to the loss is given by the systems for which $\omega\tau \approx 1$. Within the STM, the transition to lower temperatures is marked by a crossover temperature given by:

$$T_m = \sqrt[3]{\frac{\omega}{Ak^3}}$$

(III.11)

This crossover temperature is indicated in Fig. V.10 by arrows and can be

approximated to be around 0.1 K for glycerol. Since the operating frequency is 1 kHz one can estimate, assuming that Eq. (III.11) holds, the important glass parameter Ak^3 (defined by Eq. III.4) that reads for glycerol the value of $Ak^3 = 10^6$ $(K^{-3}s^{-1})$. For comparison, Esquinazi et al. [122] estimated a value of $Ak^3 = 8 \cdot 10^7$ $(K^{-3}s^{-1})$ for SiO_2 using acoustic measurements.

At higher temperatures T > 1 K, the plateau value can provide information concerning the tunneling strength C that is related to the density of tunneling states $\bar{P}$ and the effective dipole moment μ of the relaxing element (as a coupling parameter of the ADWP to the external electric field):

$$\tan \delta = \frac{\pi}{2}C, C = \frac{\bar{P}\mu^2}{3\varepsilon_0 \varepsilon'}$$

(Eq. III.8, III.9)

The equation above is derived assuming that the TLS dipole moments are randomly oriented, and the expression may need (small) corrections for including the effects of the local field [118]. The density of states $\bar{P}$ can be directly accessed only by heat release experiments, where no coupling to external field is involved [123].

		System	C
Molecular glasses	Type A	2-picoline	$7.4 \cdot 10^{-5}$ (1 kHz)
		PC	$5.3 \cdot 10^{-4}$ (1 kHz)
		Glycerol	$7.5 \cdot 10^{-5}$ (1 kHz)
		Salol	$2.2 \cdot 10^{-5}$ (1 kHz)
	Type B	m-TCP	$1.7 \cdot 10^{-4}$ (1 kHz)
		m-FAN	$1.7 \cdot 10^{-4}$ (1 kHz)
		PB330	$1.1 \cdot 10^{-5}$ (1 kHz)
		Toluene	$2 \cdot 10^{-6}$ (1 kHz)
		CCH	$2.2 \cdot 10^{-5}$ (1 kHz)
Inorganic glasses		Suprasil (<1.5 ppm OH)	10^{-5} (2.2 kHz) from [124]
		GeO_2+0.1 % Na_2O	$6 \cdot 10^{-5}$ (1 kHz) from [124]
		BK7	$3 \cdot 10^{-4}$ (1 kHz) from [74]
		PMMA	$3.4 \cdot 10^{-5}$ (10 kHz) from [74]
		CKN	$3 \cdot 10^{-5}$ (10 kHz) from [74]
		$LiCl \cdot 7H_2O$	$3 \cdot 10^{-4}$ (50 kHz) from [119]

Table V.2 The tunneling strength C for all the molecular glasses investigated here. For comparison we included some data for the inorganic glasses as found in the literature.

The values of plateau strength C obtained for the molecular systems, together with the previous results for inorganic glasses are posted in Table V.2. Neglecting the weak frequency dependence displayed in Fig. V.9 (b), the constant C varies among the molecular glasses by a factor of about few hundreds.

As discussed in IV.4.3, the dielectric loss ε" for molecular systems at lowest temperatures can be collapsed to a system independent constant value by scaling out the value of the molecular dipole moment (see Fig. IV.29 re-plotted below as Fig. V.11 b, now in logarithmic T-axis). The tunneling strength C appears to correlate with the value of molecular dipole moment that dictates the amplitude of the α-peak. Since the STM theory provides no picture about the microscopic origin of the relaxing tunneling elements, it is tempting to check if there is indeed a direct connection between effective dipole moment μ$_{eff}$ of the tunneling centers and the molecular dipole moment μ$_{mol}$.
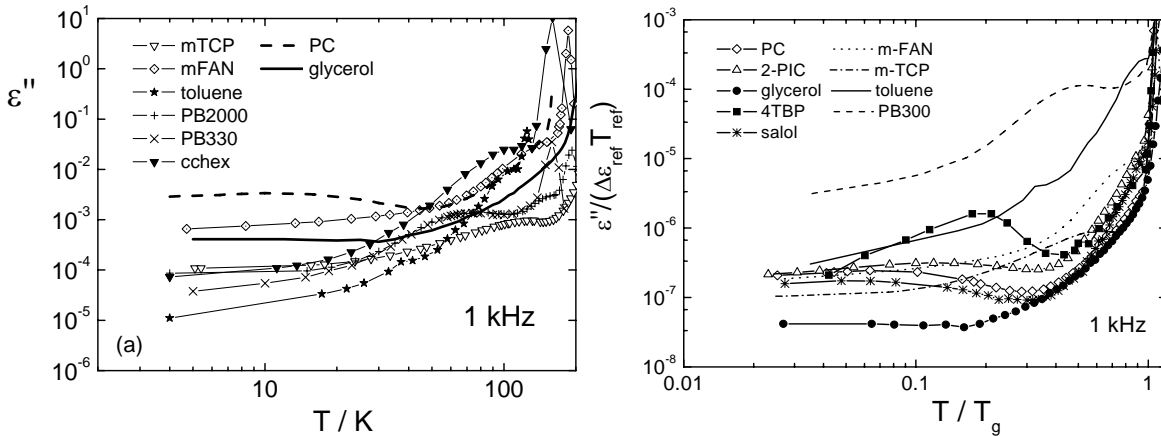
Fig. V.11 (a) Temperature dependence of ε" at 1 kHz for the molecular systems investigated here as function of temperature in logarithmic representation (b) The imaginary part of permittivity ε" scaled by the molecular dipole moment in the logarithmic reduced T/T$_g$ scale for all the molecular glasses below T$_g$.

As explained in IV.4.3, from the Curie law evaluated at highest temperature T$_{ref}$:

$$\mu_{mol}^{2} = \frac{3\varepsilon_0 k T_{ref} \Delta\varepsilon_{ref}}{n} \tag{IV.4}$$

On the other hand, using Eq. (III.9) one can write for the tunneling regime:

$$\varepsilon''(2K) = \frac{\pi}{2}\frac{\bar{P}\mu_{eff}^2}{3\varepsilon_0} \Rightarrow \bar{P}\mu_{eff}^2 = \frac{6\varepsilon_0\varepsilon''(2K)}{\pi} \tag{V.1}$$

93

From Eq. (V.1) and (IV.4) one may calculate the ratio:

$$\frac{\bar{P}\,\mu_{eff}^2}{\mu_{mol}^2} = \frac{2n\varepsilon''(2K)}{\pi k T_{ref}\,\Delta\varepsilon_{ref}} \tag{V.2}$$

As observed in Fig. V.11 (b), one can assume for all the molecular systems a value for $\varepsilon''(2K)/(T_{ref}\Delta\varepsilon_{ref}) \approx 2*10^{-7}$ (1/K). Glycerol is an exception, and this may be due to the failure of the Curie law (Eq. IV.4) for this system even at highest temperatures [117]. Polybutadiene exhibits a peculiar relaxation behavior at low temperatures that is discussed separately in Chapter VII.

The number density n = ρ/M_w, where ρ is the volume density and M_w the molecular weight. One can assume that in the high temperature liquid regime, where Eq. (IV.4) should hold best, the density of all molecular systems may be considered close to the one of the water, _i.e._ $\rho = 10^3$ kg/m^3. The values of M_w for the systems under discussion vary within a factor 4. For a value of M_w = 100 u = 100*1.66*10^{-27} kg, one can estimate, cf. Eq. (V.2):

$$\frac{\bar{P}\,\mu_{eff}^2}{\mu_{mol}^2} = 5.6\cdot 10^{43}\,J^{-1}m^{-3} \tag{V.3}$$

In literature one finds only little information for the values of the density of the tunneling states $\bar{P}$ in organic glasses. From the heat release experiments, $\bar{P}$ was evaluated for poly (methyl methacrylate) (PMMA) and polystyrene (PS) in $J^{-1}g^{-1}$ units. In order to get comparable results one should transform the quantity in (V.3) using that (for water) 1 m^3 weights 10^6 g:

$$\frac{\bar{P}\,\mu_{eff}^2}{\mu_{mol}^2} = 5.6\cdot 10^{37}\,J^{-1}g^{-1}.$$

The values for $\bar{P}$ found in literature for the two polymers are $\bar{P} \approx 5*10^{38}$ $J^{-1}g^{-1}$.

Assuming that $\bar{P}$ is a universal quantity, it results that the effective dipole moment of the tunnelling centres μ_{eff} has the same order of magnitude as the molecular dipole moment μ_{mol}. Alternatively, if $\mu_{eff} = \mu_{mol}$ than $\bar{P}$ in molecular glasses is by a factor 10 smaller than the value measured in polymers. This result is in agreement with the one indirectly obtained for the inorganic glasses from the internal friction data, cf. Pohl et al. [62]. According to the

compilation done by these authors, $\bar{P}$ for inorganic glasses varies within a factor 20.

V.3 The thermally activated Asymmetric Double Well Potential (ADWP) dynamics (10 K < T < T$_{CL}$)

V.3.1 Systems with weak β-contribution

Next we discuss the origin of the relaxation behavior in the temperature range in between the tunneling plateau and the true constant loss identified at T$_{CL}$. For 2-picoline, PC and salol, ε''(T) exhibits a maximum and then a minimum while heating, cf. Fig. V.2 (a-c), and the exponent γ(T) exhibit a shallow minimum, cf. Fig. V.3. The maximum of the loss is better seen when the data are plotted linearly, as done for 2-picoline measured at three different frequencies in Fig. V.12 (a). As observed here, the behavior of ε''(T) is similar to that found in silica (amorphous SiO$_2$) although the maxima for 2-picoline occur at somewhat lower temperatures. In silica and other inorganic glasses these maxima are attributed to thermally activated jumps within ADWPs (see III.3.2 and ref. therein).

Extending the STM model to higher temperatures for which the thermally activated transitions over the ADWP barriers are expected, Gilroy and Phillips considered an exponential distribution of barrier heights g(V) with no low-energy cut-off. When a low energy cut-off is missing in g(V), a peak is expected in ε''(T) but not in the spectra ε''(ν), cf. discussion in III.3.2. Indeed, this is the behavior observed in, *e.g.*, silica and CKN data obtained by light scattering and acoustic attenuation techniques [70] – and, as depicted from Figs. V.2 and V.12 – also for the molecular glasses PC, salol and 2-picoline measured here. For 4-TBP and m-TCP the relaxation peak is observed in both ε''(ν) and ε''(T), cf. Fig. V.5 and V.6 discussed above. For glycerol no peak is discernible at all, a behavior found also for some other inorganic glasses as, *e.g.* LiCl·5H$_2$O [119].
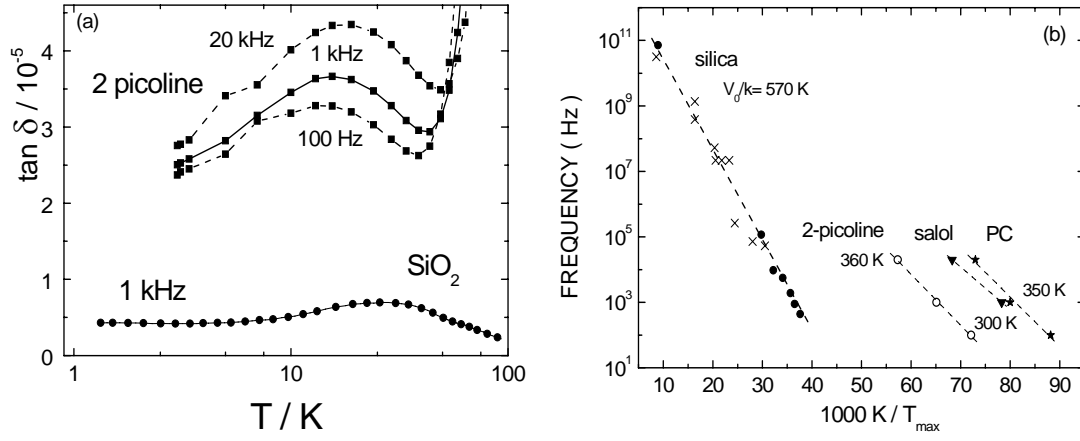
Fig. V.12 (a) Loss peaks of 2-picoline and silica [65] in linear temperature scale; (b) Frequency vs. inverse peak temperature for PC, 2-picoline and salol. Data are compared with dielectric measurements of the thermally activated peak of silica [125].

Eq (III.19) describes the evolution of the dielectric loss within the Gilroy-Phillips model:

$$\varepsilon''(\omega,T) \propto \frac{k_B T}{V_0}(\omega\tau_0)^{\frac{k_B T}{V_0}} \qquad \omega\tau_0 <<1 \qquad\qquad (III.19)$$

where $\tau_0 \sim 10^{-12} - 10^{-13}$ sec is a typical molecular attempt time. A peak in $\varepsilon''(T)$ is expected that follows the Arrhenius law. The derivation of Eq. (III.19) leads to:

$$\omega_{max} = \tau_0^{-1} \exp(-V_0/kT_{max}) \qquad\qquad (V.4)$$

T_{max} is the temperature corresponding to the maximum in $\varepsilon''(T)$. The value for the peak amplitude is given by:

$$\varepsilon''_{max} \propto kT_{max}/V_0 \qquad\qquad (V.5)$$

According to Eq. (V.4) and (V.5), one expects that the maximum of ε'' (or tanδ) shifts to higher temperatures with increasing frequency and that the maximum's value ε''_{max} increases with temperature. Clearly, the evolution of the peak observed in molecular systems resembles the predicted behavior (see Fig. V.12 for 2-picoline). From the shift of the maximum, the mean activation energy V_0 can be estimated, cf. Eq. (V.4). Accordingly, one may plot the frequency versus inverse peak temperature T_{max}, as done in Fig. V.12 (b) for PC, 2-picoline and salol. Here are also added the results obtained for silica [125]. Though the accessible frequency range provided by the bridge is relatively small, an approximate value for V_0/k_B can be extracted for each

system. As indicated by the values in Fig. V.12 (b), V_0 is similar among the molecular systems and within a factor 2 smaller than the value for silica.

Having an estimation for the mean activation barrier V_0, one can calculate the spectra $\varepsilon''(\nu)$ for different temperatures by using the Gilroy-Phillips model. In Fig. V.13 (a), some spectra calculated accordingly are plotted for few temperatures between 10 K and 30 K. The mean activation energy was chosen $V_0 = 300$ K. For comparison, the spectra of PC measured at similar temperatures are presented in Fig. V.13 (b). Clearly, the model predictions resemble the measured spectra $\varepsilon''(\nu)$.

Within this model the susceptibility is obtained by integrating over the distributions of barrier heights g(V) and the distribution of asymmetries f(Δ) of the ADWPs. If f(Δ) is considered flat with a cut-off $\Delta_{max} \propto$ T, the loss is given by Eq (III.19). Using the change of the variable as V = kTln(x/$\omega\tau_0$), with x=$\omega\tau$, one may rewrite the integral as [72]:

$$\varepsilon''(\omega,T) \propto T \int_{\omega\tau_0}^{\infty} \frac{x}{1+x^2} g(V)d(x) \qquad . \qquad (V.6)$$

Assuming a broad distribution g(V), the Debye term can be ignored in the convolution, thus $\varepsilon''(\omega)$ in (V.6) yields directly the distribution of barriers g(V):
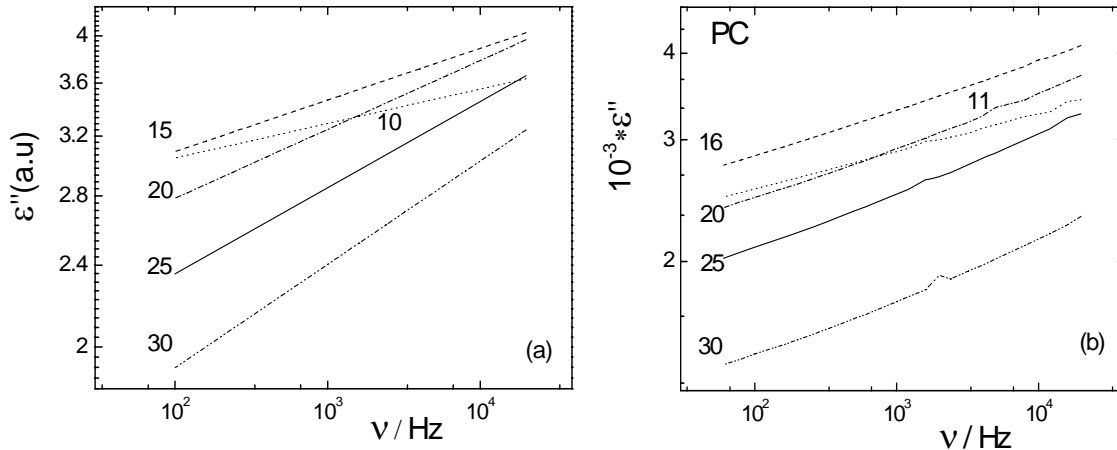
Fig. V.13 (a) $\varepsilon''(\nu)$ curves calculated using Eq. (III.25); the chosen frequency range matches the one experimentally accessed in this Work. (b) spectra of PC at similar (indicated) temperatures.

$$\varepsilon'' \propto Tg(V) \Rightarrow g(V) \propto \varepsilon''/T \qquad (V.7)$$

$$V/k = T\ln(\nu_0/\nu) \qquad (V.8)$$

where $\nu_0 = 1/(2\pi\tau_0)$.

Thus, as long as g(V) is broad enough and, by definition, temperature independent, one should be able to scale the spectra in order to directly obtain g(V). Explicitly, the ε''-axis is divided by T and the logν-axis is multiplied with T (cf. Eq. V.7 and V.8).

The data for PC, 2-picoline and salol are scaled accordingly in Fig. V.14. Here the results are compared with the ones obtained for CKN by light scattering investigations [70]. As observed, the scaling works well for the three molecular systems in the temperature range above 10 K up to T$_{CL}$, and even above, as discussed next. The only parameter necessary for the scaling is the attempt frequency ν_0. For all three glasses a value of $\nu_0 = 10^{12}$ Hz was used to collapse more than ten spectra for every system. While the distribution g(V) is exponential in the case of CKN, for the molecular systems g(V) appears more stretched.
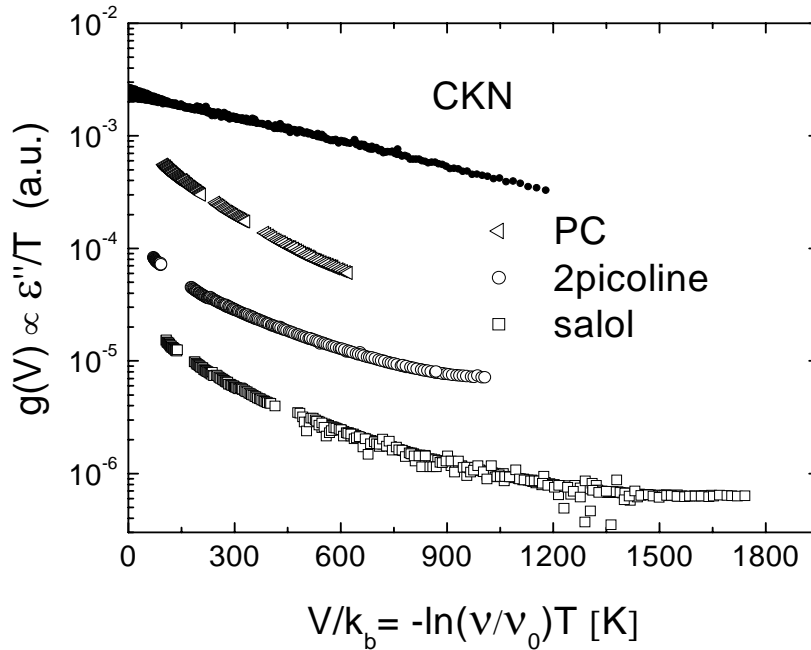
Fig. V.14 Distribution of activation barriers g(V) extracted from the spectra for PC, 2-picoline and salol. The scaled data of CKN obtained in GHz range are added from ref. [70].

One should keep in mind that the dielectric measurements presented here are performed in the kHz range, therefore the thermally activated ADWP dynamics and, implicitly the g(V) distribution are accessed only at very low temperatures (cf. Eq. V.4). This is not the case for the light scattering investigations that are performed in the GHz range. The low investigating

frequencies may not yield the correct g(V), since at low temperatures, say below 30 K, influence from the tunneling contribution might play an important role. If true, the tunneling contribution should also affect the temperature evolution of the power-law exponent γ characterizing the spectra in this temperature range. In Fig. V.3 one can observe that in the small temperature range below the minimum in γ(T), the exponent γ is linear in T but not proportional with T, as expected from the Gilroy - Phillips model ($\gamma \propto kT/V_0$ cf. Eq. III.25).

It is theoretically not well established how to describe the crossover from the tunneling regime to the thermally activated dynamics. Some attempts have been made but none of them fully successful. One important assumption is that both processes are statistically dependent and the total transition rate is simple given by the sum of the individuals [126]. In order to single out the individual contribution of the thermally activated dynamics, one can proceed with subtracting from the overall spectra the spectrum measured in the tunneling regime, *i.e.* at the lowest temperature, say at 4 K. This additive approach can be tested only for few spectra at temperatures around the maximum in ε''(T). As indicated by Fig. V.9 (a) and V.12 (a) this is due to the decrease of the signal amplitude in the minimum range (at temperatures above T$_{max}$) below the value of the tunneling plateau, thus the subtraction analysis becomes obsolete here. For this reason, the analysis for PC is practically impossible, yet it can be tested for 2-picoline and salol.

One example of how such a subtraction works is given in Fig. V.15 (a) for the 2-picoline spectrum measured at 16 K. As observed here, ε''(ν) measured at the lowest temperature (3 K) shows a weak frequency dependence, typical for the tunneling regime, as discussed. The spectrum at 16 K can be interpolated by a power-law with exponent $\gamma \approx 0.05$, not much higher than the one of the tunneling spectrum. However, the exponent changes by a factor 2 when the latter is simply subtracted (cf. Fig. V.15 a).

In Fig. V.15 (b) the exponent γ characterizing the spectra before, and after this subtraction, is plotted for the two molecular glasses 2-picoline and salol. As clearly observed, the temperature dependence -γ(T) strongly changes after

subtraction and the exponent γ appears now as proportional with T, in accordance with the Gilroy-Phillips model.
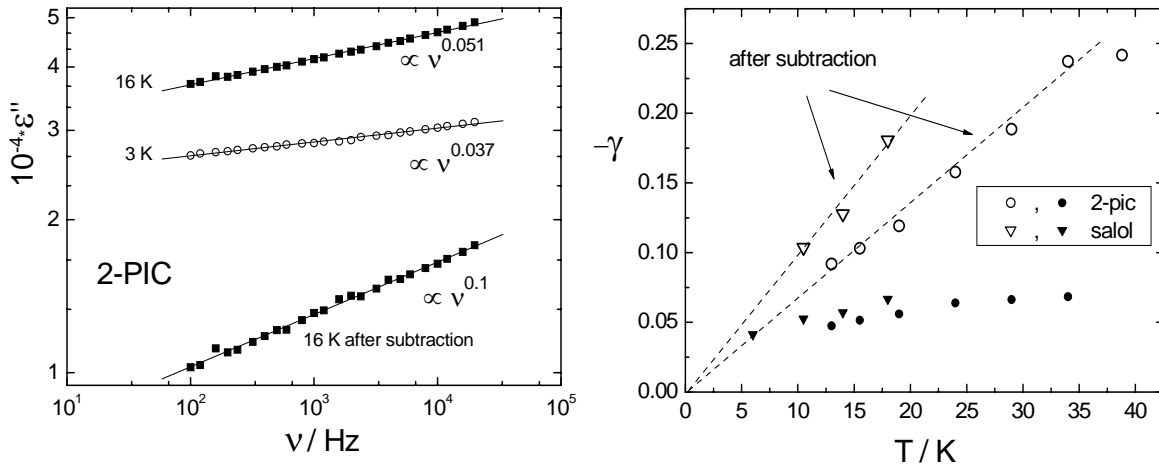
Fig. V.15 (a) Dielectric spectra of 2-picoline measured at 3 and 16 K (upper spectra) plotted together with the subtracted $\varepsilon''(\nu)=\varepsilon''_{16K}(\nu)-\varepsilon''_{3K}(\nu)$ (lower spectrum). Solid lines: fits with power-laws. (b) Temperature dependence of the power-law exponent γ of the spectra ($\varepsilon''(\omega) \propto \omega^\gamma$) for temperatures below 40 K before (full symbols) and after (open symbols) the subtraction of the tunneling spectrum; dashed lines are linear interpolations.

Moreover, the extracted spectra yield a distribution g(V) close to exponential (cf. Fig. V.16).
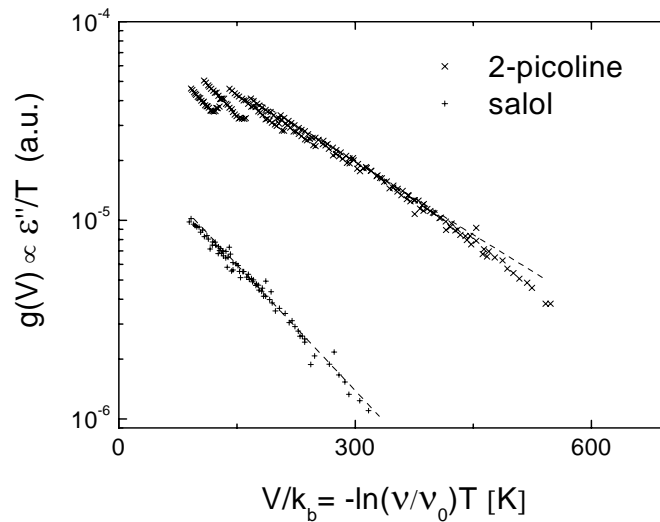
Fig. V.16 The g(V) scaling for 2-picoline and salol after the subtraction of the tunneling spectrum (see text). The dashed lines are interpolations with an exponential law $g(V) \propto \exp(-V/V_0)$.

One can interpolate the newly obtained $g(V) \propto \exp(-V/V_0)$, yielding the values $V_0 = 103$ K for salol and $V_0 = 193$ K for 2-picoline. These values are lower than

those estimated from the shift of the peak maximum in $\varepsilon''(T)$, indicated in Fig. V.12 (b). However, they are consistent with those extracted from the slope of the temperature dependence of $\gamma(T)$ after the subtraction of the tunneling spectrum. The slopes of the dashed lines ($\gamma = kT/V_0$) in Fig. V.15 (b) gives the values of $V_0 = 150$ K for 2-picoline and 100 K for salol.

V.3.2 Systems with strong β-contribution

The scaled distribution g(V) appears as stretched for molecular glasses. As shown above, one reason may be the influence of the tunneling. One the other hand, as the β-process is also a thermally activated process, its presence may also manifest at high barriers V. Note that the main difference between the thermally activated ADWP process and the β-process is given by the characteristic activation heights. For the former process the barriers V (in K) are in the order of hundreads of K [65,70], while for the latter in the order of thousands of K [26].

As discussed in IV.1.2, for the systems with pronounced β-contribution, the spectra below T_{CL} are very similar among different glasses and highly resemble the behavior observed for glycerol, cf. Figs. V.7 and V.1 (d). Explicitly, there are no direct indications for thermally activated ADWP dynamics, as no maximum in $\varepsilon''(T)$ nor a minimum in $\gamma(T)$ is observed below T_{CL}.

However, since for a given system the ADWP peak maximum ε''_{max} depends, via T_{max}, on the investigated frequency (cf. Eq. V.4 and V.5), for a certain (low) frequency ε_{max} can reach the value observed for the tunneling plateau $\varepsilon''_{plateau}$, and the maximum cannot be resolved. Thus, the appearance of the peak in $\varepsilon''(T)$ dependence is favored by the situations of small V_0, high investigating frequencies and sufficiently small value of the tunneling plateau (dictated by the molecular dipole moment, as discussed). This may explain why no peak in $\varepsilon''(T)$ is observed below T_{CL} in the data of these systems when measured in the kHz range. Thus, it is difficult to draw any conclusion regarding the absence or the presence of thermally activated ADWP

dynamics, especially for systems that clearly exhibit contribution from the other thermally activated process (β-process) at higher temperatures.

We recall that if the spectra appear as the manifestation of thermally activated ADWP dynamics, one should be able to scaled them yielding directly the distribution of activation barriers g(V), as demonstrated for the type A glasses 2-picoline, PC and salol in the previous paragraph. Next the same procedure is tested for m-FAN spectra starting from the lowest temperature close to 4 K. The result of the scaling is presented in Fig. V.17. Surprisingly, this scaling works well in the temperature range from 4 K up to temperatures above T$_{CL}$ (T$_{CL}$ = 54 K for m-FAN, see Table V.1), close to 100 K where the relaxation is dominated by the β-process, cf. Fig. V.7 (a).
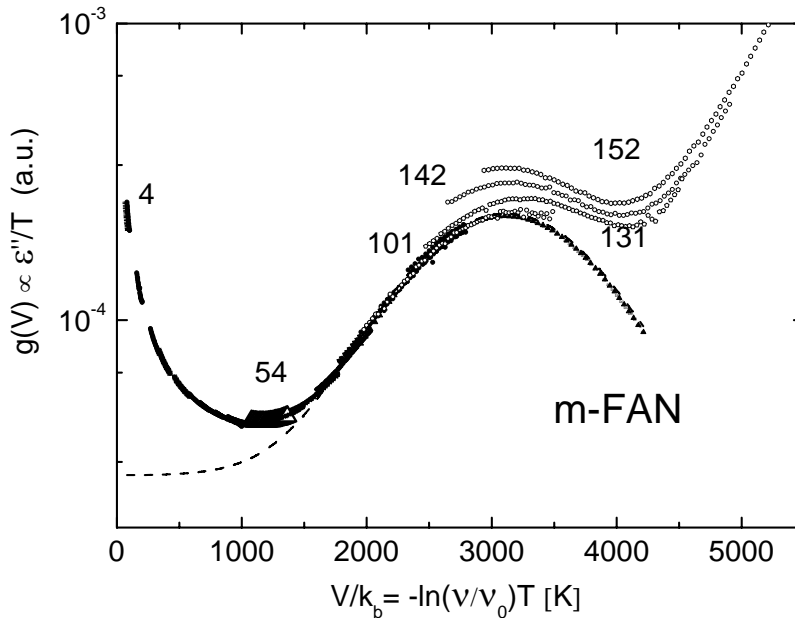
Fig. V.17 Distribution of activation barriers g(V) extracted from the spectra for m-FAN below T$_g$. Temperatures are indicated for few scaled spectra. For temperatures above 100 K the open symbols are obtained by the scaling of the raw broadband data and the full triangles are the same data scaled after the subtraction of the EW (see text for details). The scaled data at T$_{CL}$ = 54 K are highlighted by larger size, open triangles.

If the distribution g(V) is flat, this corresponds to a flat spectrum, as observed at temperatures close to T$_{CL}$. For example, in Fig. V.17 the minimum of g(V) for m-FAN corresponds to the spectra measured at 54 K, *i.e.* T$_{CL}$. Note that for barriers V larger than the ones at the minimum in g(V) is obtained by scaling the spectra measured at T > T$_{CL}$.

The scaling fails above 100 K (plotted with open symbols in Fig. V.18). As discussed in IV.3.2, within approach II, at similar temperatures (close to 100 K) the EW starts to significantly contribute to the overall spectra as a power-law spectrum $\varepsilon''_{EW} = A\nu^{-\gamma}$ with a temperature independent exponent $\gamma = 0.2$ and the prefactor A increasing exponentially with temperature. The same behavior was discussed for glycerol, the only difference to m-FAN being the smaller amplitude of the β-process. One may attempt to scale the m-FAN data for temperatures above 100 K after the subtraction of the EW contribution (as presented in Fig. IV.18 b). As shown in Fig. V.17, after the subtraction of this EW one can collapse now, according to Gilroy-Phillips model, all the spectra measured from 4 K up to temperatures close to T_g.

For large V's, the distribution g(V) has a Gaussian shape as indicated by the interpolation of the data for V > 2000 K (dashed line in Fig. V.17). This result is in concordance with previous investigations suggesting that in the glass the β-process can be described by a Gauss distribution of activation energies [26]. However, for m-FAN the <u>symmetric</u> Gaussian shape is clearly revealed only after the subtraction of the EW contribution in the spectra. The Gaussian interpolation gives a value of the mean activation energy of $E_a = 3115$ K ≈ 18 T_g, in agreement with the result obtained in IV.3.2 applying approach II.

The fact that the g(V) scaling works must be a consequence that the relation (V.6) holds. However, this equation is derived under the assumption that the thermally activated jumps are taking place within the *asymmetric* double well potentials. According to the model, the distribution of the asymmetries f(Δ) is considered flat with a cut-off $\Delta_{max} \propto T$. Only under this condition the prefactor of the integral in Eq. III.19, *i.e.* the dielectric strength of the thermally activated process becomes temperature independent. Since this temperature invariance of $\Delta\varepsilon_\beta$ is indeed observed experimentally for the β-peak in the glass [26], the scaling indicates that the Gilroy-Phillips model can be extended to temperatures were the spectra are dominated by the β-process. Accordingly, the β-process is a thermally activated process within the *asymmetric* double well potentials with a flat distribution of the asymmetries f(Δ)= constant and $\Delta_{max} \propto kT$, and with a Gaussian distribution of the barriers g(V).

Another interesting observation is that at low V's (say V < 1000 K) the stretched g(V) appears as similar with the distribution obtained for the ADWP dynamics in type A glasses salol, PC and 2-picoline. In order to single out the contribution g$_{ADWP}$(V) at low V barriers we may consider the total g(V) as given by the sum g(V) = g$_{ADWP}$(V) + g$_\beta$(V), and than subtract the Gaussian contribution of the β-process (dashed line in Fig. V.18) from the overall distribution. The results for m-FAN after subtraction are plotted as solid line in Fig. V.18. The extracted g$_{ADWP}$(V) appears as exponential at high V. For comparison, the results of g(V) obtained for glycerol and salol, previously discussed and now extended to temperature above T$_{CL}$ are also added here.
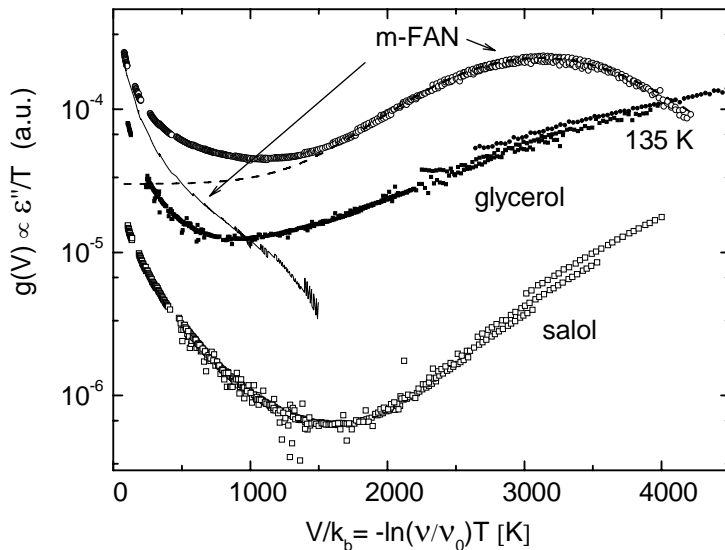
Fig. V.18 Distribution of activation barriers g(V) extracted from the spectra for m-FAN before and after (solid line) the subtraction of g$_\beta$(V). For comparison the scaled data of glycerol and salol are added. The dashed line is interpolation with a Gaussian function.

According to Approach II, the NCL (observed in some systems with no well-resolved β-peak below T$_g$) results from the contribution of both EW and β-process, however with the EW dominating close to T$_g$. At lowest temperatures close to T$_{CL}$, as the EW shifts stronger with temperature than the β-process (see IV.4.2), the spectra here are dominated here by the thermally activated β-contribution. As indicated by Fig. V.18, the data of glycerol and salol can be scaled in a restricted temperature range above T$_{CL}$ (for glycerol up to 135 K, cf. Fig. V.19). As approach II predicted, the spectra close to T$_{CL}$ are dominated by the β-process, and, as the EW contribution becomes stronger close to T$_g$, the latter spoils the g(V) scaling here.

V.4 Conclusions

For all the molecular systems investigated three relaxation regimes can be identified for temperatures below T$_g$.

Below 10 K we find clear indications that the tunneling regime is reached for the molecular glasses. Here the dielectric loss ε'' as a function of temperature saturates to a plateau and its frequency dependence appears as universal. In particular, the spectra can be interpolated by power-laws with a temperature independent exponent $-\gamma = 0.04 \pm 0.002$ for all systems, including inorganic glasses. As the plateau value appears to be controlled by the molecular dipole moment μ_{mol}, one can estimate that the effective dipole moment of the tunneling center μ_{eff} is proportional to μ_{mol} or, equivalently, scaling the ε'' data by μ^2_{mol} leads to a very similar values for the density of the tunneling centers. At lowest temperatures, below 0.1 K we find indications that the fastest tunneling relaxation occurs at 1 kHz for glycerol. The glass parameter A containing the coupling constants of the tunneling systems to the phonon bath can be estimated for glycerol and its value does not differ much from the one previously obtained (from acoustic experiments) for silica.

At higher temperatures (10 K > T > 50 K) indications are found for thermally activated ADWP dynamics for the molecular systems. The data for 2-picoline, PC and salol display a peak as function of temperature ε''(T) but not in the spectra ε''(ν), in accordance with Gilroy-Phillips model. The distribution of the activation barriers g(V) can be determined by scaling the spectra in accordance with this model. However, g(V) does not appear exponential as predicted, but more stretched. The explanation may be that at lowest barriers tunneling contributions may play a significant role as the measurements are performed at relatively low frequencies, in the kHz range. On the other hand the thermally activated β-process may contribute to the g(V) shape for high barriers. As the Gilroy-Phillips scaling appears to work also for the spectra clearly dominated by the β-process, one may conclude that the latter is a thermally activated process within asymmetric double wells with barriers g(V) distributed as a Gaussian. The distribution of asymmetries for the β-process is also flat and only the wells with asymmetries $\Delta < kT$ contributes to the

dielectric response, as in the Gilroy-Phillips model. This may justify the temperature independence of the relaxation strength $\Delta\varepsilon$ of the β-process below T$_g$.

Finally, at the highest temperatures close to T$_g$ the secondary processes emerging above T$_g$ and surviving in the glass give the main contribution to the spectra here.

VI. Results; A joint study of glycerol by dielectric spectroscopy, field cycling NMR and light scattering.

As already discussed in Chapter IV, the nature of the excess wing (EW) and also the way to disentangle it from the dielectric spectral contribution of the α-process is not *a priori* clear, thus further experiments are needed to address this point. Two-dimensional (2D) NMR techniques [50,101,128,129] suffer from the problem that in glass formers with no β-peak above the glass transition temperature T_g both α-process and EW are not well separated in time, and below T_g the relaxation strength is too small and time scale too slow to be probed by 2D NMR. For example, in the systematic 2D NMR studies carried out by the Sillescu group, the reorientational process in molecular glass formers was identified by random walk simulations comprising a mixture of small ($2 - 3^o$) as well as large angle ($30 - 50^o$) jumps [50,130,131]. However, these experiments do not easily allow to explain the particular shape of the susceptibility with its characteristic high frequency tail. On the other hand, NMR spin-lattice relaxation data identified the EW, however, as typical for conventional solid-state NMR, relaxation data at only few frequencies were presented [132,133,134]. For instance, in the case of glycerol, Blochowicz et al. demonstrated that a quantitative comparison of dielectric and NMR spectroscopy is possible [42]. A broader range of frequencies may be covered by applying fast (electronic) field cycling (FFC) relaxometry, *i.e.* the frequency dispersion of the spin-lattice relaxation is studied by fast switching the external magnetic field [135,136]. However, early experiments provided limited information and, in particular, did not address the phenomenon of the EW. With progress in instrumentation [137,138] and with the appearance of a commercial FFC spectrometer the situation changed.

The approach II introduced in IV.3, allows keeping the frequency-temperature superposition (FTS) for the α-relaxation at all temperatures above T_g. Moreover, in strong contrast to previous approaches, the EW exponent γ is also chosen as temperature independent and the EW amplitude decreases with temperature, opposite to what is found for the β–process [114]. The above interpretation for the temperature evolution of the dielectric susceptibility in molecular glass formers will be tested in the following also for the relaxation data obtained by field cycling NMR and

light scattering (LS). This Chapter presents a systematic study of the paradigmatic glass former glycerol by dielectric spectroscopy (DS), FFC NMR and LS covering a broad temperature range of 75 – 360 K, *i.e.* the relaxation of glycerol is investigated above as well as below T_g = 186 K. By this means a comparison between the orientational correlation functions of rank *l* = 1 (probed by DS) and *l* = 2 (probed by FFC NMR and light scattering) is carried out. This Chapter is self contained and closely follows publication [150].

VI.1. Theoretical background – dispersion of spin-lattice relaxation

The FFC method is based on measuring the dispersion of spin-lattice relaxation time $T_1(\omega)$ by cycling the external magnetic field B_o. In the case of proton nucleus ^{1}H, most often used in FFC NMR, the decay of magnetization expressed by T_1 is due to fluctuations of the dipolar interactions of proton spins. Then, the interaction Hamiltonian involves a sum over all pairs of spins *i, j* in the sample. The interaction term of a particular pair of spins *ij*, separated by $\mathbf{r}_{ij}$, depends on the polar (ϑ) and azimuthal (φ) angles with respect to the magnetic field, as well as on the distance r_{ij}. Generally, the sum can be separated into intra- and inter-molecular contributions that, assuming their statistical independence, contribute additively to the spin-lattice relaxation rate [137,143]:

$$1/T_1 = 1/T_1^{intra} + 1/T_1^{inter} \tag{VI.1}$$

However, due to the short-range nature of dipole-dipole interaction, one expects that the main contribution to the interaction sum stems from the nearest protons belonging to the same molecular unit, and that inter-molecular terms are relatively unimportant, so that $T_1 \approx T_1^{intra}$. Even if there is some intermolecular contribution, in super-cooled liquids the corresponding spectral densities of intra- and intermolecular fluctuations are expected to be similar. One thus assumes in the following that distinct intermolecular contributions are negligible in first approximation, so that the proton NMR data mostly reflect reorientation dynamics. One should note that the problem is similar with the one in dielectric relaxation where, in super-cooled liquids, the cross relaxation effects are usually ignored, cf. II.1.

Orientational dynamics enters the calculation of the relaxation rate $1/T_1$ via the correlation functions $F_2^m(t)$ of the second rank spherical harmonics $Y_{2,m}(\vartheta,\varphi)$:

$$F_2^m(t) = <Y_{2,m}(\vartheta_o,\varphi_o)Y_{2,-m}(\vartheta_t,\varphi_t)> / <|Y_{2,m}(\vartheta_o,\varphi_o)|^2> \qquad \text{(VI.2)}$$

where <...> indicates the ensemble average, whereas the indices *0* and *t* refer to the initial and final times. The orientational average for a macroscopically isotropic system yields an *m*-independent expression for the reorientational correlation function, expressed through the second-rank Legendre polynomial $P_2(\cos\vartheta)$ = ½(3cos$^2\vartheta$ -1) [134,137,144]:

$$F_2(t) = <P_2(\cos\vartheta_o)P_2(\cos\vartheta_t)> / <|P_2(\cos\vartheta_o)|^2> \qquad \text{(VI.3)}$$

with the corresponding spectral density

$$J(\omega) = \text{Re}\int_0^\infty F_2(t)\, e^{-i\omega t}\, dt \qquad \text{(VI.4)}$$

The proton spin-lattice relaxation rate $1/T_1$ is related to the spectral density $J(\omega)$ through the well-known Bloembergen, Pound, Purcell expression [134,137,144,145]:

$$1/T_1(\omega) = C\left[J(\omega) + 4J(2\omega)\right] \qquad \text{(VI.5)}$$

where ω = γB_0 is the Larmor frequency depending on the gyromagnetic ratio γ and the magnetic field B_0, whereas C is the NMR coupling constant, which depends on the nuclear separation r_{ij} of the relevant spin pairs and is connected to the second moment of the solid-state ^{1}H NMR spectrum.

According to the fluctuation-dissipation theorem the spectral density of thermal equilibrium orientational fluctuations is related to the linear response of the molecular orientations to a weak external perturbation, *i.e.* to a response (susceptibility) function. Specifically, the loss (imaginary) part of the susceptibility is given by $\chi''(\omega) \approx \omega J(\omega)$. This "molecular orientation" susceptibility would be an (average) response of a molecule to external torque, and thus cannot be "measured" in a NMR experiment. However, several experimental techniques, such as the optical Kerr effect and dielectric spectroscopy, do access response functions that are related to molecular reorientation dynamics and therefore are comparable with the

"orientational" susceptibility discussed above. We therefore transform Eq. (VI.5) into the susceptibility form [112,146]:

$$\omega/T_1 = C[\chi''(\omega) + 2\chi''(2\omega)] \equiv C\,\chi''_{NMR}(\omega) \tag{VI.6}$$

where the object in square brackets is called "normalized NMR susceptibility", or simply "NMR susceptibility" in the following. Even though it is in fact a weighted sum of two susceptibility terms, for a broad relaxation spectrum it is barely distinguishable from the individual susceptibilities. Analyzing the NMR susceptibility $\chi''_{NMR}(\omega)$ rather than the relaxation rate $1/T_1(\omega)$ itself allows a direct comparison with dielectric spectra the latter yielding $\chi''_{DS}(\omega) = \varepsilon''(\omega)/\Delta\varepsilon$ where $\Delta\varepsilon$ denotes the relaxation strength of the slow dynamics.

VI.2 Experimental results

VI.2.1. Dielectric spectroscopy (DS)

The dielectric measurements of glycerol discussed in this Chapter are performed in Bayreuth by employing five different spectrometers for data acquisition in the temperature range from 273 K down to 4 K. Four of them are discussed in II.2. In addition, the investigations below T_g, for temperatures 74 K < T < 173 K, are carried out by R. Kahlau in Bayreuth by applying a newly purchased Alpha-A spectrometer from Novocontrol. These measurements cover a broader frequency range as compared to those previously presented in V.1.1 and obtained with a Schlumberger spectrometer.

The imaginary part of the dielectric permittivity ε'' of glycerol is presented in Fig. VI.1 (a) for temperatures above T_g, and in Fig. VI.9 for temperatures below T_g. Data in Fig. VI.1 (a) are normalized by the relaxation strength $\Delta\varepsilon = \varepsilon_s - \varepsilon_\infty$, where ε_s is the static susceptibility, and ε_∞ the dielectric constant at frequencies much larger than the main relaxation including α–peak and EW, is determined from the real part $\varepsilon'(\nu)$, cf. Fig. VI.1 (b).

Usually, the spectra contain a rather strong contribution from ionic conductivity which is removed in most spectra of Fig. VI.1 (a), except for T = 233 K. Operating the time

domain spectrometer in the discharge mode allows to significantly suppress the conductivity contribution, cf. data at T = 194 K. Then, the low frequency flank of the main relaxation is well resolved which is needed for a comparison with the NMR data, as discussed later.
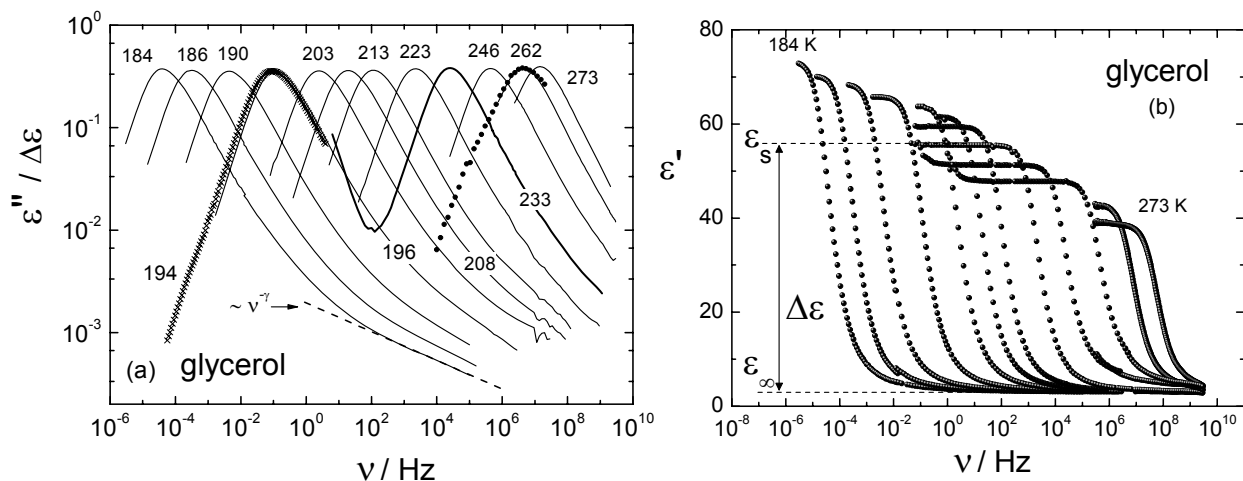
Fig. VI.1 (a) Imaginary part of normalized dielectric permittivity $\varepsilon''/\Delta\varepsilon$ of glycerol above T_g. For T = 194 K the results are obtained using the time domain spectrometer operating in the discharging mode. For T = 262 K comparison with the NMR susceptibility (dots) is shown; high-frequency power-law (EW) is indicated. (b) Real part of dielectric permittivity ε' of glycerol at same temperatures as in (a).

VI.2.2 ^{1}H Nuclear Magnetic Resonance (NMR)

The dispersion of the ^{1}H spin-lattice relaxation time T_1 is measured in the temperature range 191 K – 360 K, cf. Fig. VI.2 (a) by employing a commercial fast field cycling spectrometer STELAR FFC2000 ("Bayreuth data"). The sample temperature is controlled by heating a flow of air or by cooling evaporated liquid nitrogen. Moreover, applying an another homebuilt electronic FFC spectrometer a temperature range 75 K – 314 K is covered ("Darmstadt data", cf. Fig. 3a). For details of the involved magnet design and the unusual Darmstadt spectrometer performance one may consult [138,141]. Despite the special cryostat design involving the use of nonmetallic materials, wherever possible, eddy currents during field switching are a major problem. Nevertheless, spin-lattice relaxation times down to about 1 ms are accessible. In both applied FFC spectrometers the temperature stability is ± 0.3 K. In all cases exponential relaxation is observed. A frequency range of 10 kHz – 40 MHz is covered by the FFC NMR technique.
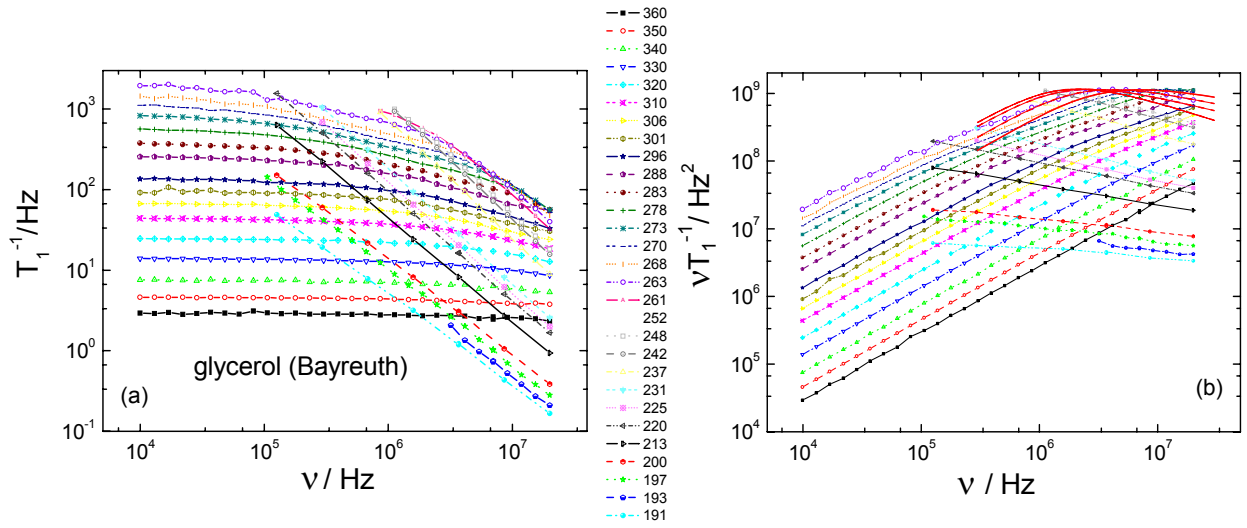
Fig. VI.2 (a) Dispersion of the spin-lattice relaxation time T_1 as measured by the Bayreuth spectrometer for indicated temperatures (in K). (b) Conversion of the data in (a) along Eq. (VI.6) into the susceptibility representation; solid (red) lines: interpolation around the relaxation maximum applying a Cole-Davidson susceptibility.
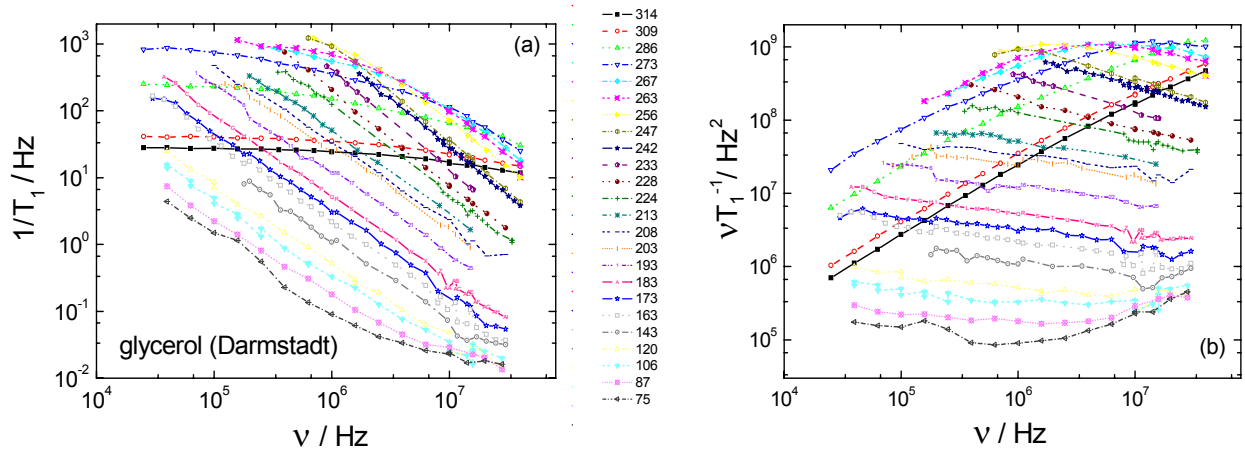
Fig. VI.3 (a) Dispersion of the spin-lattice relaxation time T_1 as measured by homebuilt Darmstadt spectrometer allowing to measure down to low temperatures. (b) Conversion of the data in (a) along Eq. (VI.6) into the susceptibility representation.

VI.2.3. Light scattering (LS)

The light scattering (LS) spectra were previously measured by applying a tandem-Fabry-Perot interferometer and a double monochromator [142]. The susceptibility spectrum is obtained from the scattered light intensity $I(\omega)$ via $\chi_{LS}''(\omega) = I(\omega)/(n(\omega)+1)$ where $n(\omega)$ denotes the Bose factor. The susceptibility

spectra are normalized along the lines described in [142] and the data are displayed in Fig. VI.4.
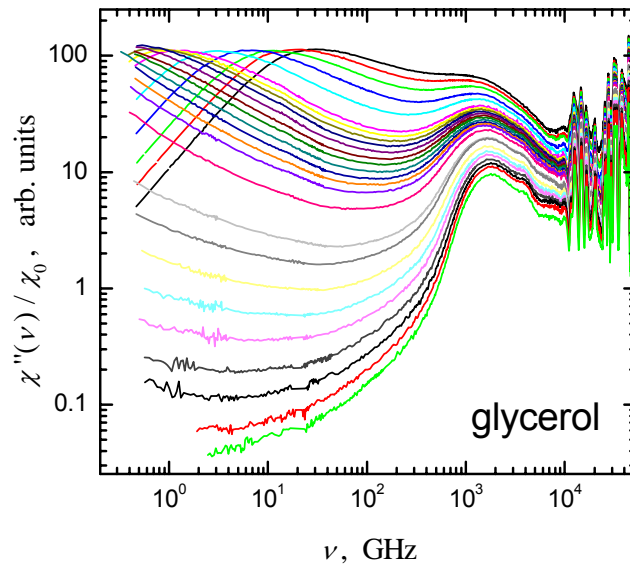
Fig. VI.4 Normalized susceptibility spectra of glycerol as obtained from depolarized light scattering in the temperature range 160 K – 430 K.

VI.3 Discussion

VI.3.1. T > T_g

As mentioned in the introduction, there are several approaches to describe the full slow response including the α-peak and the high frequency wing. The following analysis sticks to the approach II introduced in IV.3. However, one should emphasize that the conclusions drawn from the following spectral analysis do not rely on this particular choice. As mentioned in IV.3, this approach assumes that the FTS principle holds for all temperatures above T_g. The corresponding stretching parameter β is taken from the high-temperature spectra, as there the spectral analysis is not yet hampered by the appearance of the EW and thus can be determined unambiguously. Moreover, it has been demonstrated that the exponent γ of the EW contribution is temperature independent, too. In order to account for the minor changes of the slow dynamics spectra (α-peak and EW) one may allow for a change of the relative weight of the EW contribution with respect to that of the α-peak.

In order to compare the relaxation data obtained by different techniques, the dielectric data displayed in Fig. VI.1 (a) are scaled by the relaxation strength $\Delta\varepsilon$, *i.e.*

113

the temperature dependence described by the Curie law (see II.1) has been eliminated. The frequency range around the relaxation maximum of the dielectric spectra can be well interpolated by applying a CD susceptibility function, as demonstrated in IV.3. Applying a stretching parameter β_{CD} = 0.64, the time constant τ_α is reliably determined and plotted in Fig. VI.5. Typical of glass forming liquids, a non-Arrhenius behavior is obtained. Given the time constant τ_α, the dielectric susceptibility data of Fig. VI.1 (a) can be displayed as a function of the reduced frequency $\omega\tau_\alpha$. As shown in Fig. VI.6 (lines), the resulting master curve extends over 12 decades in frequency for the dielectric spectra including the α–peak and the EW. Note that this scaling is nothing else than the "peak scaling" discussed in relation to Fig. IV.5.
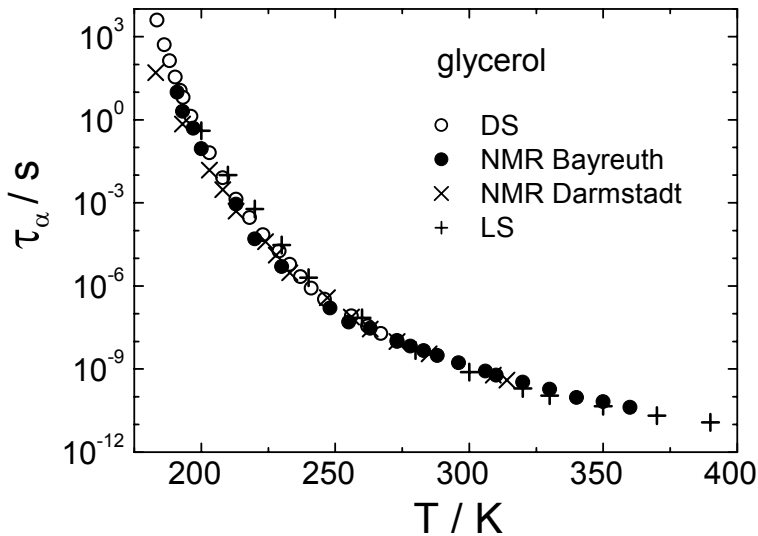
Fig. VI.5 Time constants of the α-process obtained from the construction of the master curves in Fig. VI.6 and Fig. VI.8 applying s NMR (Bayreuth and Darmstadt), dielectric spectroscopy (DS) and depolarized light scattering (LS)

Around the relaxation maximum, the master curve in Fig. VI.6 is well interpolated by a CD function with a width parameter β_{CD} = 0.64 (dashed line). As typical for simple liquids, the low frequency flank ($\omega\tau_\alpha \ll 1$) essentially follows a $\chi''(\omega) \propto \omega^1$ behavior, *i.e.* a slowest Debye limit is found. Due to the time domain measurements (at 194 K) suppressing the conductivity contribution, one can follow the low frequency flank down to an amplitude of 10^{-3}.
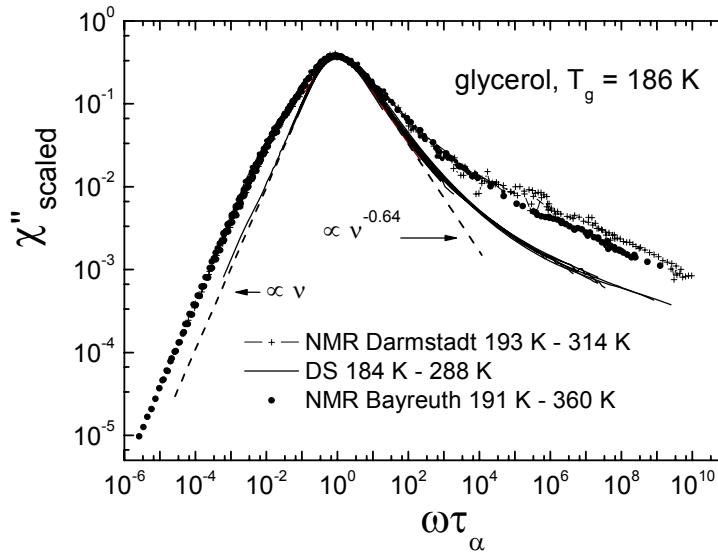
Fig. VI.6 Master curves obtained from dielectric spectroscopy (cf. Fig. VI.1a) and from NMR relaxation data (cf. Fig. VI.2b and Fig. VI.3b), spectra from the temperature range indicated were used; dashed line: interpolation of maximum with a Cole-Davidson function using β_{CD} = 0.64.

One may apply a similar procedure for the NMR data, as shown next. According to Eq. (VI.6) the T_1^{-1} data from Fig. VI.2 (a) and Fig. VI.3 (a) are converted into the susceptibility form and displayed accordingly in Fig. VI.2 (b) and Fig. VI.3 (b). For some temperatures, the susceptibility spectra exhibit a maximum which shifts towards low frequencies upon cooling. This maximum reflects the main relaxation process, *i.e.* the α–relaxation. On the high frequency side of the susceptibility peak the flank becomes progressively flatter upon cooling indicating that the relaxation is not of Debye type, but rather characterized by an asymmetric broadening, as typically observed for molecular glass formers (*e.g.* in the dielectric spectra displayed in Fig. VI.1 a). Below T_g = 186 K (cf. Fig. VI.3 b), a flat power-law dispersion is found with a small negative exponent, which is virtually not changing upon cooling. At lowest temperatures, an indication of a crossover to a positive exponent is observed at the highest accessed frequencies.

A closer look to the low frequency side of the relaxation maximum (cf. Fig. VI.2 b) reveals an additional spectral feature usually not observed in the susceptibility dielectric spectra of simple glass formers: instead of a Debye behavior with $\chi''(\omega) \propto \omega^1$, a shoulder is recognized in the NMR spectra which may indicate the presence of a further low frequency process.

In order to get an estimate of some NMR time constants we interpolated the NMR susceptibility curves which show a relaxation maximum by a CD function, cf. Fig. VI.2 (b). Of course, the low frequency shoulder in the NMR data cannot be interpolated

but still reliable time constants are extracted when fitting the peak region only. Then, the NMR susceptibility data are displayed as a function of $\omega\tau_\alpha$ and included in Fig. VI.6, where the amplitudes of the NMR spectra were scaled by a single factor for all temperatures to allow a direct comparison with the dielectric spectra. To justify this, note that the coupling constant C in Eq. (VI.6) is essentially temperature independent [144]. The other curves in Fig. VI.2 (b) which do not exhibit a relaxation maximum, were shifted horizontally to agree best with the others. A remarkable master curve results also for the NMR data covering about 15 decades, and the corresponding time constants (extracted from the shift factors) are included in Fig. VI.5. They closely follow those compiled from DS. The data sets from the two field cycling spectrometers employed in the present study agree well with each other, in particular at low reduced frequencies. At high frequencies the scatter increases somewhat and very small systematic differences are observed which may be considered not worth to be further discussed. Both NMR data sets show the low frequency shoulder already anticipated when discussing Fig. 2b and 3b.

In order to inspect in detail the particularities at the low frequency side we display in Fig. VI.7 the NMR and DS master curves in a selected frequency range of $10^{-6} < \omega\tau_\alpha < 1$. Here are also included some LS data from Fig. VI.4. The low frequency shoulder is now well recognized in the NMR master curve, but not in the DS and LS data. However, we note that some very weak shoulder is recognized in the part of the dielectric master curve extending to lowest amplitudes respectively frequencies. It leads to a weak systematic excess intensity of the dielectric susceptibility with respect to the CD fit at $\omega\tau_\alpha < 10^{-2}$. Whether this feature is related to the much stronger relaxation feature observed in the NMR data is not yet clear. It follows that NMR probes an additional low frequency process which is essentially not reflected in the reorientation of the molecular dipole moment of glycerol. Regarding its spectral shape we note that the NMR master curve in the range $10^{-3} >> \omega\tau_\alpha >> 1$ can be interpolated by a power-law susceptibility, $\chi''(\omega) \propto \omega^\alpha$, with an exponent $\alpha = 0.65$. At lower reduced frequencies the master curve crosses over to a Debye behavior with an exponent $\alpha = 1.0$. The power-laws are indicated in Fig. VI.7.
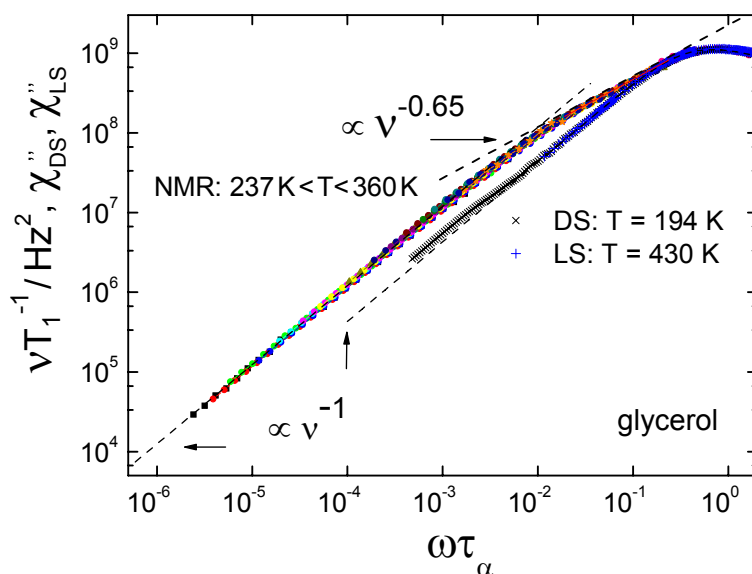
Fig. VI.7 Susceptibility master curve of glycerol in the low frequency range as compiled by NMR, DS and LS; temperature range used for NMR is indicated; dashed lines show power-law interpolations.

Though glycerol is a glass former being studied intensively since long, FFC NMR reveals a relaxation phenomenon with correlation times significantly longer than those of the structural relaxation, not recognized in simple liquids before. As other glass forming systems like o-terphenyl and tristytrene, recently also investigated by FFC NMR [146], do not show such a slow relaxation one may speculate that this special spectral contribution originates from particularities associated with the network of hydrogen bonds present in glycerol. Thereby, the formation of larger clusters may be a possibility. However, it is not easy to imagine a reorientational motion of the presumably rigid molecule glycerol (cf. below) probed by the fluctuations of dipolar couplings among the protons but essentially not by those of the dipole moment.

Comparing the two master curves in Fig. VI.6, pronounced differences are observed not only at low frequencies but also at $\omega\tau_\alpha \gg 1$, in particular, regarding the high frequency wing. Although this EW appears to exhibit a similar exponent γ, its amplitude is significantly stronger for the NMR susceptibility; roughly a factor three is found for the difference of the amplitudes.

In Fig. VI.8 we re-plotted the two master curves from DS and NMR (now only the NMR data from Fig. VI.2 b are taken) for $\omega\tau_\alpha > -1$. In addition, we included the master curve obtained from the LS data in Fig. VI.4. In order to do this, CD fits were carried out for the high temperature LS spectra of glycerol [142] and the low temperature LS

data not showing a relaxation maximum are horizontally shifted to provide also a LS master curve after the static susceptibility is eliminated, cf. [142]. The extracted time constants match well with those from NMR and DS, cf. Fig. VI.5. Together, the three techniques provide correlation times covering the range 10^{-11}s – 10^3 s. The high frequency envelope of the LS curve nicely agrees with the corresponding one measured by NMR. This demonstrates that the EW is also observed by LS and its amplitude appears to be the same as in the case of NMR.

Although distinct from each other, at low as well as at high reduced frequencies, the master curves supplied by the different probing techniques, extending over many decades in frequencies, are a strong indication that the spectral shape of the dynamic susceptibility does virtually not change upon cooling, *i.e.* the FTS principle works very well in case of glycerol. Moreover, as is obvious from the data in Fig. VI.5, the time constants agree very well. This is explicitly shown in Fig. VI.1 (a) where the dielectric and NMR susceptibilities for T = 262 K are directly compared. It becomes clear that FFC NMR allows to reach much lower frequencies and/or amplitudes as compared to DS since in NMR there is no conductivity contribution to interfere at all.
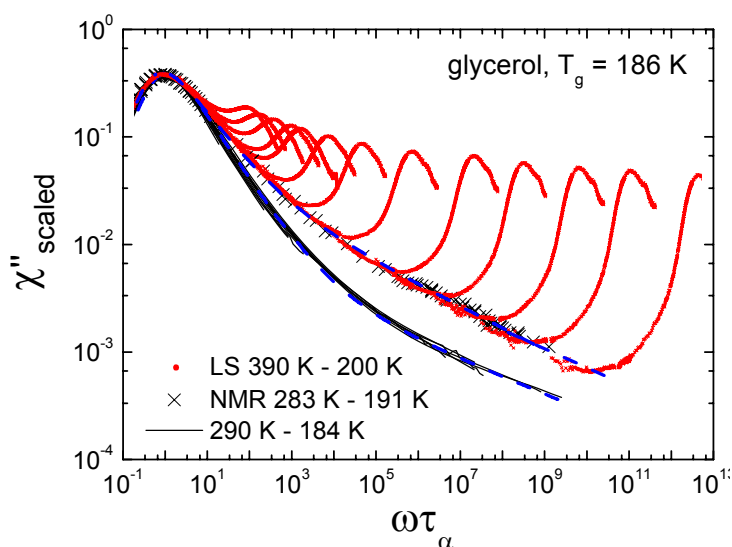
Fig. VI.8 Comparison of the susceptibility master curves of glycerol compiled from NMR, dielectric spectroscopy (DS) and depolarized light scattering (LS); temperature range used as indicated; dashed (blue) lines: interpolations assuming a relaxation described by a Cole-Davidson function (β_{CD} = 0.64) together with a power-law contribution with exponent γ = 0.20.

The following question arises: is it possible to rationalize the difference of the master curves at high reduced frequencies among DS on the one side, and NMR and LS on the other? As shown next, the quantitative differences of the same relaxation feature

recognized in the spectra at high frequencies (EW) can be routed back to probing of the same reorientation by the different techniques.

In first approximation, DS probes the reorientational correlation function of rank $l = 1$ of the Legendre polynomial whereas FFC NMR as well as LS that of rank $l = 2$ (see, *e.g.*, [128]). It is well established that different mechanisms of molecular reorientations may be differently reflected in the two correlation functions, $l = 1$ and $l = 2$, respectively. For example, in the case of rotational diffusion, *i.e.* small angular step rotation, the time constants are different by a factor of $\tau_l/\tau_2 = 3$ whereas $\tau_l = \tau_2$ holds for the case of a random jump mechanism [50]. As demonstrated here, however, the time constants probed by the different techniques agree very well suggesting that the mechanism reflected in the low frequency part of the susceptibility spectrum in the super-cooled liquid is close to the random jump limit, or more precisely, close to the limit of large angle reorientations. In the following will be shown that given two processes the respective relaxation strengths in the correlation function may depend on the rank l, as well.

For the context of the present discussion, one may assume that the reorientational process yielding α–process and EW can be described by two distinct processes, a slow one (α–process) and a fast one (EW). Moreover, one assumes that in first approximation they are statistically independent, as done in IV.3 within approach II discussion. Later it is shown that these assumptions do not spoil the conclusion. Then, a two-step correlation function results which can be described as follows:

$$C_l(t) = C_{excess}(t)C_\alpha(t) = \left[(1 - f_l)\phi_{fast}(t) + f_l\right]\phi_\alpha(t) \qquad \text{(VI.7)}$$

1 − f_l is the correlation losses brought about by the EW $\phi_{fast}(t \rightarrow \infty) = 0$, and f_l is the relaxation strength of the α–process. Note that $1-f_{l=1}$ is identical with $1-S_{ex}$ in approach II considerations. As shown by Lebon et al. [134], Blochowicz et al. [42] or Brodin et al. [142], in the case of the fast process proceeding via small angular steps:

$$1 - f_2 = 3(1 - f_1) \qquad \text{(VI.8)}$$

leading to

$$\chi_2''(\omega) = 3\chi_1''(\omega) \qquad \text{(VI.9)}$$

at high frequencies.

In order to describe quantitatively the master curves in Fig. VI.8 one may recourse to the approach II considerations. Yet, the chosen approach for interpolating the spectra does not change the overall interpretation.

The master curves are fitted by a convolution of two Cole-Davidson functions, with the exponents fixed, as explained in IV.3. The model has only one free spectral shape parameter, the relative relaxation strength *1 – f_{ex}* of the excess wing. It turns out that the fits are close to perfect, without any detectable systematic deviation from the data. This is demonstrated in Fig. VI.8 by the blue dashed lines. Both master curves are well interpolated by this approach, the only difference being the weight *1 – f* of the excess wing. As in IV.3, β = 0.64 and γ = 0.2 were used for both master curves. As a fitting result, only the amplitude of the EW differs by a factor 2.8, very close to the prediction cf. Eq. (VI.8). Thus, one may conclude that the EW contribution is associated with small angle reorientations. One should emphasize again that within this approach, the "apparent" width of the α–relaxation peak being clearly different from each other when probed by NMR and LS or DS, is solely controlled by the relaxation strength *1 – f* of the EW.

VI.3.2. T < T_g

Concerning dielectric investigations at T < T_g, the static permittivity ε_s is not any longer accessible, *i.e* normalized dielectric spectra cannot be obtained. Therefore, in order to compare the NMR and dielectric spectra below T_g we use the raw dielectric spectra. The $\varepsilon''(\nu)$ are displayed in Fig. VI.9 together with the NMR relaxation data divided by temperature T and scaled by a single factor for all temperatures. As the NMR coupling constant C, cf. Eq. (VI.6), is essentially temperature independent, the NMR spectrum ν/T_1 is a kind of normalized susceptibility. According to the fluctuation dissipation theorem the temperature dependent susceptibility is given by

$$\chi''_{NMR}(\nu) \propto 1/T(\nu/T_1).$$ (VI.11)

Apparently, similar power-law spectra with amplitudes exhibiting the same temperature dependence are probed by NMR and DS. The DS spectra measured by applying the high precision bridge [139] (cf. also V.1.1) are included, as well as new broad band data benefiting from the better resolution of new instrumentation (Alpha-A spectrometer).
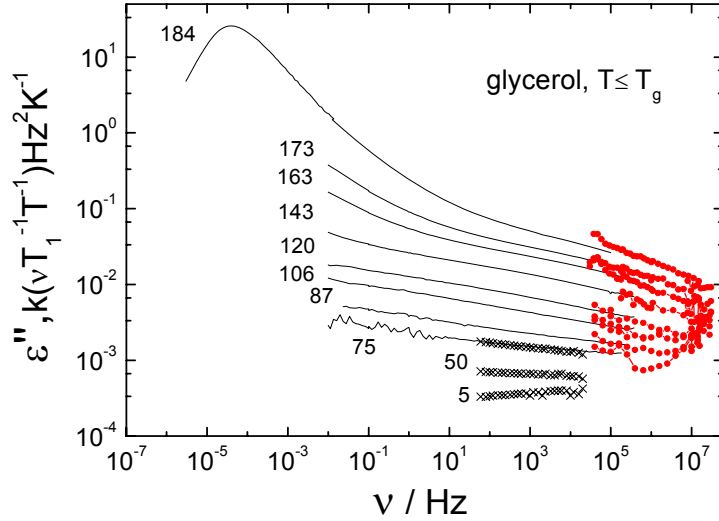
Fig. VI.9 Dielectric (lines and crosses) and NMR susceptibility (red circles) spectra compared to each other at temperatures below T_g; the NMR data are scaled by a single factor k.

As discussed in Chapter V, applying the high precision bridge, dielectric data down to cryogenic temperatures can be compiled and explained within the tunneling model at lowest temperatures. Up to this author's knowledge the NMR data presented here are the first FFC data measured below T_g. Due to the strong local field determined by the dipolar coupling among the proton spins the frequency range covered in the glass is reduced to roughly three decades, cf. Fig. VI.3.

Clearly, the NMR data match well with the dielectric spectra. One can conclude that the temperature dependence of the dynamic susceptibility probed by NMR and DS is the same, specifically we can write

$$\varepsilon''(\omega) \equiv \chi''_{glass}(\omega) \quad \propto \quad (\omega/T_1)/T \tag{VI.12}$$

It appears that the EW emerging first well above T_g persists below T_g, and in the temperature interval investigated by both techniques NMR and DS, the susceptibility $\chi''_{glass}(\omega)$ can be approximated by a power-law with an exponent appearing to be frozen at a value $\gamma \cong 0.1$. Explicitly,

$$\chi''_{glass}(\omega) \propto \omega^{-\gamma} \tag{VI.13}$$

The slight curvature recognized in the spectra may be caused by the presence of a very weak β-process in addition to the EW (in the light of approach II).

121

In Fig. VI.10 (a) the temperature of the different susceptibilities at 4 MHz (NMR) and 20 kHz (DS) are directly compared. The ^{1}H NMR results from Akagi and Nakamura [147] measured at the same (single) frequency and reaching temperatures down to 4 K are also added for comparison. The latter NMR data agree quite well with those compiled from FFC NMR of the present work. Regarding the NMR relaxation rate $1/T_1$ (also included in Fig. VI.10a), a qualitatively different temperature dependence is revealed.

At $T \leq T_g$ down to say 40 K the temperature dependence of $\chi''_{glass}(T)$ may be approximated by an exponential law (dashed line in Fig. VI.10 a),

$$\chi''_{glass}(T) \propto \exp(T/T_0) \tag{VI.14}$$

as was shown previously for several glass formers by dielectric spectroscopy, cf. III.2.3. Accordingly, a value of $T_0 = 33$ K is found.

At lowest temperatures, $\chi''_{glass}(T)$ bends over to a much weaker temperature dependence, characteristic for the tunneling regime (see V.2).
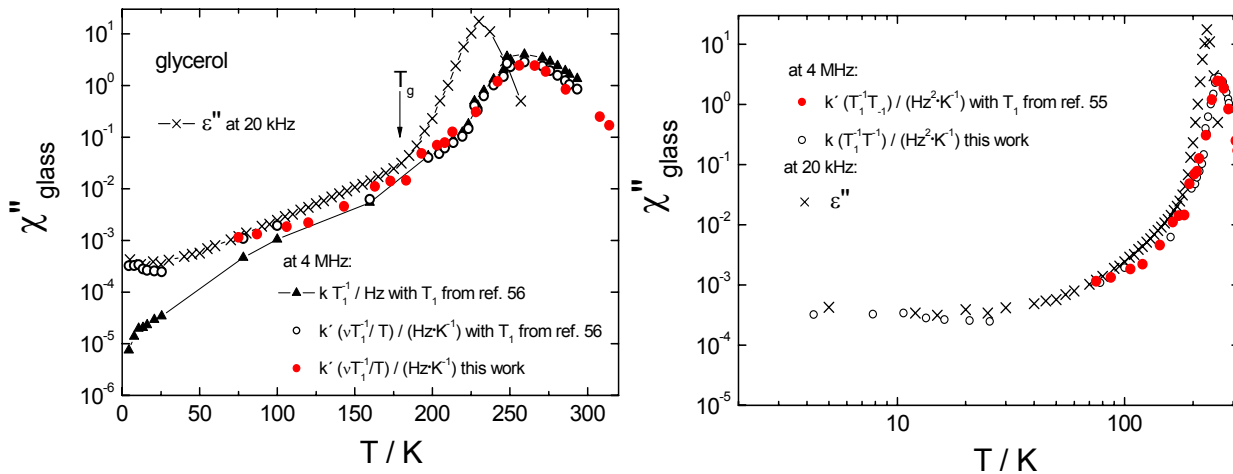
Fig. VI.10 (a) Temperature dependence of the NMR susceptibility (scaled by factor k´) as measured in the present work compared to one obtained from the data reported by Akagi and Nakamura [147] and the imaginary part of the dielectric permittivity $\varepsilon''(T)$; (b) Susceptibilities compared on logarithmic temperature scale.

This regime is better recognized when the susceptibilities are displayed on a logarithmic temperature scale as done in Fig. VI.10 (b). Here the plateau is well recognized, *i.e.* below say 10 K the susceptibility virtually does not change any longer. Thus, it turns out that NMR and dielectric spectroscopy probe the same fluctuations, and as usually NMR data are compiled at higher frequencies as

compared to standard dielectric experiments, both techniques provide complementary information.

VI.4 Conclusions

Regarding the slow relaxation including the α–peak and its high frequency wing (EW), a systematic comparison between the reorientational correlation function of rank $l = 1$ (DS) and $l = 2$ (NMR and LS) becomes possible for the first time by converting relaxation data to the susceptibility representation. Since frequency temperature superposition (FTS) works quite well in the case of glycerol a master curve is obtained extending in frequency over 15 decades.

Considering the temperatures T > T_g, significant differences in the spectral shape of the susceptibility of rank $l = 1$ and $l = 2$ are recognized at the low frequency ($\omega\tau_\alpha$ << 1) as well as at the high frequency side ($\omega\tau_\alpha$ >> 1) of the susceptibility peak. In contrast, the time constants provided by NMR, DS and LS turn out to be the same within experimental error.

An additional relaxation feature in glycerol at the low frequency side of the relaxation maximum is essentially only probed by FFC NMR. Regarding the systematic differences observed at high frequencies for the susceptibilities of rank $l = 1$ and $l = 2$, one may explain them by assuming that the fast dynamics proceeds via small angles whereas the slow dynamics associated with frequencies close to the relaxation maximum is associated with large angle jumps. In such a case, the relative relaxation strength $1 - f_{ex}$ depends on the rank l of the reorientational correlation function. As experimentally found the relaxation strength of the fast respectively high frequency motion is by factor close to 3 three stronger for the $l = 2$ in comparison with the $l = 1$ susceptibility. Both NMR as well as LS spectra exhibit similar relative relaxation strengths of the EW.

In accordance with the approach II interpretation, a strong EW contribution, as is found in the NMR and LS data, broadens the overall relaxation peak, although the contribution of the α–process itself may be taken to follow FTS with a width parameter β being independent on the technique, as the underlying motional mechanism involving large angle reorientations. Since the scaling works well also for the LS data measure far above the melting point, this interpretation has an important consequence. As different strength of the EW controls the different apparent width of

the susceptibility, the latter has to be present already at highest temperatures ($T > T_x$) though obscured by the presence of the fast dynamics contribution. Then, the appearance of the excess wing at $\tau_\alpha \cong 10^{-8}$s may not be taken as a physically meaningful crossover temperature, in accordance with the discussion related to Fig. IV.21 (b).

Regarding the temperatures range below T_g, the susceptibilities probed by NMR and DS reflect the same dynamics. Apparently, reminiscences of the EW, the latter emerging in the super-cooled liquid, also govern the susceptibility at $T \leq T_g$. At still lower temperatures a crossover to the tunneling regime is expected, and, hopefully, in near future FFC NMR experiments will also reach this temperature regime.

VII. Results; Dielectric properties of 1,4 Polybutadiene

Polybutadiene (PB) is a well-known glass forming polymer. Its monomer unit may appear in three different structural configurations as *cis*, *trans* and *vinyl* (displayed in Fig. VII.1), and their percentages depend on the chemical method used for the PB polymerization [109,110]. Previous studies revealed that in addition to its variation with the molecular weight (M), the glass transition temperature T_g of PB is strongly influenced by the content of vinyl units [109].

The absence of the side-groups makes the PB chain structure rather simple, favoring numerous investigations by, *e.g.*, light scattering [100,104], NMR [88.101], neutron scattering [102,103] or molecular dynamics simulations [105,106]. Nevertheless, up to now, a systematic study of the PB dynamics in the full temperature range from the melt down to cryogenic temperatures is missing.

Some PB systems with high M were also investigated with dielectric spectroscopy [26,108]. These dielectric measurements are limited in the temperature range covered due to the relative small dipole moment of the cis and vinyl units. Due to their symmetry, the trans group has no dipole moment, thus it does not contribute to the dielectric response.
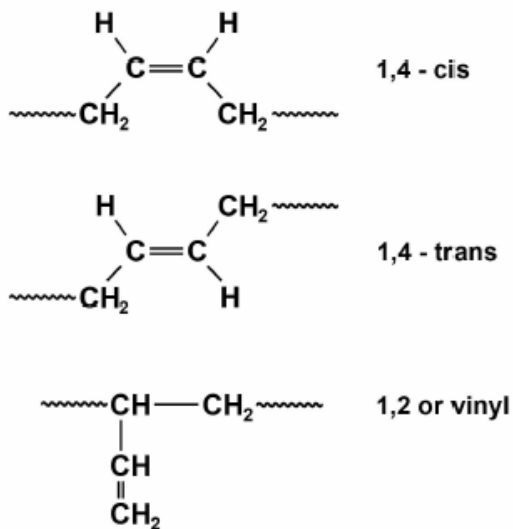
Fig. VII.1. The isomers of PB monomer unit. Figure from [109].

The dielectric spectra of PB with M = 20 000 g/mol were discussed by Kudlik et al. [26] in the temperature range 203 K – 131 K. In addition to the α-peak reflecting the segmental dynamics, a secondary β-peak emerges at high temperatures close to 200 K and survives below T_g ($\approx$ 172 K). The time constants of the β-process follow an Arrhenius temperature dependence with an activation energy $E_a \approx 24 \cdot T_g$. Hansen and

Richert investigated PB with M_w= 12 400 g/mol down to 25 K using a single frequency bridge and found indications for a third relaxation process below 100 K [108]. In the following we extend the measurements by applying the multifrequency bridge AH 2700 A in the temperature range down to 4 K. The study was motivated by NMR investigations in our group, indicating the presence of an additional relaxation process with a time constant much shorter than the one of the β-process [51,88].

We present in Fig. VII.2 (a) the dielectric results for PB with M_w = 20 000 g/mol, extended now for temperatures down to 4 K. The dielectric loss ε'' is presented as a function of both temperature and frequency, and two datasets are included: the broadband spectra previously measured by Kudlik et al. [26] and the high precision spectra measured in this Thesis. A good agreement is observed in the temperature range above 100 K, as the investigations below are possible only with the AH bridge. According to the broadband data, one recognizes at highest temperatures the α-peak. Lowering temperature, the β-process evolves and below T_g the latter dominates the spectra. At temperatures close to 100 K the β-peak shifts out and a new relaxation feature enters in the frequency window provided by the bridge, in accordance with the single frequency measurements by Hansen and Richert [108]. However, as our bridge accesses a frequency interval of almost three decades, one can identify this relaxation feature, called γ-process in the following, now as a distinct peak in the spectra ε''(ν), cf. Fig. VII.2 (b).
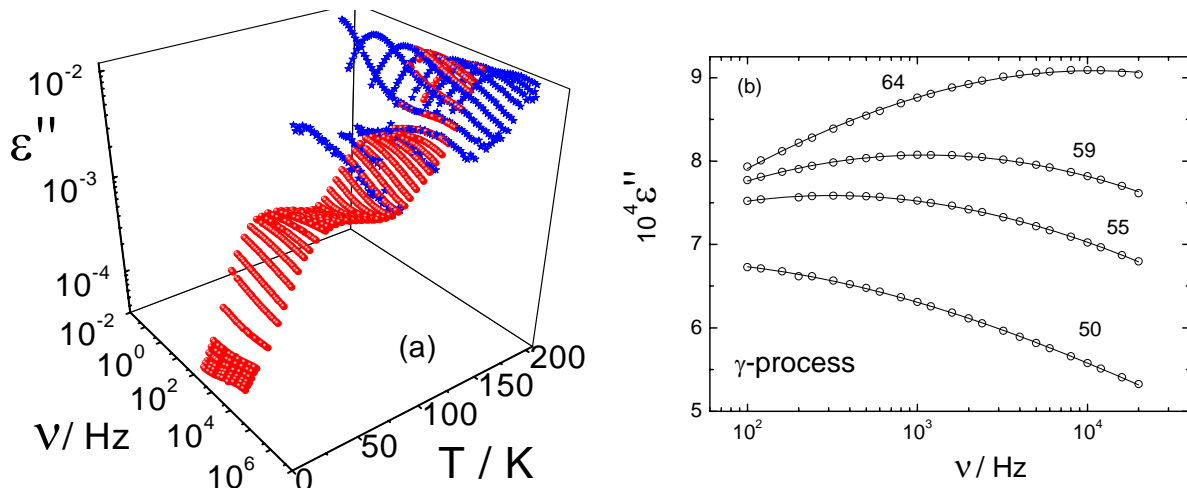
Fig. VII.2. Imaginary part of the complex permittivity ε'' for 1,4 PB with M_w = 20 000 g /mol as function of frequency and temperature; stars: broadband data from [26], dots: high-precision data. (b) Dielectric spectra of the γ-process with corresponding log Gauss fits; indicated temperatures are in Kelvins.

For a better understanding of the nature of the γ-process, we investigated a series of 1,4 PB with different M: 330 g/mol (PB-330), 557 g/mol (PB-557), 777 g/mol (PB-777), 1450 g/mol (PB-1450), 2010 g/mol (PB-2010), 11 400 g/mol (PB-11400), 20 000 g/mol (PB-20000) and 87 000 g/mol (PB-87000). The samples were purchased from Polymer Standards Service (Mainz). In addition, a PB sample with M = 25 000 g/mol (PB-25000) was investigated (courtesy A.P. Sokolov). For comparing the results obtained for the different PB samples, we plot in Fig. VII.3 the temperature dependence for the dielectric loss normalized by its maximum value $\varepsilon''/\varepsilon''_{max}$, obtained at a single frequency of 1 kHz. Note that scaling the data by the ε''_{max} (corresponding to the α-peak) we suppress the weak variation of $\Delta\varepsilon_\alpha$ within the different samples. This representation allows for a direct comparison of the relative dielectric strength of the secondary processes (β and γ) with respect to the relaxation strength of the α-process.
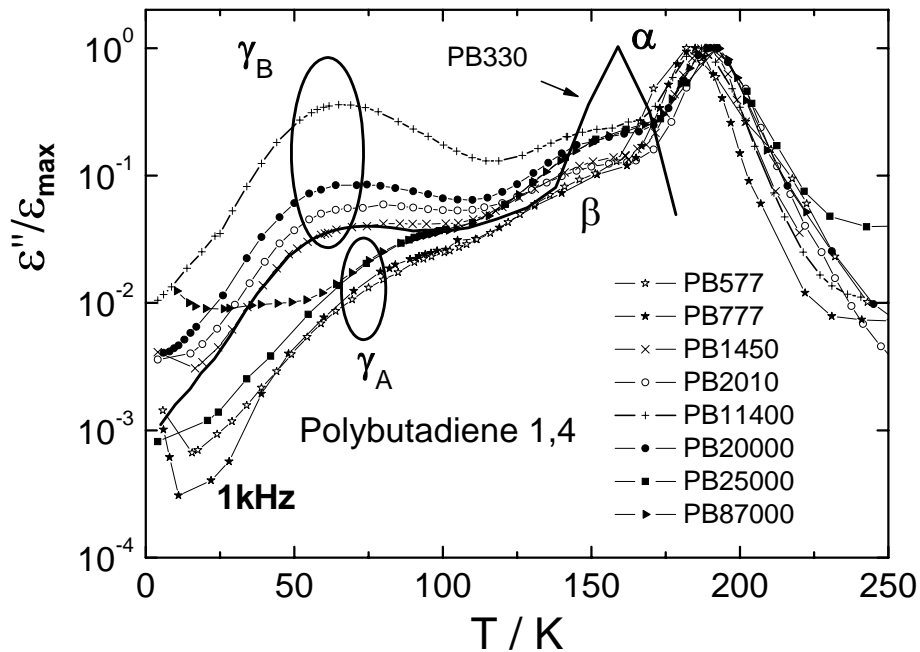
Fig. VII.3. The imaginary part of permittivity scaled by its maximum value $\varepsilon''/\varepsilon''_{max}$ measured at single frequency of 1kHz as function of temperature for different PB samples with indicated M.

We observe that the γ-process is present in all the samples independent of the molecular weight, however with different relative relaxation strengths among the systems. Both β- and γ-peak heights do not show any systematic trend with changing M. Except for PB87000, it appears as the two processes are related: the higher is the amplitude of the β peak, the larger is the γ contribution. Concerning the peak

positions, we remark a weak variation for the α- and the β-peaks with M. The PB330 sample shows a peculiar behavior, as for this system the corresponding α-peak appears at very low temperature (around 160 K). Since for PB330 (the solid line data) only one relaxation peak is observed in below T_g, similar, cf. Fig. VII.3 and the analysis below, with the γ-peak observed for the other samples, it appears that the α-process "drowns" the β-contribution by its shift. This strong shift of the α-process reflects the fact that $T_g(M)$ dependence gets stronger in the low M limit, in accordance with other studies by light scattering [111] and NMR [112].

Concerning the temperature dependence of the γ-process two groups can be distinguished: for PB11400, PB20000, PB2010, PB1450 and PB330 the peak maximum appears at temperatures around 60 K, while for the others PB87000, PB25000, PB777 and PB577 it is found at roughly 20 K higher. For convenience we denote the first group γ_B and the second γ_A. The groups are indicated in Fig. VII.3 by ovals. In order to obtain quantitative results for the time constants τ_γ we interpolated the spectra containing the γ-peak by a log Gauss function $G(\ln\nu)$. For the three samples with lowest molecular weights PB330, PB577 and PB777 the analysis was not possible because the γ-peak is not well-resolved.

Examples of such interpolations are given in Fig. VII.2 (b) for PB20000 and in Fig. VII.4 for spectra of two different PB systems, representative for the γ_B / γ_A situations. Note that the spectra of the γ-process are much broader than a Debye peak and they are quite similar among each other, though measured at different temperatures.
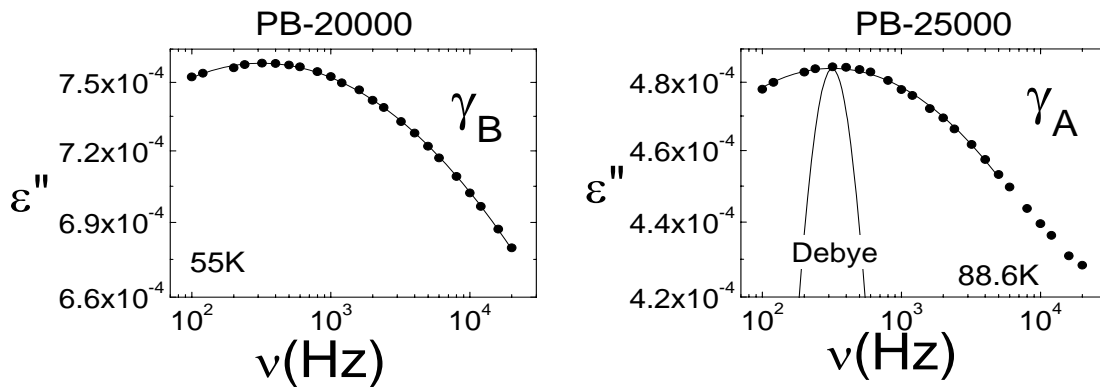
Fig. VII.4. Dielectric spectra of PB2000 at 55 K and PB25000 at 88.6 K on linear scale. Fits using a log Gauss function are included. A Debye peak is displayed for comparison.

From the shift of the maximum ν_γ one obtains the temperature dependence of τ_γ calculated from $\tau_\gamma = 1/(2\pi\nu_\gamma)$. The results are presented in Fig. VII.5 together with the

time constants for α and β processes. The time constants of the α- and β-processes are similar within the different systems with M $\geq$ 557 g/mol. Concerning the well separated γ-process, its time constants τ_γ are very similar within one group (γ_A or γ_B), and exhibit a thermally activated behavior. Fits with an Arrhenius law provide the mean activation energy E_γ. We find $11 < E_{\gamma B} < 14$ kJ/mol for the γ_B group and $17.5 < E_{\gamma B} < 20$ kJ/mol for γ_A.

For comparison, we included the time constants of the secondary process observed by Ding et al. in the light scattering experiments for PB25000 [111]. Inspecting the light scattering data one may tentatively assume that a γ_A process is observed for PB25000. However, as these measurements are performed at high temperatures, the straight line in Fig. VII.5 suggests that the Arrhenius dependence is preserved up to the melt. Note that this is one of the rare situations when a secondary relaxation maximum is identified by an experimental technique other than dielectric spectroscopy.
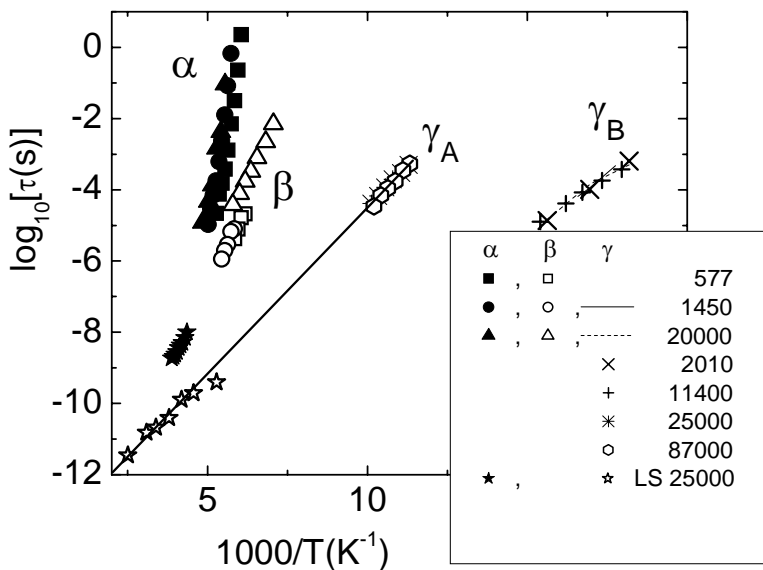
Fig. VII.5. The time constants for the various processes in PB. Data plotted as stars are obtained from light scattering by Ding et al [111]. The line is an Arrhenius interpolation.

To summarize our results, the dielectric investigations of PB below T_g clearly reveal, in addition to a typical β-process a further relaxation process at lower temperatures, here-called γ-process,. The relaxation peak associated with the γ-process is significantly broader than a Debye peak. Its relaxation strength $\Delta\varepsilon_\gamma$ does not show any systematic change with molecular weight. The time constants τ_γ obey a weaker Arrhenius temperature dependence than the one of the β-process. The PB systems can be divided into two groups depending on the activation energy of the γ-process.

^{2}H NMR studies of PB [88] indicated that the reorientational motion involved in the γ-process is highly restricted and can be described by a cone model. For the PB87000 sample, the upper limit for the cone semiangle was determined to be around 8^0 at T < T_g. However, one should keep in mind that the relaxation strength of the γ process strongly varies within the investigated polymers. The extreme case is PB11400, for which the amplitude of the γ-process is larger than the one of the β-process and only by a factor 3 smaller than the one of the α-process, cf. Fig. VII.3.

Concerning the evolution of the spectra at lowest temperatures, below the ones associated with the γ-process, PB shows again an "exotic" behavior: the shift of the γ-process is followed by the appearance of a fourth relaxation peak (δ) at lowest temperatures. One example is shown in Fig. VII.6 (a) for the PB2010 sample: at temperatures below 35 K the signal increases again as a curvature that develops into a peak at lowest temperature T = 4 K. This δ-peak is observed in all PB samples with $M_w \geq 577$ g/mol (cf. Fig. VII.7) and it is responsible for the increase of the $\varepsilon''(T)$ at lowest temperatures in Fig.VII.2. The PB330 system is an exception again: cf. Fig. VII.6 (b) the spectrum at lowest temperature can be interpolated by a power-law with a small positive exponent, resembling the behavior of low molecular weight glasses discussed in Chapter V.
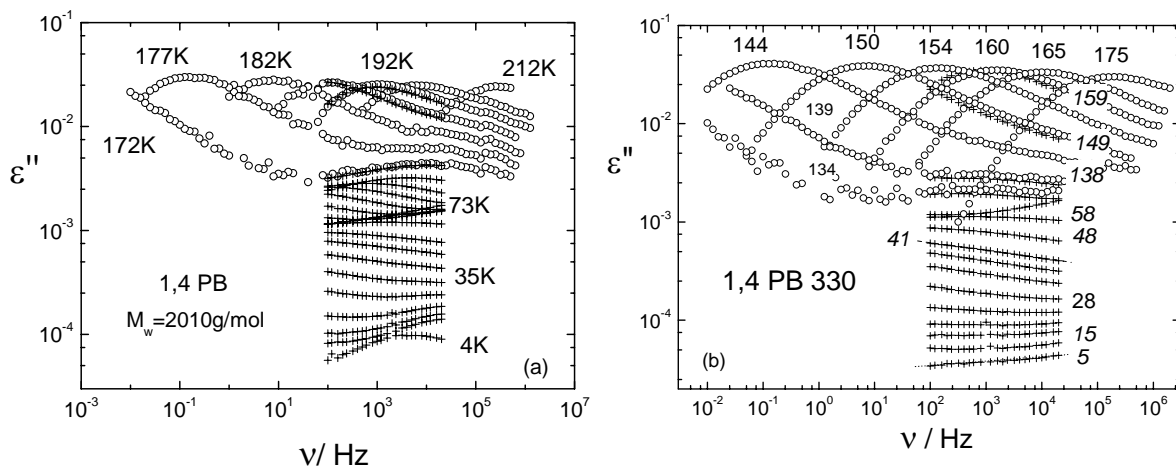
Fig. VII.6. Dielectric spectra of (a) PB2010 and (b) PB330. The high precision data (crosses) are compared with those measured by our broadband techniques (open circles). Few temperatures are indicated. Dashed lines in (b) are interpolations by power-laws.

.
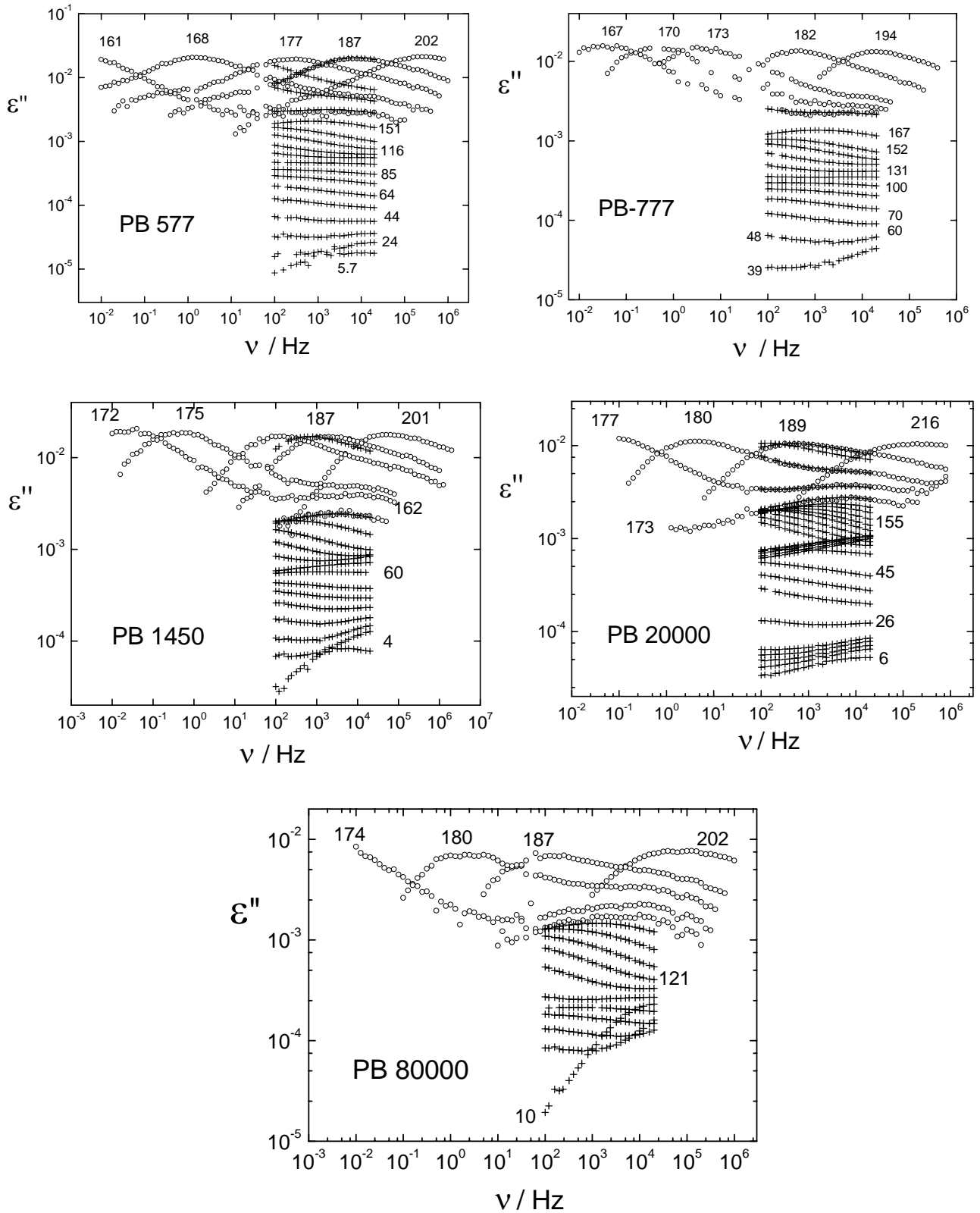
Fig. VII.7. Dielectric spectra of some PB samples discussed above. The high precision data (crosses) are compared with those measured by our broadband techniques (open circles). Few temperatures are indicated.

VII Dielectric properties of 1,4 Polybutadiene

VIII. Summary

The main purpose of this Thesis is to extend the dielectric investigations of molecular glass forming systems down to cryogenic temperatures (2 K), but also to complement previous work above the glass transition temperature T_g. The measurements were performed on systems composed of simple, mostly rigid molecules.

Having at hand a large collection of data, previously compiled in Bayreuth group, this work starts with analyzing the characteristic relaxation features in molecular systems above T_g. Here, secondary relaxation processes emerge on the high frequency side of the main (α) relaxation peak, namely the excess wing (EW) and the β-process. The EW manifests itself in the dielectric spectra as a power-law ($\propto \nu^{-\gamma}$), while β-process as a second relaxation peak. A new approach is introduced to disentangle the different spectral contributions (α-process, EW and β-process). At variance with previous interpretations, the spectral shape of the α-process is assumed to be temperature invariant, obeying frequency temperature superposition (FTS) in the full temperature range above T_g. Its corresponding stretching parameter is taken from the high-temperature spectra, where the analysis is not hampered by the appearance of secondary processes. As a result of this constraint, the EW exponent γ turns out to be not only temperature, but also system independent, $\gamma \approx 0.2$. Thus, the overall spectral evolution for systems with no β-peak above T_g (previously called type A glass formers) is simply described by a small variation of the relative weight of the EW with respect to the α-peak. This weight grows upon cooling, in contrast to the behavior of a β-process. These now called "type A characteristics" are always spoiled by a more or less pronounced manifestation of a β-process. Based on their different temperature changes, the EW and the β-process contributions are disentangled close to T_g, and aging experiments carried out in this work are interpreted within the new scenario. In the glass, the interplay of both EW and β-process determines the relaxation pattern. The β-process appears as the only feature spoiling the universality in the evolution of the dynamics in molecular glass formers, since its relaxation strength does not correlate with the molecular dipole moment.

Based on the above scenario, a consistent comparison between the orientational correlation functions of rank $l = 1$ (probed by dielectric spectroscopy) and $l = 2$ (probed by field cycling NMR and light scattering) is carried out. As demonstrated for glycerol, the NMR and light scattering spectra above T_g are scaled according to FTS over 15 decades in frequency. Significant differences in the spectral shape of the susceptibilities of different ranks are recognized at the low, as well as at the high frequency side of the scaled relaxation peak. In contrast, the time constants provided by the three techniques turn out to be essentially the same. Regarding the systematic differences observed at high frequencies, they are explained by assuming that the fast dynamics (EW) proceeds via small angles. Below T_g, NMR and dielectric spectroscopy reflect the same dynamics for glycerol, *i.e.* an experimental temperature dependence of the susceptibility is revealed.

The evolution of the secondary processes (EW and β-process) is monitored for temperatures well below T_g by applying a high-precision bridge. The bridge was employed to investigate extremely low losses ($\tan\delta < 10^{-5}$), and, for the first time, the frequency dependence (within three decades) of the permittivity down to cryogenic temperatures was accessed for molecular glasses. Two additional relaxation regimes are identified: below 10 K clear indications are found that the tunneling regime is reached. Here the dielectric loss saturates to a plateau when plotted as a function of temperature and the corresponding weak frequency dependence appears as universal $\varepsilon'' \propto \nu^{-0.04}$, at variance with the standard tunneling model predicting no frequency dependence here. Scaling out the molecular dipole moment collapses the plateau heights to an approximately system independent value, indicating a common density of tunneling centers in molecular glasses. At higher temperatures (10 K > T > 50 K) indications for thermally activated dynamics in asymmetric double well potentials are found for these systems. Here, for some systems, the dielectric loss displays a peak when plotted as a function of temperature but not as a function of frequency. This is in accordance with the Gilroy-Phillips model, previously used to interpolate the data for inorganic glasses in this regime. The distribution of the activation barriers g(V) is directly accessed by scaling the spectra in accordance with this model. However, g(V) extracted for molecular glasses appears as a stretched exponential.

Zusammenfassung

Das Hauptanliegen dieser Arbeit ist sowohl die Ausweitung der dielektrischen Untersuchungen an molekularen Glasbildnern bis in den Tieftemperaturbereich (2K), als auch die Ergänzung bisheriger Ergebnisse oberhalb der Glasübergangstemperatur T_g. Die Messungen wurden an Systemen durchgeführt, die aus einfachen, meist starren Molekülen bestehen.

Oberhalb von T_g weisen all diese Systeme sekundäre Relaxationsprozesse auf, die als „excess wing" (EW) bzw. β-Prozess auf der Hochfrequenzseite des α-Peaks hervortreten. Der EW manifestiert sich in den dielektrischen Spektren als Potenzgesetz ($\sim \nu^{-\gamma}$), während der β-Prozess als ein zweites Relaxationsmaximum zum Vorschein kommt. Die Analyse dieser Phänomene für eine Vielzahl von zum Teil bereits in früheren Arbeiten vermessenen molekularen Glasbildnern steht im Fokus des ersten Teils dieser Arbeit. Es wird hierbei ein neuer Ansatz vorgestellt, mit dem es möglich ist, die Temperaturabhängigkeiten der verschiedenen Spektralbeiträge (α-Prozess, EW und β-Prozess) quantitativ zu beschreiben. Im Widerspruch zu bisherigen Betrachtungsweisen wird angenommen, dass die spektrale Form des α-Prozesses temperaturunabhängig ist und somit im gesamten Temperaturbereich oberhalb von T_g der Frequenz-Temperatur-Superposition (FTS) genügt. Der Breitenparameter des α-Prozesses wird aus den Hochtemperaturspektren gewonnen, deren Analyse nicht durch das Auftreten sekundärer Prozesse beeinträchtigt wird. Infolge dieser Randbedingung stellt sich heraus, dass der EW-Exponent γ nicht nur temperatur-, sondern auch systemunabhängig ist ($\gamma \approx 0.2$). Folglich kann die Gesamtentwicklung der Spektren von Systemen ohne β-Peak (früher "Typ A" genannt) oberhalb von T_g durch kleine Variationen der relativen Gewichtung des EW bezüglich des α-Peaks beschrieben werden. Im Gegensatz zum Verhalten des β-Prozesses nimmt sein spektrales Gewicht während des Abkühlens zu. Diese nun "Typ-A-Charakteristika" sind immer von einer mehr oder weniger ausgeprägten Manifestation des β-Peaks überlagert. In der Nähe von T_g sind EW- und β-Prozeß-Beiträge voneinander getrennt, und Aging-Experimente werden in diesem Szenarium interpretiert. Im Glas bestimmt das Zusammenspiel von

EW und β-Prozess das Relaxationsmuster. Der letztere ist der einzige Beitrag, der die Universalität der Evolution der Dynamik molekularer Glasbildner zu stören scheint, da seine Relaxationsstärke nicht mit dem molekularen Dipolmoment korreliert ist.

Basierend auf dem oben erläuterten Szenarium wird für Glyzerin ein Vergleich der Orientierungskorrelationsfunktionen des Ranges l=1 (dielektrische Spektren - DS) bzw. l=2 (Field-Cycling NMR und Lichtstreuung - LS) durchgeführt. Wie gezeigt, werden die DS-, NMR- und LS-Spektren oberhalb von T_g gemäß des FTS über 15 Dekaden in der Frequenz skaliert. Sowohl an der Nieder- als auch an der Hochfrequenzseite des skalierten Relaxations-Peaks erkennt man signifikante Unterschiede in den spektralen Formen der Suszeptibilitäten verschiedener Ränge. Im Gegensatz dazu sind die von den drei Meßmethoden erhaltenen Zeitkonstanten im Wesentlichen gleich. Die bei hohen Frequenzen beobachtbaren, systematischen Unterschiede kann man durch die Annahme erklären, dass die schnelle Dynamik (EW) im Rahmen einer Kleinwinkelbewegung vonstatten geht. Unterhalb von T_g sondieren NMR und dielektrische Spektroskopie die gleiche Dynamik und weisen die gleiche exponentielle Temperaturabhängigkeit auf (im Fall von Glyzerin).

Die Entwicklung der Sekundärprozesse (EW und β-Prozess) wird für Temperaturen deutlich unterhalb von T_g mit Hilfe einer Hochpräzisionsmeßbrücke verfolgt. Die Brücke deckt frequenzmäßig drei Dekaden ab und detektiert dabei äußerst kleine dielektrische Verluste ($\tan\delta < 10^{-5}$), was die Untersuchung molekularer Gläser bis zu sehr tiefen Temperaturen erstmals ermöglichte. Zwei zusätzliche Relaxationsregimes werden identifiziert: unterhalb von 10K werden klare Anzeichen dafür beobachtet, dass das Tunnelregime in molekularen Gläsern erreicht wird. Der dielektrische Verlust erreicht hier als Funktion der Temperatur ein Plateau, und die schwache Frequenzabhängigkeit erweist sich als universell, d.h. $\varepsilon''(2\,K - 4\,K) \propto \nu^{0.04}$. Skaliert man die Daten mit dem molekularen Dipolmoment, erweisen sich die Plateauwerte als näherungsweise systemunabhängig, was auf ähnliche Tunnelzentrendichten in molekularen Gläsern hindeutet. Bei höheren Temperaturen (10K < T < 50K) werden Hinweise auf thermisch aktivierte Dynamik in asymmetrischen Doppelmuldenpotentialen gefunden. Für mache Systeme weist hierbei der dielektrische Verlust als Funktion der Temperatur ein Maximum auf, nicht aber als Funktion der Frequenz. Dies stimmt mit dem Gilroy-Phillips-Modell überein, das bisher zur Interpolation der Daten anorganischer Gläser in diesem

Regime verwendet worden ist. Die Verteilung der Aktivierungsenergiebarrieren g(V) wird direkt gewonnen, indem man die Spektren gemäß diesem Modell skaliert. Die für molekulare Gläser gewonnene Verteilung g(V) erweist sich als gestreckt exponentiell.

__Zusammenfassung__

Appendix

A. Systems investigated in this work

Type A systems

System	T_g (K)	Abbreviation	Investigation details	
			Temperature range	*Spectrometers*
Glycerol	189	GLY	316 K– 0.05 K	HF, BB, TD, HPB, home build cryostat
Propylene Carbonate	158	PC	170 K – 2 K	TD, HPB
2-Picoline	130	2-pic	144 K – 3 K	HPB
Propylene Glycol	168	PG	233 K – 53 K	BB, TD, HPB
4-tertbutyl pyridine	166	4-TBP	184 K – 7 K	HPB
m-tricresyl phosphate	205	m-TCP	232 K – 5 K	HPB
o-terphenyl	245	OTP	264 K – 190 K	HPB
Salol	220	SAL	237 K – 3 K	HPB

Type B systems

System	T_g (K)	Abbreviation	Investigation details	
			Temperature range	*Spectrometers*
1,4 Polybutadiene	-	PB	200 K – 4 K	BB. HPB
Toluene	117	TOL	124 K – 4 K	HPB
m-Fluoroaniline	172	FAN	191 K – 3 K	HPB
Polybutadiene	-	PB	400 K – 4 K	BB, HPB
Trimethyl phosphate	136	TMP	230 K – 60 K	HF, BB
Cyano cyclohexane	134	CCH	70 K – 4 K	HPB

HF – high frequency Hewlet Packard 4291 B network analyzer.

BB – broad band Impedance Analyzer Schlumberger SI1260 from Novocontrol.

TD – time domain spectrometer.

HPB – high precision bridge AH 2700 A from Andeen-Hagerling.

Appendix A

B. Dielectric response of 2-methyl tetrahydrofuran
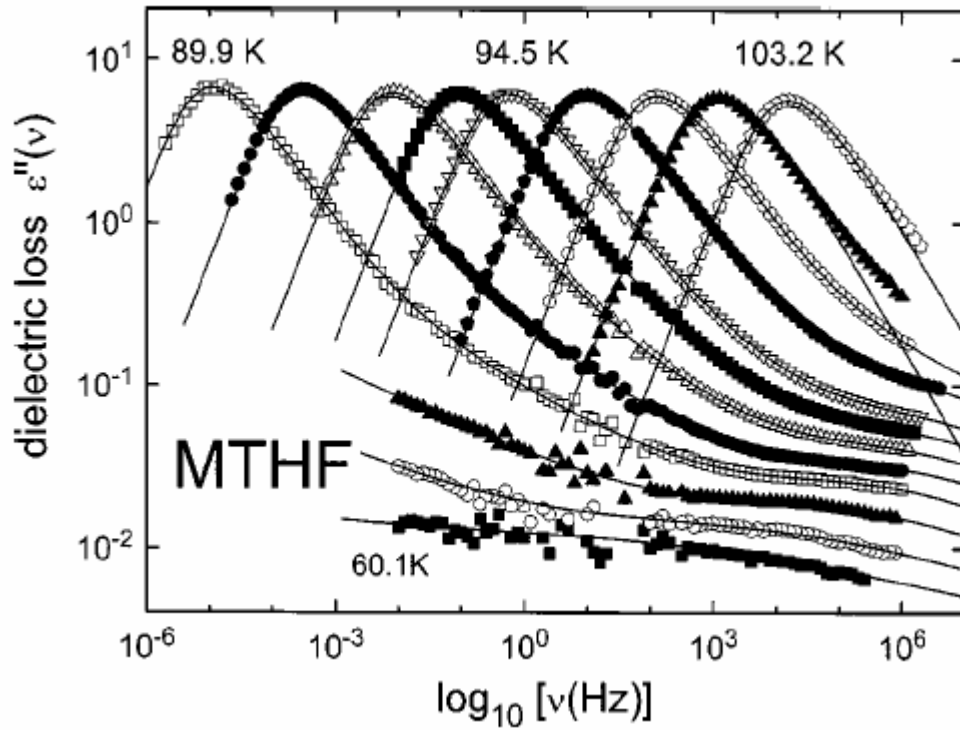
Fig. B.1. Double logarithmic representation of the frequency-dependent dielectric loss ε'' of MTHF for temperatures of 60.1, 70.1, 79.9, 89.9, 91.4, 92.5, 93.5, 94.5, 96.3, 98.3, 100.3, and 103.2 K. The lines are fits using the GGE function, in accordance with approach I. Figure taken from [80].

C. The spectra analysis using approach I; scaling relations.

.

As discussed in IV.2, within approach I one identifies two temperature regimes for the evolution of the slow dynamics in type A glass-formers. They are easily identified when the parameters β and γ of the GGE function are discussed as functions of temperature. As seen in Fig. C.1 (a), whereas γ and β for glycerol and PC do not change at high temperatures $T > T_x$ (*i.e.* FTS applies here), a linear decrease is recognized below the crossover temperature T_x.
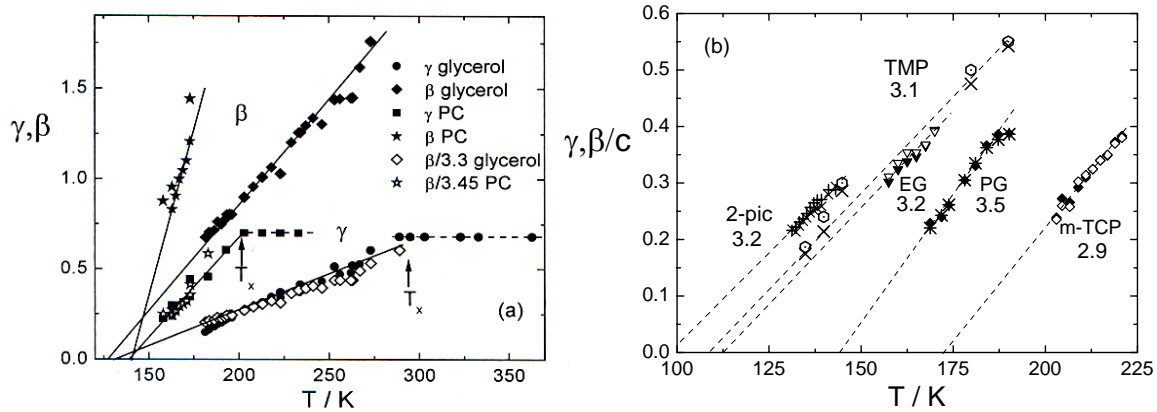
Fig. C.1 (a) The parameters β and γ fixing the power-law exponents in the GGE distribution for glycerol and propylene carbonate (PC) as a function of temperature; β is divided by a factor c demonstrating that the exponents β and γ are proportional to each other in the low temperature regime; data of high-temperature regime from analyzing the spectra measured by Lunkenheimer et al. [25] for glycerol and PC are also included and the crossover temperature T_x is indicated. (b) the parameters γ and β/c for 2-picoline (PIC), ethylene glycol (EG), trimethyl phosphate (TMP), propylene glycol (PG) and tricresyl phosphate (m-TCP) (Figure from [43]).

It appears that for each system β and γ extrapolate to zero at a similar temperature therefore β and γ are proportional to each other. This is indeed the case, as seen in Fig. C.1. (b) where γ (T) is similar with $\beta(T)/c$, with c being a constant indicated in the figure for every system.

In the low temperature regime $T < T_x$ one finds:

$$\beta/\gamma = c = 3.2 \pm 0.3$$

$$\gamma = A \, (T - T_\gamma) \tag{C.1}$$

where T_γ is the temperature for which γ(T) extrapolates to 0 in Fig. C.1 (b).

Below T_x the spectral shape of the slow dynamics appears to change in a characteristic way: the excess wing emerges as a power-law with an exponent γ that shows a linear temperature dependence. The question arises how $\gamma(T)$ and $\tau_\alpha(T)$ are

related in detail. Interpolating the linear $\gamma(T)$ dependency (the solid line in Fig. C.1 a) and using the Stickel linearization of the VFT, cf. Eq. (I.1):

$$S = \left(\frac{-d\lg\tau_\alpha}{dT}\right)^{-1/2} = D^{-1/2}(T - T_0)$$

one can identify T_γ from Eq. (B.1) with T_0, yielding a proportionality between the Stickel parameter S and the exponent γ [43]. This can be easily checked by plotting S^* (the Stickel parameter normalized by its value at T_g) as function of γ. We observe in Fig. C.2 that, within the scatter, for all systems S^* is proportional with the EW exponent γ.
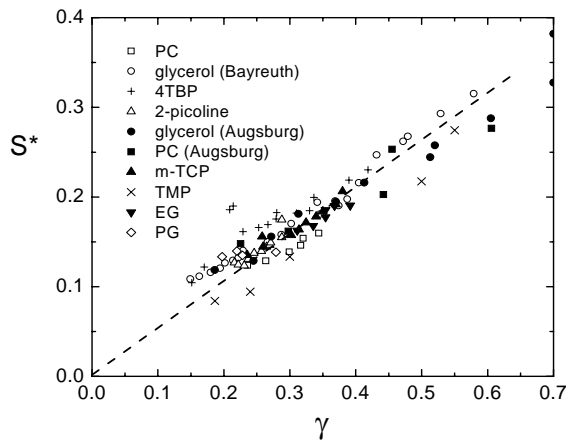
Fig. C.2 The normalized Stickel ($S^*=S/S_{T=T_g}$) parameter as a function of the exponent γ. Dashed line: guide for the eye.

It is well established that the low-temperature VFT equation fails above a certain temperature T_S [23,24]. It becomes interesting to find whether there is a connection between T_X marking the crossover in the evolution of the susceptibility line shape and the temperature T_S separating different temperature dependences of the structural relaxation time $\tau_\alpha(T)$. Using the Stickel representation it may be difficult to identify T_s because it involves the derivative $d\tau_\alpha/dT$ that usually scatters strongly. To better determine T_s one may try a linearization of the VTF as following: defining T_g as the temperature at which $\tau_\alpha(T_g) = \tau_g = 100$ s, one can rewrite the VFT equation (I.1) as:

$$\log\frac{\tau_\alpha}{\tau_0} = \frac{K_0^2}{m(T/T_g - 1) + K_0} \tag{C.2}$$

where $K_0 = \log(\tau_g/\tau_0)$ and m is the fragility, defined by Eq. (I.2). The values of T_g are given in Table C.I for every system used in the following analysis. Plotting $\lg(\tau_\alpha)$ as a function of $z = m(T/T_g -1)$ a master curve is expected for all glass formers, type A as well type B, assuming that the time constants follow a VFT dependence and τ_0 is similar for the systems under consideration. The results, before and after the scaling,

are shown in Figs. C.3 (a) and (b), respectively. The only parameter used for the scaling of all data in (b) is the fragility m. The values obtained for *m* are also given in Table C.I. For m-TCP and 2-picoline the time constants in the high temperature range were obtained using the DC conductivity and light scattering spectra [35].
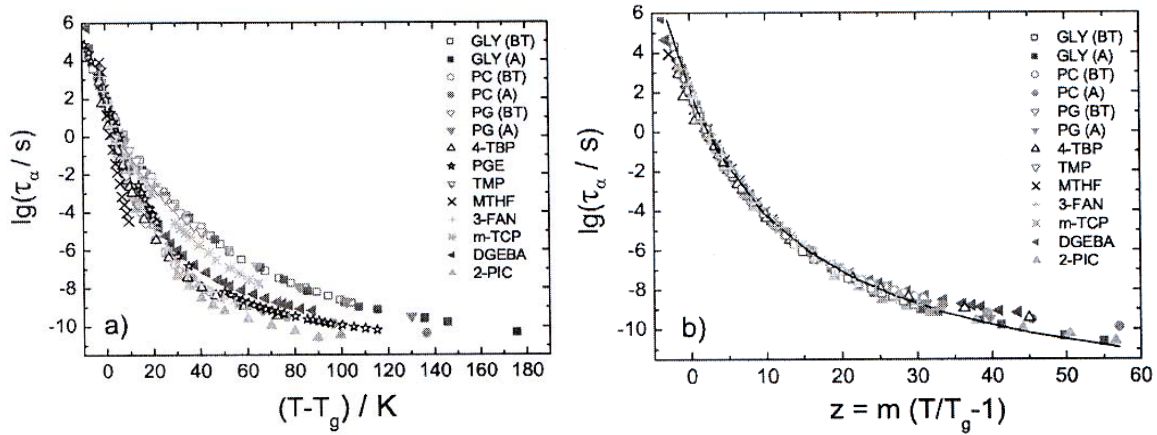
Fig. C.3 (a) The average relaxation times τ_α of all the systems investigated. (b) the effect of individual fragilities at T_g is removed and a master curve is obtained; solid line is calculated using Eq. (C.2) with $K_0 = 17$ ($\tau_0 = 10^{-15}$ s).

According to Fig. C.2 (b), it is clearly recognized that the time constants of all systems follow the master curve (C.2) up to a value of z around 25. At higher temperatures, some curves spread apart, indicating that deviations from the VFT behavior occur, maybe due by a system dependent τ_0 parameter. Using that

$$\log(\tau_\alpha / \tau_0) = \log(\tau_\alpha / \tau_g) + \log(\tau_g / \tau_0) \tag{C.3}$$

eq. (C.2) can be rewritten as:

$$\log\frac{\tau_\alpha}{\tau_g} = -\frac{zK_0}{z + K_0} \tag{C.4}$$

Figure C.4 upper half shows the linearization of VFT equation, *i.e* τ_α now as a function of $zK_0/(z+K_0)$. For every system K_0 (implicitly τ_0) is chosen in the way that the slope −1 is obtained in the low temperature regime. The corresponding values of τ_0 obtained as such are posted in Table C.1 They vary around $\tau_0 \approx 10^{-15}$ s for all systems discussed here. This analysis is more sensitive with respect to the Stickel one since no derivative of the data points is involved.

In order to extract the value of τ_S that marks the crossover, we plot the values of $\lg(\tau_\alpha/\tau_{VFT})$ in the lower half of Fig. C.4. Here τ_{VFT} refers to the τ_α satisfying Eq. (C.4), *i.e.*, the VFT law.
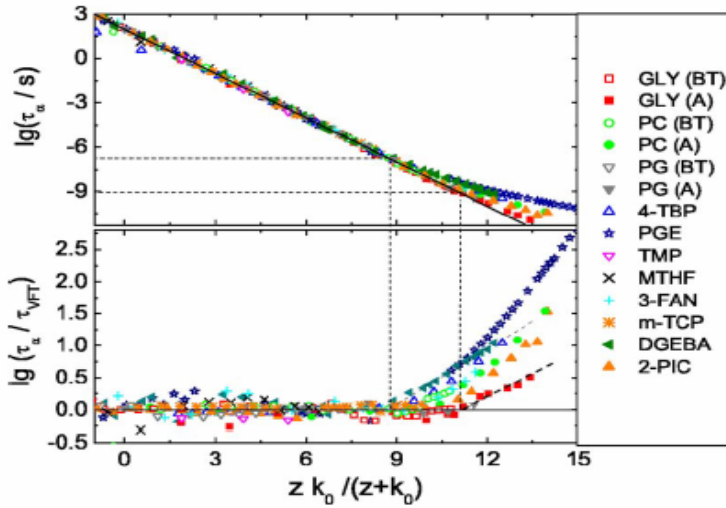
Fig. C.4 The master curve for all the systems under investigation. Upper part: the solid line represents Eq. (C.4). Lower part: the ratio $\log(\tau_\alpha/\tau_{VFT})$ indicates the deviations from the VFT behavior; dashed lines are guide for the eye.

Comparing the upper and lower parts of Fig. C.4 one can easily read off a value for the crossover to the VFT failure at $\lg\tau_S \cong -9$ for PC, glycerol and 2-PIC. This value corresponds to the crossover temperature T_s and is very similar with the one marking the crossover in the line shape of susceptibility spectra, cf. Figs. C.1. Similar temperatures (T_S) with the ones obtained here were reported by applying the Stickel derivative analysis [24]. The crossover temperatures identified on the one hand from the changes of the relaxation spectra and on the other hand from deviations from the low temperature VFT behavior of $\tau_\alpha(T)$ are found to coincide within the accuracy of the experimental data for the three type A systems glycerol, PC and 2-picoline. We included in our analysis the data for DGEBA and PGE (phenyl glycid ether [82]), even though a spectral shape analysis including a contribution from the excess wing cannot be performed for these two systems due to a strong β-process contribution. However, their time constants clearly show a deviation from the VFT behavior at $\lg\tau_S \cong -7$, demonstrating that τ_S is an individual quantity. Accordingly, the so-called "magic relaxation time" discussed in [96] becomes obsolete.

System	GLY	PC	2-PIC	4-TBP	TMP	PG	m-FAN	MTHF	m-TCP	EG	DGEBA	PGE
T_g(K)	188.6	158	129.8	165.5	136.2	168	172.4	91.5	205.4	152	250.4	192.8
m	53.4	101.5	81.8	102.6	80.6	51.3	94.6	101.4	76.4	50	124.2	81.3
α	10	20	5	4	3	30	5	10	2	20	3	4
$\lg\tau_0$	-15	-14.5	-16	-15.3	-15	-14.3	-16	-14	-14.6	-15	-15	-20

Table C.1. Parameters of the systems investigated with approach I.

D. Aging experiment on 4-tertbutyl pyridine (4-TBP)

The peculiarity of 4-TBP is that at T_g (165 K) and slightly below it reveals in its spectra a stronger curvature with respect to the other type A systems, cf. Fig. IV.2. This strong curvature may indicate the presence of a faster or stronger β-process with respect to the α-process and offers the possibility to get completely resolved by aging.

In Fig. D.1 we present the results for 4-TBP aged at 155 K, almost 10 K below T_g. At this temperature the structure fully relaxes within 150 h, as the spectrum does not change afterwards. The effect of the aging is stronger than in the case of the measurements in glycerol (cf. Fig. IV.11 a), as the spectrum at lowest frequencies changes horizontally by a factor 10. In the following we apply the same analysis as done for glycerol in IV.3.1. For determining the stretching parameter β of the α-peak we used the spectrum at 187 K, where the EW influence is assumed to be minimal. As shown in Fig. D.1, a value $\beta = 0.54$ is obtained.
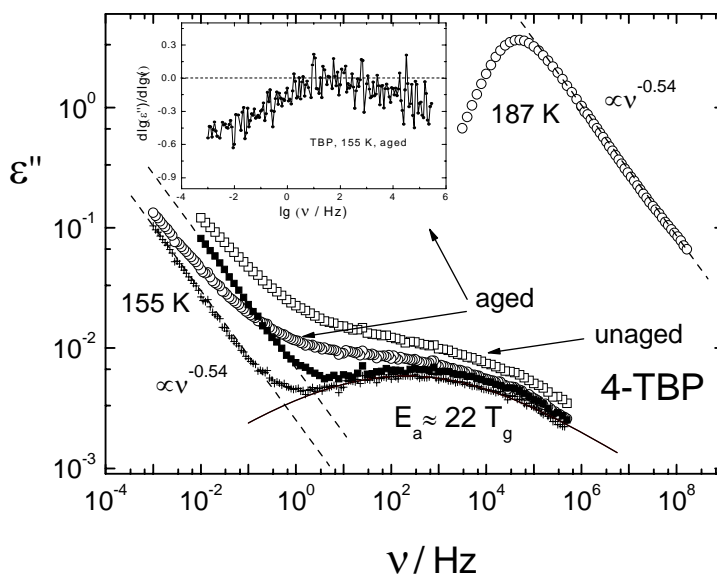
Fig. D.1 Aging analysis of 4-TBP at 155 K. Inset: the derivative of the equilibrium spectrum.

From both spectra measured at 155 K, aged and non-aged, respectively, we subtract the EW as a power-law with exponent γ, such that the remaining spectral contributions are the high-frequency flank for the α-peak as $\nu^{-0.54}$ and a symmetric β-peak. The exponent of the EW was found, as for glycerol, $\gamma = 0.21$. The position of the β-peak indicates a value for its activation energy $E_a \approx 22\ T_g$ (cf. discussion in

IV.3.1), a value close to the one found in type B glasses, and also in glycerol within the same analysis.

In the inset of Fig. D.1 we plotted the derivative of the spectrum measured in equilibrium $dlg(\varepsilon'')/dlg(\nu)$, *i.e.* the apparent exponent in the spectrum at different frequencies. Within the scatter, the value of the derivative gets close to 0 at frequencies around 100 Hz, as the aged spectrum gets almost flat here. As a maximum in the spectra is defined when the $dlg(\varepsilon'')/dlg(\nu)$ curve exceeds the 0 value, one concludes that the β-peak could not be separated in this experiment. However, as the derivative of the measured data is very close to the 0 value (closer than the ones obtained by Schneider et al. for glycerol and PC aged for 5 weeks), it may be worthwhile, in order to separate the β-peak, to investigate 4-TBP at even lower temperatures and for longer aging times.

Bibliography

[1] C.J.F. Böttcher, and P. Bordewijk, *Theory of electric polarization I: Dielectrics in static fields*, Elsevier, Amsterdam, London, New York, 1978.

[2] ----, *Theory of electric polarization II: Dielectrics in time-dependent fields*, Elsevier, Amsterdam, London, New York, 1978.

[3] F. Kremer, and A. Schönhals, (Eds.) *Broadband dielectric spectroscopy*, Springer, Berlin, 2003.

[4] H. Frölich, *Theory of Dielectrics*, Clarendon Press, Oxford, 1968.

[5] A.K. Jonscher, *Dielectric relaxation in solids*, Chelsea Dielectric Press, London, 1983.

[6] L. Onsager, J. Am. Chem. Soc., **58**, 1486 (1938).

[7] D. Forster, *Hydrodynamic Fluctuations, Broken Symmetry, and Correlation Functions*, Addison - Wesley, London, 1975.

[8] E.V. Russell, N.E. Israeloff, L.E. Walther and H. Alvarez-Gomariz, Phys. Rev. Lett., **81**, 1461 (1998).

[9] E.V. Russell and N.E. Israeloff, Nature **408**, 695 (2000).

[10] W. Götze, *Aspects of structural glass transitions,* in Liquids, Freezing and Glass Transition (Les Houches, Session LI), J. P. Hansen, D. Levesque and J. Zinn-Justin (Eds.), North-Holland, Amsterdam, Oxford, New York, 1991.

[11] T. Blochowicz, *Broadband Dielectric Spectroscopy in Neat and Binary Molecular Glass Formers*, PhD thesis, Bayreuth, 2003.

[12] H. Wagner and R. Richert, J. Phys. Chem. B, **103,** 4071 (1999).

[13] A. Kudlik, *Dielectrische Spektroskopie an organische Glasbildnern - Ein Beitrag zur Linienform der dynamischen Suszeptibilität*, PhD Thesis, Bayreuth, 1997.

[14] T. Wagner, PhD thesis, Bayreuth (1995).

[15] D.W. Davidson and R. H. Cole, J. Chem. Phys., **18**, 1417 (1950).

[16] C. A. Angell, K. L. Ngai, G. B. McKenna, P. F. McMillan and S. W. Martin, J. Appl. Phys., **88**, 3113 (2000).

[17] E. Donth, *The Glass Transition: Relaxation Dynamics in Liquids and Disordered Materials*, Springer-Verlag, Berlin, Heidelberg, New York, 2001.

[18] M. D. Ediger, C. A. Angell and S. R. Nagel, J. Phys. Chem., **100**, 13200 (1996).

[19] G. Tammann and W. Hesse, Z. Anorg. Allg. Chem., **156**, 245 (1926).

[20] H. Vogel, Phys. Z., **22**, 645 (1921).

[21] C.A. Angell, J. Non-Cryst. Solids, **131-133**, 13 (1991).

[22] R. Böhmer, K. L. Ngai, C. A. Angell and D. J. Plazek, J. Chem. Phys., **99**, 4201 (1993).

[23] F. Stickel, E.W. Fischer and R. Richert, J. Chem. Phys. **102**, 6251 (1995)

[24] F. Stickel, *Untersuchung der Dynamik in niedermolekularen Flüssigkeiten mit Dielektrischer Spektroskopie*, PhD Thesis, Mainz, 1995

[25] P. Lunkenheimer, U. Schneider, R. Brand and A. Loidl, Contemporary Physics, **41**, 15 (2000).

[26] A. Kudlik, S. Benkhof, T. Blochowicz, C. Tschirwitz and E. Rössler, J. Mol. Struct., **479**, 201 (1999).

[27] S. Benkhof, *Dielektrische Relaxation zur Untersuchung der molekularen Dynamik in unterkühlten Flüssigkeiten und plastischen Kristallen*, PhD thesis, Bayreuth, 1999.

[28] M. Goldstein, J. Chem. Phys., **51**, 3728 (1969).

[29] G. P. Johari, J. Chem. Phys., **58**, 1766 (1973).

[30] S. Adichtchev, T. Blochowicz, C. Gainaru, V. N. Novikov, E. A. Rössler and C. Tschirwitz. J. Phys.: Cond. Matt., **15**, S835, (2003).

[31] U. Schneider, R. Brand, P. Lunkenheimer and A. Loidl, Phys. Rev. Lett., **84**, 5560 (2000).

[32] G.P. Johari, Ann. New York Acad. Sci. **279**, 117 (1976).

[33] W. Götze and L. Sjögren, Rep. Prog. Phys., **55**, 241 (1992).

[34] N.B. Olsen, T. Christensen and J.C. Dyre, *Phys. Rev. Lett.*, **86**, 1271 (2001).

[35] S. Adichtchev, T. Blochowicz, C. Tschirwitz, V.N. Novikov and E.A. Rössler, Phys. Rev. E, **68**, 01154 (2003).

[36] S. Adichtchev, N. Bagdassarov, S. Benkhof, T. Blochowicz, V.N. Novikov, E. Rössler, N. Surovtsev, C. Tschirwitz, and J. Wiedersich, J. Non-Cryst. Solids, **307-310**, 24 (2002).

[37] S. Adichtchev, *The dynamics of molecular glasses studied by light scattering*, PhD Thesis, Bayreuth, 2006.

[38] P. K. Dixon, L. Wu, S. R. Nagel, B. D. Williams, and J. P. Carini, Phys. Rev. Lett., **65**, 1108 (1990).

[39] A. Kudlik, S. Benkhof, R. Lenk and E. Rössler, Europhys. Lett., **32**, 511 (1995).

[40] R.V. Chamberlin, Phys. Rev. Lett., **82**, 2520 (1999).

[41] K.L. Ngai, P. Lunkenheimer, C. Leon, U. Schneider, R. Brand and A. Loidl, J. Chem. Pjys., **115**, 1405 (2001).

[42] T. Blochowicz, C. Tschirwitz, S. Benkhof and E. Rössler, J. Chem. Phys., **118**, 7544 (2003).

[43] T. Blochowicz, C. Gainaru, P. Medick, C. Tschirwitz, E.A. Rössler, J. Chem. Phys., **124**, 134503 (2006).

[44] F. Fujara, S. Wefing and H.W. Spiess, J. Chem. Phys. **84**, 4579 (1986).

[45] T. Blochowicz and E. A. Rössler. Phys. Rev. Lett., **92**, 225701 (2004).

[46] K. L. Ngai and M. Paluch, J. Chem. Phys., **120**, 857 (2004).

[47] N. B. Olsen, J. Non-Cryst. Solids, **235**, 399 (1998).

[48] M. Paluch, C.M. Roland, S. Pawlus, J. Ziolo and K.L. Ngai, Phys. Rev. Lett., **91**, 115701 (2003).

[49] K.L. Ngai and S. Capaccioli, Phys. Rev. E, **69**, 031501 (2004).

[50] R. Böhmer, G. Diezemann, G. Hinze and E. Rössler, Prog. NMR Spectrosc., **39**, 191 (2001).

[51] S. Lusceac, *Study of relaxation processes in simple glass formers by means of ^2H NMR spectroscopy*, PhD Thesis, Bayreuth, 2006.

[52] G. Johari, J. Non-Cryst. Solids, **307-310**, 317 (2002).

[53] G. Williams and D.C. Watts, Trans. Farad. Soc., **67**, 1971, (1971).

[54] M. Vogel and E. Rössler, J. Phys. Chem. B, **104**, 4285 (2000).

[55] M. Vogel and E. Rössler, J. Chem. Phys., **114**, 5802 (2001).

[56] M. Vogel and E. Rössler, J. Chem. Phys., **115**, 10883 (2001).

[57] L. Wu and S. Nagel, Phys. Rev. B, **46**, 198 (1992).

[58] W.A. Phillips, Rep. Prog. Phys. **50**, 1657 (1987).

[59] S. Hunklinger, Physica A **261**, 26 (1998).

[60] P. Esquinazi (Ed.), *Tunneling Systems in Amorphous and Crystalline Solids*, Springer, Berlin, 1998.

[61] J. Classen, T. Burkert, C. Enss and S. Hunklinger, Adv. Sol. St. Phys., **40**, 279 (2000).

[62] R.O. Pohl, X. Liu and E. Thompson, Rev. Mod. Phys. **74**, 991 (2002).

[63] P. Debye, Ann. Phys. (Leipzig) **39**, 789 (1912).

[64] R.C. Zeller and R.O. Pohl, Phys. Rev. B, **4**, 2039 (1971).

[65] W.A. Phillips (Ed.), *Amorphous Solids: Low-Temperature Properties*, Springer, Berlin, 1981.

[66] W.A. Phillips, J. Low Temp. Phys., **7**, 351 (1972).

[67] P.W. Anderson, B.I. Halperin and C.M. Varma, Philos. Mag., **25**, 1 (1972).

[68] J. Classen, C. Enss, C. Bechinger, G. Weiss and S. Hunklinger, Ann. Physik **3**, 315 (1994).

[69] K.S. Gilroy and W.A. Phillips, Philos. Mag. B **43**, 735 (1981).

[70] J. Wiedersich, *Quasi-elastische Lichtstreuung von Gläsern*, PhD Thesis, Bayreuth, 2000.

[71] K.A. Topp and D.G. Cahill, Z. Phys. B **101**, 235 (1996).

[72] J. Wiedersich, S.V. Adichtchev and E. Rössler, Phys. Rev. Lett., **84**, 2718 (2000).

[73] L. Hayler and M. Goldstein, J. Chem. Phys. **66**, 4736 (1977).

[74] J.G. Gilchrist and G.P. Johari, Philos. Mag. B **54**, 273 (1986).

[75] C. Hansen and R. Richert, J. Phys.: Condens. Matter **9**(**44**), 9661 (1997).

[76] H.Z. Cummins, G. Li, Y.H. Hwang, G.Q. Shen, W.M. Du, J. Hernandez and N.J. Tao, Z. Phys. B **103**, 501 (1997).

[77] E. Rössler and H. Sillescu in *Materials Science and Technology*, R.W. Cahn, P. Haasen, E.J. Kramer (Eds), Vol 12., Verlag Chemie, Weinheim, 1991.

[78] A. Döß, M. Paluch, H. Sillescu, and G. Hinze, Phys. Rev. Lett. **88**, 095701 (2002).

[79] K.L. Ngai, Physica A, **261**, 36 (1998).

[80] F. Qi, T. El Goresy, R. Böhmer, A. Döß, G. Diezemann, G. Hinze, H. Sillescu, T. Blochowicz, C. Gainaru, E.A. Rössler and H. Zimmermann, J. Chem. Phys. **118**, 7431 (2003).

[81] A. Brodin, E.A. Rössler, R. Bergman and J. Mattsson, European Physics J. B, **36**, 349 (2003).

[82] A. Justl, S. Capaccioli, T. Blochowicz, C. Tschirwitz, P.A. Rolla, E.A. Rössler, unpublished data.

[83] N. Menon and S.R. Nagel, Phys. Rev. Lett. **74**, 1230 (1995).

[84] C. Gainaru, T. Blochowicz, A. Brodin, H. Schick, P. Medick, Ch. Tschirwitz, E.A. Rössler, J. Non-Cryst. Sol. **352**, 4735 (2006)

[85] P.K. Dixon, N. Menon and S.R. Nagel, Phys. Rev. E*,* **50,** 1717 (1994).

[86] S. Hensel-Bienkowka and M. Paluch, Phys. Rev. Lett., **89**, 025704 (2002).

[87] R. Böhmer, G. Hinze, T. Jörg, F. Qi and H. Sillescu, J. Phys.: Condens. Matter, **12**, 383, (2000).

[88] S.A. Lusceac, C. Gainaru, M. Vogel, C. Koplin, P. Medick, E.A. Rössler, Macromolecules, **38**, 5625 (2005).

[89] M. Vogel, *^{2}H NMR-Untersuchung der Sekundärrelaxation in organischen Glasbildnern*, PhD thesis, Bayreuth, 2000.

[90] compendiu matematica

[91] V. Porokhonskyy, *Dielectric spectroscopy of some high-permittivity ceramics with structural disorder*, PhD thesis, Prague, 2004.

[92] L. Wu, Phys. Rev. B, **43**, 9906 (1991)

[93] I. Chang, F. Fujara, B. Geil, G. Heuberger, T. Mangel, H. Sillescu, J. Non-Cryst. Sol., **172-174**, 248-55 (1994).

[94] H. Wagner, R. Richert, J. Non-Cryst. Sol., **242**, 19 (1998).

[95] N. Theodorakopoulos, J. Jäckle, Phys. Rev. B **14**, 2637 (1976).

[96] V.N. Novikov, A.P. Sokolov, Phys. Rev. E **67**, 031507 (2003).

[97] C.B. Sawyer, C.H. Tower, Phys. Rev. **35**, 269 (1930).

[99] C. Enss, S. Hunklinger in *Tieftemperaturphysik*, Springer, Berlin 2000, p. 264.

[100] Y. Ding, V.N. Novikov, A.P. Sokolov, J. Pol. Sci., Part B: Polym. Phys. **42**, 994 (2004).

[101] M. Vogel, C. Tschirwitz, G. Schneider, C. Koplin, P. Medick, E. Rössler, J. Non-Cryst. Sol. **307-310**, 326 (2002).

[102] D. Richter, R. Zorn, B. Frick, L.J. Fetters, B. Farago, Phys. Rev. Lett. **68**, 71 (1992).

[103] A. Arbe, D. Richert, J. Colmenero, B. Farago, Phys. Rev. E. **54**, 3853 (1996).

[104] A. Auardi, M.J. Lebon, C. Dreyfus, B. Strube, W. Steffen, A. Patkowski, R.M. Pick, J. Phys.: Condens. Matter **9**, 3803 (1997).

[105] R.H. Gee, R.H. Boyd, J. Chem. Phys. **101**, 8028 (1994).

[106] E.G. Kim, W.L. Mattice, J. Chem. Phys. **117**, 2389 (2002).

[107] A. Kudlik, C. Tschirwitz, T. Blochowicz, S. Benkhof, E. Rössler, J. Non-Cryst. Solids **235-237**, 406 (1998).

[108] C. Hansen, R. Richert, Acta Polym. **48**, 484 (1997).

[109] A. Hofmann, A. Alegria, J. Colmenero, L. Willner, E. Buscaglia, N. Hadjichristidis, Macromolecules **29**, 129 (1996).

[110] H. Sato, K. Takebayashi, Y. Tanaka, Macromolecules **20**, 2418 (1987).

[111] Y. Ding, A. Kisliuk, A.P. Sokolov, Macromolecules **37**, 161 (2004).

[112] S. Kariyo, C. Gainaru, H. Schick, A. Brodin, V.N. Novikov, E.A. Rössler, Phys. Rev. Lett. **97**, 207803 (2006).

[113] H. Cang, V. N. Novikov, M.D. Fayer, J. Chem. Phys. **118,** 2800 (2003).

[114] A. Brodin, E.A. Rössler, J. Chem. Phys. **125,** 114502 (2006).

[115] A. Brodin, C. Gainaru, V. Porokhonskyy, E.A. Rössler, J. Phys.: Condens. Matter **19**, 205104 (2007).

[116] A. Justl, S. Capaccioli, V. Porrochonskyy, C. Gainaru, E.A. Rössler, unpublished data (2006).

[117] C. Tschirwitz, *Untersuchung der Sekundärrelaxation einfacher organischer Glasbildner mittels dielektrischer Spektroskopie*, Diplomarbeit, Bayreuth, 1997.

[118] R. Höhler, G. Kasper, S. Hunklinger, Phys. Rev. B. **43**, 9220 (1991).

[119] V. Röhring, T. Saatkamp, G. Kasper, S. Hunklinger, J. Non-Cryst. Solids **107**, 166 (1989).

[120] M.A.Il'in, V.G. Karpov, D.A. Parshin, Sov. Phys. JETP **65**, 165 (1987).

[121] C. Enss, S. Hunklinger, Phys. Rev. Lett. **79**, 2831 (1997).

[122] P. Esquinazi, R. König, F. Pobell, Z. Phys. B **87**, 305 (1992).

[123] A. Nittke, S. Sahling, P. Esquinazi, in *Tunneling Systems in Amorphous and Crystalline Solids*, Springer, Berlin, 1998, p. 9.

[124] M. Zobel, PhD. Thesis, Bristol, 1971

[125] S. Hunklinger, M.v. Schickfus, in *Amorphous Solids: Low-Temperature Properties*, Springer, Berlin, 1981, p. 81.

[126] P. Esquinazi, R. König in *Tunneling Systems in Amorphous and Crystalline Solids*, Springer, Berlin, 1998, p. 166.

[127] A. Hoffmann, F. Kremer, E.W. Fischer, A. Schönhals, in *Disorder Effects on Relaxation Processes*, Eds: Richert, R. and Blumen, A., Springer, Berlin, 1994, p. 309.

[128] T. Blochowicz, A. Brodin, E.A. Rössler, Adv. Chem. Phys. **133** Part A, 127 (2006).

[129] M. Vogel, P. Medick, E.A. Rössler, Annual Reports on NMR Spectroscopy **56,** 231 (2005).

[130] G. Hinze, Phys. Rev. E **57**, 2010 (1998).

[131] R. Böhmer, G. Hinze, J. Chem. Phys. **109**, 241 (1998).

[132] Th. Dries, F. Fujara, M. Kiebel, E. Rössler, H. Sillescu, J. Chem. Phys. **88**, 2139 (1988).

[133] W. Schnauss, F. Fujara, H. Sillescu, J. Chem. Phys. **97**, 1378 (1992).

[134] M.J. Lebon, C. Dreyfus, Y. Guissani, R.M. Pick, H.Z. Cummins, Z. Phys. B **103**, 433 (1997).

[135] F. Noack, G. Preissig, Z. Naturforsch. **24a**, 143 (1969).

[136] F. Noack, Progr. NMR Spectr. **18**, 171 (1986).

[137] R. Kimmich, E. Anoardo, Progress in NMR spectroscopy **44**, 257 (2004).

[138] O. Lips, D. Kruk, A. Privalov, F. Fujara, Solid State Magnetic Resonance **31**, 141 (2007).

[139] C. Gainaru, A. Rivera, S. Putselyk, G. Eska, E.A. Rössler, Phys. Rev. B **72**, 174203 (2005).

[140] C. Gainaru, A. Brodin, V.N. Novikov, E.A. Rössler, preprint cond-mat/0604597 (2006).

[141] O. Lips, A. F. Privalov, S. V. Dvinskikh, F. Fujara, J. Magn. Res. **149**, 22 (2001).

[142] A. Brodin, E.A. Rössler, Eur. Phys. J. B **44,** 3 (2005).

[143] M. Kehr, N. Fatkullin, R. Kimmich, J. Chem. Phys.**126**, 094903 (2007).

[144] A. Abragam, *The Principles of Nuclear Magnetism*, Clarendon Press, Oxford, 1961.

[145] N. Bloembergen, R.V. Pound, E.M. Purcell, Phys. Rev. **73**, 679 (1948).

[146] S. Kariyo, A. Brodin, C. Gainaru, A. Herrmann, H. Schick, V.N. Novikov, E.A. Rössler, Macromolecules (2007), submitted.

[147] Y. Akagi, and N. Nakamura, J. Phys. Condens. Matter **12**, 5155 (2000).

[148] C*. Tschirwitz, S. Benkhof, T. Blochowicz, E.A. Rössler*, J. Chem. Phys. **117**, 6281 (2002).

[149] Novocontrol Technologies, *Alpha-A high resolution dielectric, conductivity, impedance and gain phase modular measurement system; User's manual,* (2004.)

[150] C. Gainaru, O. Lips, A. Troshagina, R. Kahlau, F. Fujara, E.A. Rössler, "On the nature of the high-frequency relaxation in a molecular glass former: A joint study of glycerol by field cycling NMR, dielectric spectroscopy and light scattering" submitted.

List of publications

1. Kariyo S., Brodin A., **Gainaru C.**, Herrmann A., Schick H., Novikov V.N., Rössler E.A. "From simple liquid to polymer melt: Glassy and polymer dynamics studied by fast field cycling NMR relaxometry - Part I: Low and high molecular weight limit ", submitted, Macromolecules.

2. Kariyo S., Brodin A., **Gainaru C.**, Herrmann A., Hitermeyer J., Schick H., Novikov V.N., Rössler E.A. "From simple liquid to polymer melt: Glassy and polymer dynamics studied by fast field cycling NMR relaxometry - Part II: Rouse regime", submitted, Macromolecules.

3. **Gainaru C.**, Lips O., Troshagina A., Kahlau R., Brodin A., Fujara F., Rössler E.A. "On the nature of the high-frequency relaxation in a molecular glass former: A joint study of glycerol by field cycling NMR, dielectric spectroscopy and light scattering" , accepted for publication, J. Chem Phys.

4. Brodin A., **Gainaru C.**, Porokhonskyy V., Rössler E.A. "Evolution of dynamic susceptibility in molecular glass-formers – a critical assessment" J. Phys.: Condens Matter (2007), 19(205104).

5. **Gainaru C.**, Brodin A., Novikov V.N., Rössler E.A. "Does frequency-temperature superposition principle hold in deeply super-cooled liquids?" Los Alamos National Laboratory, Preprint Archive, Condensed Matter (2006), 1-5 rXiv:cond-mat/0604597.

6. Kariyo S.; **Gainaru C.**; Schick H.; Brodin A.; Novikov V.N.; Rossler E.A. "From a Simple Liquid to a Polymer Melt: NMR Relaxometry Study of Polybutadiene." Physical Review Letters (2006), 97(20).

7. Blochowicz Th., **Gainaru C.**, Medick P., Tschirwitz Ch., Rössler E.A. "The dynamic susceptibility in glass forming molecular liquids: The search for universal relaxation patterns II" Journal of Chemical Physics (2006), 124(13).

8. **Gainaru C.**, Blochowicz Th., Brodin A., Schick H., Medick P., Tschirwitz Ch., Rössler E.A. "Supercooled liquids and plastically crystalline phases: Indications for a similar manifestation of a crossover in the evolution of the dielectric spectra" Journal of Non-Crystalline Solids (2006), 352(42-49).

9. **Gainaru C.**, Rivera A., Putselyk S., Eska G., Rössler E.A. "Low temperature dielectric relaxation of molecular glasses: crossover from the nearly constant loss to the tunneling regime" Phys. Rev. B (2005), 72, 174203

10. Lusceac S.A., **Gainaru C.**, Vogel M., Koplin C., Medick P., Rössler E.A. "Secondary relaxation processes in polybutadiene studied by 2H nuclear magnetic resonance and high-precision dielectric spectroscopy" Macromolecules (2005), 38(13), 5625-5633.

11. Rivera A., Blochowicz Th., **Gainaru C.**, Rössler E.A. "Spectral response from modulus time domain data of disordered materials" J. Appl. Phys. (2004), 96(10) 5607-5612.

12. Adichtchev S., Blochowicz Th., **Gainaru C.**, Novikov V.N., Rössler E.A., Tschirwitz Ch. "Evolution of the dynamic susceptibility of simple glass formers in the strongly supercooled regime" Journal of Physics: Condensed Matter (2003), 15(11), S 835.

13. Qi F., El Goresy T., Bohmer R., Doss A., Diezemann G., Hinze, G., Sillescu H., Blochowicz Th., **Gainaru C.**, Rössler E.A., Zimmermann H. "Nuclear magnetic resonance and dielectric spectroscopy of a simple supercooled liquid: 2-methyl tetrahydrofuran" J. Chem. Phys. (2003), 118(16), 7431-7438

14. Rivera A., Santamaria J., Leon C., Blochowicz Th., **Gainaru C.**, Rössler E. A. "Temperature dependence of the ionic conductivity in Li3xLa2/3-xTiO3: Arrhenius versus non-Arrhenius" Appl. Phys. Lett. (2003), 82(15), 2425-2427

Acknowdledgements

The author would like to express its gratitude regarding all people contributing (more or less) to this thesis.

First in the list is, by all means, Prof. Dr. Ernst Rössler who trusted and offered me a position in his group. His scientific support, his kindness and, nonetheless, his patience during the thesis preparation are fully appreciated. Also, I thank Prof. Dr. Dumitru D. Sandu for introducing me in the field of dielectric spectroscopy and Prof. Frantz Fujara for giving me the opportunity to analyze the field cycling NMR data measured in his group in Darmstadt. Also many thanks to Prof. Dr. Roland Böhmer for accepting to referee this thesis.

There are many others whom I would like to acknowledge: Thomas Blochowitz, the "guru" of the dielectric lab at the time of my initiation, Christian Tschirwitz for its kindness, scientific and social skills, other dielectric people as Alberto Rivera (always a "sunshine" in the cloudy Bayreuth) and Viktor Porokhonskyy (the calmest guy I've ever meet). Regarding the "NMR people", special regards to my conational Sorin Lusceac, with whom I spent many evenings discussing and enjoying german beer. From the "Light Scattering group" all the best to Sergei Aditchev who helped and supported me during our common time in Bayreuth. His kitchen will always be remembered. Also the criticism and sometimes the "cinism" of Alex Brodin are, at this time, fully appreciated.

Many considerations also for the youngsters, Axel Herrmann, Björn Micko, Nikolaus Petzold and Robert Kahlau, the latter helping also with the correction of this thesis. I miss having grill with them on the roof of NWII. Taking about grills, many greeting to my friends Lukasz Kotula, Dominik Neugebauer and Chris Mayer.

Last but not least I thank my wife Roxana for her patience during the time needed for the thesis accomplishment.